Final Report

FHWA/IN/JTRP – 2006/16

Fatigue Strength and Evaluation of Sign Structures
Volume 1: Analysis and Evaluation

by

Xuejun Li
Graduate Research Assistant

Timothy M. Whalen
Continuing Lecturer

and

Mark D. Bowman
Professor of Civil Engineering

School of Civil Engineering
Purdue University

Joint Transportation Research Program
Project No: C-36-56DDD
File No: 9-10-63
SPR-2494

Conducted in Cooperation with the
Indiana Department of Transportation
And the U.S. Department of Transportation
Federal Highway Administration

Purdue University
West Lafayette, Indiana
June 2006

TECHNICAL REPORT STANDARD TITLE PAGE

1. Report No.	2. Government Accession No.	3. Recipient's Catalog No.
FHWA/IN/JTRP-2006/16		

4. Title and Subtitle	5. Report Date
Fatigue Strength and Evaluation of Sign Structures	June 2006
	6. Performing Organization Code

7. Author(s)	8. Performing Organization Report No.
Xuejun Li, Timothy M. Whalen, and Mark D. Bowman	FHWA/IN/JTRP-2006/16

9. Performing Organization Name and Address	10. Work Unit No.
Joint Transportation Research Program 550 Stadium Mall Drive Purdue University West Lafayette, Indiana 47907-2051	
	11. Contract or Grant No. SPR-2494

12. Sponsoring Agency Name and Address	13. Type of Report and Period Covered
Indiana Department of Transportation State Office Building 100 North Senate Avenue Indianapolis, IN 46204	Final Report
	14. Sponsoring Agency Code

15. Supplementary Notes

Prepared in cooperation with the Indiana Department of Transportation and Federal Highway Administration.

16. Abstract

This report is a two-volume final report presenting the findings of the research work that was undertaken to evaluate the fatigue behavior of sign structures and, based on that evaluation, to recommend an inspection plan that can be effectively used to detect and minimize possible deterioration due to wind induced loadings of sign structures. The study included a number of signs that are commonly used in Indiana: single-mastarm and double-mastarm cantilever sign structures, box-truss sign structures, tri-chord sign structures, and monotube sign structures. Sign structures with typical dimensions and details were selected as prototypes for each of the various types of sign structures in the study and were subjected to various wind loading environments. The predicted fatigue behavior of the sign structures was used to identify the types of signs and the structural details that were most susceptible to fatigue damage. This information was used to develop an inspection guideline that provides information on where to look during an inspection for fatigue damage. An inspection plan was formulated by using a crack propagation analysis to evaluate crack growth under the most critical wind loading environment. Based on these analyses, an inspection period of four years was recommended for single and double mastarm cantilever sign structures (Class A) and an eight year inspection cycle was recommended for box-truss, tri-chord, and monotube sign structures.

The titles of the two volumes are listed below:

Volume 1: Analysis and Evaluation
Volume 2: Sign Structure Inspection Manual

17. Key Words	18. Distribution Statement
fatigue, sign, crack, wind loading, inspection, monitoring, remaining life	No restrictions. This document is available to the public through the National Technical Information Service, Springfield, VA 22161

19. Security Classif. (of this report)	20. Security Classif. (of this page)	21. No. of Pages	22. Price
Unclassified	Unclassified	133 + 64	

Form DOT F 1700.7 (8-69)

ACKNOWLEDGEMENTS

This research project was financially supported by the Federal Highway Administration and the Indiana Department of Transportation through the auspices of the Joint Transportation Research Program. The authors would like to express their grateful acknowledgement for sponsorship of this research.

The advice and input provided throughout the study by the Study Advisory Committee for the research project is greatly appreciated. Members of the Study Advisory Committee include Messrs. Dale Louie, Pankaj Patel, Prakash Patel, and Scott Newbolds of the Indiana Department of Transportation and Mr. Ed Ratulowski of the Federal Highway Administration.

Thanks are also due to those that assisted in various aspects of the study. In particular, appreciation is extended to Messrs. Ed Sinchai and Matt Kilgour, and Dr. Piya Chotickai.

TABLE OF CONTENTS

Page
LIST OF TABLES vi

LIST OF FIGURES vii

ABBREVIATIONS xi

CHAPTER 1. INTRODUCTION 1
1.1. Research Problem Statement 1
1.2. Objectives of Study 2
1.3. Scope and Method of Study 3
1.4. Organization of the Report 4

CHAPTER 2. BACKGROUND 6
2.1. NCHRP Report 412 6
2.1.1. Types of Wind Loading on Sign Structure 7
2.1.2. Fatigue Categorization of Connection Details 8
2.1.3. Proposed Fatigue Limit State Loads for Sign Structures 10
2.2. Background on Wind Engineering 11
2.2.1. Critical Wind Load for Fatigue on Sign Structures 11
2.2.2. Wind Spectrum 13
2.2.3. Weibull Distribution for Wind Speed Distribution 15
2.3. Background on Fatigue 16
2.3.1. AASHTO Fatigue Life Rules and S-N Curves 17
2.3.2. Miner's Rule 18
2.3.3. Rainflow Counting 20
2.3.4. Fatigue Limits 21

CHAPTER 3. FINDINGS 25
3.1. Finite Element Modeling of Sign Structures 25
3.1.1. Modeling of Double-Mastarm Cantilevered Sign Structure 26
3.1.1.1. Prototype Sign Structure 26

3.1.1.2. Description of Finite Element Model 26
3.1.2. Modeling of Single-Mastarm Cantilevered Sign Structure 28
3.1.2.1. Prototype Sign Structure 28
3.1.2.2. Description of Finite Element Model 28
3.1.3. Modeling of Box-Truss Sign Structure 29
3.1.3.1. Prototype Sign Structure 29
3.1.3.2. Description of Finite Element Model 29
3.1.4. Modeling of Monotube Sign Structure 30
3.1.4.1. Prototype Sign Structure 30
3.1.4.2. Description of Finite Element Model 30
3.1.5. Modeling of Tri-Chord Sign Structure 31
3.1.5.1. Prototype Sign Structure 31
3.1.5.2. Description of Finite Element Model 31
3.2. Wind Speed Distribution and Wind Load Simulation 32
3.2.1. Wind Speed Distribution for Locations in Indiana 32
3.2.2. Wind Load Simulation 33
3.2.2.1. Wind Load Simulation Procedure 34
3.2.2.2. Application of Wind Load Simulation 37
3.3. Fatigue Analysis and Sign Structure Life Expectancies 39
3.3.1. Analytical Procedure 40
3.3.2. Fatigue Analysis Results for Double-Mastarm Cantilevered Sign Structure 42
3.3.2.1. Modal Analysis 42
3.3.2.2. Fatigue Analyses and Life Results for Connection Details 42
3.3.2.3. Sensitivity of Fatigue Lives to Load Simulation 49
3.3.3. Fatigue Analysis Results for Box-Truss Sign Structure 51
3.3.3.1. Modal Analysis 51
3.3.3.2. Fatigue Analyses and Life Results for Connection Details 52
3.3.4. Fatigue Analysis Results for Monotube Sign Structure 56
3.3.4.1. Modal Analysis 56
3.3.4.2. Fatigue Analyses and Life Results for Connection Details 56
3.3.5. Fatigue Analysis Results for Tri-Chord Sign Structure 59
3.3.5.1. Modal Analysis 59
3.3.5.2. Fatigue Analyses and Life Results for Connection Details 59
3.3.6. Fatigue Analysis Results for Single-Mastarm Cantilever Sign Structure 61
3.3.6.1. Modal Analysis 61
3.3.7. Conclusions and Discussions 63

CHAPTER 4. INSPECTION OF SIGN STRUCTURES 109
4.1. Introduction of NDE 109
4.2. NDE Methods 110

4.2.1. Visual Inspection 111
4.2.2. PT 112
4.2.3. MT 113
4.2.4. UT 116
4.3. In-Service Inspection of Sign Structures 117
4.4. Inspection Frequency 118
4.4.1 Crack Propagation Calculation 119

CHAPTER 5. CONCLUSIONS 125
5.1. Summary and Conclusions 125
5.2. Implementation of Study Results 128
5.3. Suggested Future Work 128

LIST OF REFERENCES 130

LIST OF TABLES

Table Page

2.1 Constants for different fatigue detail categories (AASHTO, 2003) 23

2.2 CAFL for different fatigue detail categories from sign structure design specification (AASHTO, 2001) 23

3.1 Section dimensions for double-mastarm cantilever prototype sign structure.....67

3.2 Section dimensions for single-mastarm cantilever prototype sign structure 67

3.3 Section dimensions for box-truss prototype sign structure.....67

3.4 Section dimensions for monotube prototype sign structure.....68

3.5 Section dimensions for tri-chord prototype sign structure.....68

3.6 Weibull parameters for different locations in Indiana 68

3.7 Life expectancies (in years) at various locations for different details of a double-mastarm cantilever sign structure.....69

3.8 COVs for cyclic fatigue lives of tested bridge weld connection details (Keating and Fisher, 1985).....69

3.9 Life expectations and statistical data for post-to-base plate socket weld connection with different simulated load 70

LIST OF FIGURES

Figure Page

2.1 S-N curves (Fisher et al. 1991) 24

3.1 A typical double-mastarm cantilever sign structure 71

3.2 Post-to-base plate detail 71

3.3 Typical cantilevered sign structure model (Model A) 72

3.4 Spider bolts (3D view) 72

3.5 Chord-to-post connection....73

3.6 Model with chord-to-post detail (Model B)....73

3.7 Chord-to-post detail in Model B 74

3.8 Hand hole detail 74

3.9 Model with hand hole detail (Model C)....75

3.10 A typical single-mastarm cantilever sign structure 75

3.11 A prototype single-mastarm cantilever sign structure model 76

3.12 A typical box-truss sign structure 76

3.13 Model A for box-truss sign structure. 77

3.14 Model B for box-truss sign structure 77

3.15 A typical monotube sign structure 78

3.16 Model A for monotube sign structure....78

3.17 Model B for monotube sign structure. 79

3.18 A typical tri-chord sign structure 79

3.19 Model A for the tri-chord sign structure model 80

3.20 Model B for the tri-chord sign structure 80

3.21 Selected locations in Indiana 81

Figure Page

3.22 Wind speed distribution curves (1) 81
3.23 Wind speed distribution curves (2) 82
3.24 Wind force time-history on the sign panel for V_{mean}=5 m/s at the center of the sign panel 82
3.25 Wind force time-history on the sign panel for V_{mean}=11 m/s at the center of the sign panel 83
3.26 Wind force time-history on the sign panel for V_{mean}=15 m/s at the center of the sign panel 83
3.27 First mode of the double-mastarm cantilever sign structure (top view) 84
3.28 Second mode of the double-mastarm cantilever sign structure 84
3.29 Third mode of the double-mastarm cantilever sign structure (top view) 85
3.30 Stress history at post-to-base plate connection for V_{mean}= 5 m/s 85
3.31 Histogram of stress cycles for post-to-base plate weld connection 86
3.32 Damage percentage for different stress ranges 86
3.33 Hand hole detail 87
3.34 Histogram of stress cycles for hand hole 87
3.35 Chord-to-post connection 88
3.36 Histogram of stress cycles for post-to-end plate connection 88
3.37 Chord-to-post connection 89
3.38 Strut to gusset plate weld connection and gusset plate to chord connection 89
3.39 First mode of the box-truss sign structure 90
3.40 Second mode of the box-truss sign structure 90
3.41 Third mode of the box-truss sign structure 91
3.42 A simple model of the box-truss sign structure 91
3.43 Post-to-socket weld connection for the box-truss sign structure 92
3.44 Histogram for post-to-socket weld connection 92
3.45 Histogram for anchor rod 93
3.46 Hand hole of a box-truss sign structure 93

Figure Page

3.47 Histogram for hand hole 94
3.48 U-bolt in chord-to-post connection for a box-truss sign structure....94
3.49 Chord-to-plate weld connection for a box-truss sign structure 95
3.50 Truss-to-chord weld connection for a box-truss sign structure. 95
3.51 Lateral-braces-to-post connection for a box-truss sign structure 96
3.52 First mode of the monotube sign structure 96
3.53 Second mode of the monotube sign structure....97
3.54 Third mode of the monotube sign structure....97
3.55 Post-to-base-plate weld detail of a monotube sign structure 98
3.56 Histogram for post to base plate weld connection....98
3.57 Anchor rods detail of a monotube sign structure....99
3.58 Histogram for anchor rod detail....99
3.59 Hand hole of a monotube sign structure 100
3.60 Histogram for hand hole detail 100
3.61 Monotube-to-end-plate welded connection for a monotube sign structure 101
3.62 Histogram for monotube to transverse plate weld detail. 101
3.63 Monotube-to-post pin connection for a monotube sign structure....102
3.64 Histogram for the ear to post weld connection....102
3.65 First mode for the tri-chord sign structure....103
3.66 Second mode for the tri-chord sign structure 103
3.67 Third mode for the tri-chord sign structure 104
3.68 Post-to-base-plate weld connection for a tri-chord sign structure 104
3.69 Histogram for post-to-base-plate weld detail of tri-chord sign structure 105
3.70 Anchor rods detail of a tri-chord sign structure....105
3.71 Histogram for anchor rod....106
3.72 Hand hole of a tri-chord sign structure 106
3.73 Histogram for hand hole detail 107
3.74 Chord-to-end-plate weld connection for a tri-chord sign structure. 107

Figure Page

3.75 Histogram for chord to transverse plate weld connection at middle span.....108

3.76 First mode of the single-mastarm cantilever sign structure.....108

3.77 Second mode of the single-mastarm cantilever sign structure 109

ABBREVIATIONS

AASHTO……..…...American Association of State Highway and Transportation Officials
ASTM…….…….American Society for Testing and Materials
AWS……..American Welding Society
BMG…….……..……..….Bloomington, Indiana
CAFL…….….Constant Amplitude Fatigue Limit
COV……..…….….Coefficient of Variation
EVV…….……..…….Evansville, Indiana
FWA……..……Fort Wayne, Indiana
IND……..…….Indianapolis, Indiana
LAF……..…….Lafayette, Indiana
LRFD…….Load and Resistance Factor Design
MT……..……..…..…..Magnetic Particle Testing
NCDC……..…..National Climatic Data Center
NCHRP……..……National Cooperative Highway Research Program
NDE…….…..Non-destructive Evaluation
PT……..……..…..Dye-Penetrant Testing
RT……..……...…..Radiographic Testing
S-N……..……..Stress Range versus Fatigue Life
SBN……..…….South Bend, Indiana
UT……..……..Ultrasonic Testing
VAFL…….…….Variable Amplitude Fatigue Limit

CHAPTER 1

INTRODUCTION

1.1 Research Problem Statement

Sign structures are used extensively on major interstate highways and at local intersections for traffic direction. Because of their long span length (often over several traffic lanes) and relatively small cross-sectional area and mass, sign structures are very flexible. This flexibility gives sign structures very low natural frequencies. The damping in sign structures is also very low, typically around one percent of critical damping (Kaczinski et al., 1998). These properties make the sign structure very susceptible to large amplitude vibration and fatigue cracking under wind loading. Cracks in sign structures due to fatigue damage have been observed in a number of states and in a few cases, sign structure failures have also been reported (Fisher et al., 1991; Dexter and Ricker, 2001).

There are five basic types of sign structures used in the State of Indiana: the cantilever structure (including the single-mastarm and the double-mastarm), the overhead bridge structure (including the tri-chord and the box-truss), the monotube structure, the wire cable span structure, and the variable message sign. (The variable message sign and the wire cable span structures were not included in this study.) Each type of sign structure has fatigue-sensitive connections and other details at which cracking can occur. It is crucial to

perform periodic inspections of the sign structures to detect potential problems and avoid a serious accident. Currently, there are no inspection procedures established for sign structures in Indiana. An inspection manual, outlining appropriate procedures and intervals for fatigue evaluation, needs to be developed. The manual should identify critical spots in the sign structures where fatigue could be a problem and instruct the inspection engineers exactly when and where to perform an inspection. To assist in decisions regarding inspection frequency and evaluation, an investigation was performed to evaluate the fatigue life of critical details in typical sign structures under wind loads.

1.2 Objectives of Study

A research program has been undertaken to evaluate the fatigue performance of sign structures under wind loading and, based on this research, to propose inspection instructions for sign structures. The specific objectives of the research are as follows:

1. Develop a fatigue analysis procedure to estimate the fatigue life expectation of details in sign structures from the results of dynamic stress analyses.
2. Identify the most critical details in the various types of sign structures and rank these details with respect to importance for inspection.
3. Propose inspection procedures for sign structures, outlining the locations in sign structures that should be inspected, the time interval at which inspection should be performed and appropriate inspection methods.

1.3 Scope and Method of Study

Finite element analyses were conducted to evaluate the fatigue performance of double-mastarm cantilever sign structures, single-mastarm cantilever sign structures, box-truss sign structures, monotube sign structures, and tri-chord sign structures. Natural wind gusts were assumed to be the wind load causing fatigue damage in the sign structures. The prototype sign structures used in this investigation were considered to be standard sign structures in Indiana. All of the welded connections were assumed to satisfy the quality control standards of the welding specifications. All the sign structures were assumed to be linear elastic in the finite element analysis.

The analytical program includes the following steps:

1. A literature review and communications with design engineers at the Indiana Department of Transportation (INDOT) were performed to identify details susceptible to fatigue cracking. These details were evaluated to determine if they are critical for wind induced fatigue damage.
2. Natural wind loadings were simulated numerically and applied in transient dynamic finite element analyses. Representative wind loading histograms were generated at locations such as the sign panel and post.
3. Dynamic stress analyses of prototype sign structures were conducted for critical details to obtain stress time histories for specific details.
4. Fatigue analyses were performed to estimate the fatigue life expectation of fatigue susceptible details under different wind environments in Indiana.

5. The fatigue life expectations of the critical details in sign structures were compared and these details were ranked with regard to importance for inspection.
6. An appropriate time interval for inspection of sign structures was recommended based upon the results of the fatigue life calculations, as well as information gathered from the literature search and INDOT inspection engineers.
7. Appropriate nondestructive evaluation (NDE) methods for potential crack inspection for different sign structure details were selected.

1.4 Organization of the Report

Chapter 2 presents a summary of NCHRP Report 412 and background on wind engineering and fatigue analysis. In the wind engineering background section, the topic of critical wind load is discussed, and the concepts of wind spectrum and Weibull distribution for wind speed distribution are explained. The background on fatigue includes S-N curves, Miner's rule, rainflow counting, and fatigue limits.

Chapter 3 is a detailed presentation of the research findings. Included in this chapter is (1) a description of the sign structure finite element models developed based on selected prototype sign structures installed in Indiana; (2) results of computed wind speed distributions for six locations in Indiana, and description of a wind load simulation procedure developed to generate wind load time histories; and (3) presentation of a fatigue analysis procedure developed to predict the fatigue lives of sign structural details, along with the resulting fatigue lives.

In Chapter 4, nondestructive evaluation (NDE) and in-service inspection of sign structures are briefly introduced. Frequencies for sign structure inspection are recommended, and a crack propagation evaluation is performed to justify the recommended inspection intervals. Finally, in Chapter 5, conclusions from the research are presented, future research is recommended, and implementation recommendations are provided.

CHAPTER 2

BACKGROUND

This study makes use of a large body of previous research on wind engineering, metal fatigue and connection behavior to evaluate the fatigue strength of sign structures. Section 2.1 summarizes the pertinent research from NCHRP Report 412 on fatigue-resistant design of cantilever sign signal, sign and light supports. Section 2.2 provides background on wind engineering, and Section 2.3 introduces background on fatigue.

2.1 NCHRP Report 412

An important source of previous research on fatigue-resistant design of sign support structures is the National Cooperative Highway Research Program (NCHRP) Report 412 (Kaczinski et al., 1998). Fatigue design procedures for sign structures included in the current version of Standard Specifications for Structural Supports for Highway Signs, Luminaires and Traffic Signals (AASHTO, 2001) are based upon work discussed in NCHRP Report 412. Experimental and analytical work was performed to develop guidelines for the fatigue design of cantilever sign, signal, and luminaire supports.

In the research reported by NCHRP Report 412, experimental and analytical work was performed to develop guidelines for the fatigue design of cantilever sign, signal, and

luminaire supports. Three major research topics in NCHRP Report 412 related to this project are summarized in the following section. Section 2.1.1 introduces the types of wind loading on sign structures that are associated with fatigue damage, Section 2.1.2 summarizes fatigue categorization of connection details, and Section 2.1.3 presents the proposed fatigue limit state loads for sign structures.

2.1.1 Types of Wind Loading on Sign Structure

As stated in NCHRP Report 412, there are four types of loading considered to make the majority of contribution to fatigue damage on sign structures: galloping, vortex shedding, natural wind gusts and truck induced gusts (Kaczinski et al., 1998). Galloping and vortex shedding, if they occur, can induce nearly constant-amplitude vibrations in the vertical direction at a natural frequency of the sign structure and can lead to fatigue failures in a short period of time after installation. On the other hand, natural wind gusts and truck induced gusts cause along-wind vibrations that can produce accumulated fatigue damage at critical connection details over the life of the structure.

Galloping is an aeroelastic phenomena in which unstable aerodynamic damping forces are created due to structural vibration-induced variations in the angle of attack of the wind flow (Simiu and Scanlan, 1986). Galloping-induced vibration occurs in the cross-wind direction. Moreover, galloping-induced oscillations primarily occur in flexible, lightly damped structures with non-symmetrical cross-sections.

Vortex shedding is caused by the passage of turbulent eddies in a regular, alternating

pattern on opposite sides of a structural element. It typically occurs during steady, uniform flows and produces resonant oscillations in a plane normal to the direction of flow. It was reported that only those structures with very large member dimensions, e.g., diameters greater than 900 mm (35 in), will potentially be susceptible to vortex-induced vibrations (Kaczinski et al., 1998). Usually, the diameters of sign structure members in Indiana are smaller than the dimension associated with vortex shedding.

Natural wind gusts arise from the naturally occurring variability in the velocity and direction of air flow. Changes in velocity and direction of air flow produce fluctuating pressures on the sign structure, which can cause it to vibrate. The magnitude of the vibration is a random variable. The variable stress ranges in the structural components of the sign structure, which are caused by the random vibrations, will produce fatigue damage in the long term.

Truck-induced wind gusts are produced by the passage of trucks beneath sign structures and act on the front area facing the oncoming traffic and underside of the members of the sign structures. It is more likely to be critical for sign structures with large projected areas parallel to the ground, e.g. the considerable thickness associated with variable message sign structures. Cantilever sign structures, on the other hand, have little dimension parallel to the ground and should not sustain large truck-induced wind loads.

2.1.2 Fatigue Categorization of Connection Details

Current fatigue design provisions state that cantilever sign structures should be

designed for infinite fatigue life in accordance with the AASHTO sign structure design specification (AASHTO, 2001). Although the sign structure fatigue limits are based primarily upon the AASHTO bridge specifications, the geometrical configuration of typical cantilever sign structures connection details vary significantly from details found in the AASHTO bridge specifications. The categorization of typical cantilever support structure connection details according to the fatigue design curves in the AASHTO Bridge specification and/or AWS Structural Welding Code – Steel (D1.1) was included in NCHRP Report 412.

The categorization of cantilever support structure connection details to the existing AASHTO and/or AWS fatigue design curves is based upon a general understanding of fatigue behavior, knowledge of previous research which has led to the development of the existing fatigue design curves, experience with structural failures which have resulted from fatigue, and engineering judgment. The link between the fatigue resistance of cantilever support structure connection details and the existing knowledge of bridge details was made by comparing the stress concentrations and locations at which cracks form (Kaczinski, et al., 1998; Fisher, et al., 1981).

The provisions of the AASHTO bridge specifications for the design of structures for fatigue are based upon a nominal stress approach in which details are grouped into categories according to their relative fatigue resistance. Based on the research in NCHRP report 412, the AASHTO specifications for sign structures (2001) contain nine design categories labeled A through K2 in order of decreasing fatigue strength. Examples of connection details relevant to sign structures include anchor bolts (Category D detail), mechanical clamps and U-bolts (Category D details), column-to-base-plate or mast-arm-to-flange-plate socket connections

(Category E' details) and hand hole openings (Category E detail). Most cantilever sign structure connection details are classified to have low levels of fatigue resistance. A description of the fatigue details and their corresponding stress categories can be found in Table 11-2 of the AASHTO sign structure specification (2001).

2.1.3 Proposed Fatigue Limit State Loads for Sign Structures

As discussed in Section 2.1.1, there are four wind-loading mechanisms that can be critical for fatigue damage to sign structures. Equivalent static load ranges were recommended for each of the four types of loading. The resulting stress values at critical details that were produced by the equivalent static load range are approximately the same as the stress ranges caused by various dynamic wind-loadings, which was verified in finite element analyses.

It was recommended that an equivalent static lift-pressure (shear force) range equal to $1000*I_f$ Pa ($21*I_f$ psf) be used in the design of cantilever sign structures for galloping-induced fatigue, where I_f is the fatigue importance factor and reflects the degree of hazard to traffic in the event of a failure. (A value of $I_f = 1.0$, the most critical value possible, was used throughout this study.) This shear force range should be applied in-plane vertically to the surface area of all sign attachments rigidly mounted to the horizontal mast arm as seen in the normal elevation. As for vortex shedding, wind tunnel tests indicated that significant vibrations did not occur from vortex shedding for cantilever sign structures. So cantilever sign structures do not need to be designed for vortex-shedding-induced fatigue.

The equivalent static natural wind gust pressure range normalized by the associated drag coefficient is 250 Pa (5.2 psf). The drag coefficient takes into account the varying types of surfaces on each sign structure. The calculated natural wind gust pressure range should be applied in the horizontal direction to the projected area of all exposed support structure members, signs and/or miscellaneous attachments. The equivalent static truck induced gust pressure range normalized by the associated drag coefficient is 1760 Pa (36.6 psf). This pressure range should be applied in the vertical direction to the area of the underside of all signs, walkways and/or lighting fixtures projected on a horizontal plane.

2.2 Background on Wind Engineering

Background information related to the selection of critical wind load and the simulation of wind load are discussed in this section, including critical wind loads for sign structures, wind spectrum and Weibull distribution for wind speed distribution.

2.2.1 Critical Wind Load for Fatigue on Sign Structures

Based on experimental work in a wind tunnel, along with engineering judgment, NCHRP Report 412 suggested that galloping caused fatigue damage to sign structures and should be considered for fatigue design of sign structures. However, an argument can be made that galloping is not an important source of fatigue-inducing vibrations for most types of sign structures, except the single-mastarm cantilever sign structure. Galloping has rarely

been observed in the field for sign structures other than single-arm cantilever sign structures. There were reports of actual supporting structures observed to have experienced vertical-plane vibrations consistent with galloping in the field in NCHRP Report 412. However, two of the three supporting structures were signal structures, which have different dynamic properties than sign structures. The third structure was a double-mastarm cantilever sign structure that collapsed as a result of propagation of fatigue cracks in the anchor bolts. Fractographic analyses of the failed anchor bolts indicated that the anchor bolts experienced a stress range between 69 and 103 MPa (10 and 15 ksi) (Fisher et al., 1991). It was assumed that this stress range could be caused by vertical-plane oscillations of the sign structure. But there is no direct evidence to prove that the failure of anchor bolts was due to galloping.

Also, the conclusions about galloping reported in NCHRP Report 412 were based upon results of wind-tunnel tests which were performed on one-eighth scale models. Galloping was only observed for single-mastarm cantilever sign structure models. No galloping phenomenon was observed for double-mastarm cantilever sign structure models.

As stated later, it was found that typically the out-of-plane vibration of the sign structure is a lower deformation mode than the in-plane vibration for double-mastarm cantilever sign structures, box-truss sign structures, monotube sign structures, and tri-chord sign structures. Because the out-of-plane vibration has a lower frequency, it can be more easily driven to deformation by natural wind gusts. Moreover, galloping acts on the sign structure vertically and will be mainly associated with higher modes of vibration. Hence, galloping will probably not have as much contribution to critical stresses as natural wind for the types of sign structures mentioned above. Also, considering that natural wind gusts blow

on the sign structures most of the time, it is reasonable to believe that natural wind gusts make a major fatigue damage contribution in the four types of sign structures. Natural wind gusts are also considered to be the major source for wind induced fatigue damage to slender vertical structures in other research (Repetto and Solari, 2001; Chen et al. 2003).

Both vortex shedding and truck induced gusts are not considered to be particularly critical for the fatigue damage of sign structures. According to NCHRP Report 412, wind tunnel tests have indicated that significant vibrations do not occur from vortex shedding for sign structures. Truck induced gusts can develop loads of a significant magnitude, but the development of these loads is very dependent upon the distance between the truck and the underside of the sign. Also, the occurrence frequency of these gusts is much less compared with natural wind gusts.

Hence, in this research, an assumption was made that natural wind is the wind loading that most significantly contributes to fatigue damage in the double-mastarm cantilever sign structure, the box-truss sign structure, the monotube sign structure, and tri-chord sign structure. It should be noted that this assumption may not be true for single mastarm cantilever structures.

2.2.2 Wind Spectrum

Sign structures are subjected to time-varying wind pressures that result in stress cycles at critical structural details. So a wind load time history is needed to perform a dynamic finite element analysis to obtain stress time histories for fatigue evaluation. To simulate the wind load, a wind spectrum is required. A spectrum describes the relative energy distribution over a

wide range of frequencies. When the spectrum value is high at a given frequency, it means that the wind has relatively more energy at that frequency than at other frequencies. A wind spectrum proposed by Kaimal (1968) was selected for this research. The expression of the spectrum is:

$$\frac{nS(z,n)}{u_*^2} = \frac{200f}{(1+50f)^{5/3}}$$

in which z is the height above ground and n is the frequency in Hertz. The f variable is known as the Monin coordinate and is defined (Simiu and Scanlan, 1986) as:

$$f = \frac{nz}{U(z)}$$

where U(z) is the mean wind speed as a function of height above ground. The u_* variable is known as the shear velocity and can be calculated (Simiu and Scanlan, 1986) from the following equation:

$$U(z) = \frac{1}{k} u_* \ln \frac{z}{z_0}$$

in which z_0 is the roughness length, and k is approximately 0.4. The roughness length is related to the roughness characteristics of the terrain - the rougher the terrain, the higher the z_0 value. If the mean wind speed at a certain height is known, then u_* can be calculated from the above equation.

There are also other spectra that can be used, such as the widely used Davenport spectrum (Davenport, 1961) that was used in NCHRP Report 412. The advantage of the Kaimal spectrum over the Davenport spectrum is that the Kaimal spectrum reflects the dependence of the spectrum on height, giving a better approximation of the real wind situation.

2.2.3 Weibull Distribution for Wind Speed Distribution

Due to extreme computation requirements, a simulation of sign structures under wind loading for a long period of time, such as one year, is not practical. So a simulation for a representative period of time, such as 10 minutes, was performed to evaluate the fatigue damage. In order to calculate the total damage for an entire year, a wind speed distribution is needed. This is a probability distribution function that gives the relative likelihoods of each mean wind speed at a given location. From this information, an estimation of the portion of time in a year that a given mean wind speed occurs can be found. The accumulated fatigue damage can then be scaled from 10 minutes to the total time period in a year based on the blowing time for that mean wind speed in a year. The Weibull distribution was used to represent the wind speed distribution in the State of Indiana for this research. It is a two-parameter function commonly used to fit the wind speed frequency distribution. This family of curves has been shown to give a good fit to measured wind speed data (Justus et al., 1976). The Weibull distribution function is given by:

$$P(v < v_i < v + dv) = P(v > 0)(\frac{k}{c})(\frac{v_i}{c})^{k-1} \exp\left[-(\frac{v_i}{c})^k \right] dv$$

where c = the Weibull scale parameter, with units equal to the wind speed units, k = the unitless Weibull shape parameter, v = wind speed, v_i = a particular wind speed, dv = an incremental wind speed, P($v<v_i<v+dv$) = the probability that the wind speed is between v and v+dv, and P(v>0) = the probability that the wind speed exceeds zero.

The parameters k and c are important in describing the wind speed distribution. An

accurate and robust method of calculating the Weibull parameters from wind speed data is given by the maximum likelihood method as suggested by Stevens and Smulders (1979). The shape factor k and the scale factor c are estimated using the following two equations (Seguro and Lambert, 2000):

$$k = \left(\frac{\sum_{i=1}^{n} v_i^k \ln(v_i)}{\sum_{i=1}^{n} v_i^k} - \frac{\sum_{i=1}^{n} \ln(v_i)}{n}\right)^{-1}$$

$$c = \left(\frac{1}{n}\sum_{i=1}^{n} v_i^k\right)^{1/k}$$

where v_i = the wind speed at time data point i, and n = the number of nonzero wind speed data points. The constant k must be solved using an iterative procedure, after which c can be determined explicitly. It should be noted that only the nonzero wind speed data points can be used in the equations.

2.3 Background on Fatigue

Fatigue can be defined as the initiation and propagation of microscopic cracks into macroscopic cracks by the repeated application of stresses. The approach taken by modern-day specifications for the fatigue design of fabricated steel structures is based on primarily on research work conducted in Great Britain (Gurney, 1979) and in the USA (Fisher, 1970; Fisher, 1984) in the late 1960's and early 1970's. The fatigue life rules and the analytical approaches used in this research are introduced in this section. Section 2.3.1 summarizes fatigue life rules from the American Association of State Highway and Transportation Officials (AASHTO) Specification as well as the S-N curves. Section 2.3.2

describes Miner's rule and the concept of equivalent stress range. Section 2.3.3 briefly explains the rainflow counting procedure. Section 2.3.4 provides information about fatigue limits.

2.3.1 AASHTO Fatigue Life Rules and S-N Curves

The fatigue design requirements published by AASHTO (2004) are among the most-widely used standards to design highway bridges for truck induced cyclic loadings. Moreover, the fatigue design requirements in AASHTO (2001) for sign structures draw heavily from the detailed information and procedures provided for bridge structures. The fatigue life predictions used in this research are mostly based on the AASHTO Specification requirements for the fatigue strength (resistance) of structure details.

The fatigue design strength given in the AASHTO bridge design specification (2004) corresponds to an S-N curves that is two standard deviations below the mean fatigue resistance. The S-N design curves are shown in Fig. 2.1 and are plotted with stress range on the vertical axis and the number of cycles to failure on the horizontal axis for eight different detail categories. Both axes are logarithmic representations. Over a portion of the range, each detail category has a sloping straight line with a slope constant m equal to 3. Beyond a certain point, which depends on the detail category, the fatigue life line is horizontal (shown as dashed line in Fig. 2.1). The value of the stress range that identifies the horizontal portion of each curve is called constant-amplitude fatigue limit (CAFL), below which the fatigue life is infinite. The sloping portions of the S-N curves can be represented as the following:

$$N = M\Delta\sigma_r^{-m}$$

where N=number of cycles to failure, $\Delta\sigma_r$ =constant-amplitude stress range, m =3, and M is a constant that depends primarily on geometry of the structural detail. The eight detail categories and corresponding M and CAFL values are listed in Table 2.1.

The fatigue strength curves are based upon a large database of constant-amplitude-loading tests of specimens with the structural detail of interest. Design curves are obtained by shifting the fitted curve from the test data horizontally to the left by roughly two standard deviations of the scattered data to provide a fatigue strength with the desired level of safety (Fisher et al., 1998).

The details of sign structures are classified based on associations with existing details categories in the AASHTO bridge specification, the AWS D1.1 structural welding code, and testing in other research (Kaczinski et al., 1998). The AASHTO Specifications for sign structures (2001) contain nine design S-N curves labeled as Categories A through K2 in order of decreasing fatigue strength, as listed in Table 2.2.

2.3.2 Miner's Rule

Miner's rule for linear damage accumulation is an accepted means for predicting fatigue lives for variable-amplitude loading. It was first proposed by Palmgren and further developed by Miner (Bannantine et al., 1990). The procedure assumes that the damage fraction that results from any particular stress range level is a linear function of the number of cycles that take place at that stress range. The total damage from all stress range levels that

are applied to the detail is, thus, the sum of all such occurrences. Failure is then initiated when:

$$\sum \frac{n_i}{N_i} = 1$$

where n_i = number of cycles that take place at stress range level i and N_i = number of cycles that would cause failure at stress range level i. It is also important to understand that the term "failure" should be interpreted as reaching the permissible fatigue life rather than the real structure failure.

This method has two major shortcomings (Bannantine et al., 1990): it does not consider sequence effects and it is independent of the average stress in the cycle. Both of these factors are not consistent with observed behavior of metal fatigue. However, when residual stresses are high and when plasticity is restricted (which is the case for sign structures under wind loading), it is known that these factors have only a small influence (Bannantine et al., 1990). In addition, the approach gives reasonable correlation with test data and it has the considerable advantage that it is easy to use (Fisher et al., 1998). The AASHTO LRFD Bridge Design Specification (AASHTO, 2004) also advises that the Miner's rule can be used to account for cumulative damage. Hence, Miner's rule is applicable to this research.

Another method that can be used to evaluate the fatigue life of a structure is the equivalent constant amplitude stress range $\Delta\sigma_e$. Here, $\Delta\sigma_e$ is a stress range that will display the same amount of damage as actually produced by the variable amplitude stress ranges. It is written as:

$$\Delta\sigma_e = \left[\sum \gamma_i \Delta\sigma_i^3\right]^{1/3}$$

where γ_i = the percentage of cycles for a particular stress range over the total number of

cycles for all stress ranges and $\Delta\sigma_i$ = the ith constant amplitude stress range in the variable amplitude stress history. The fatigue life of the structure then can be computed from the S-N curve using $\Delta\sigma_e$. This method is commonly used to evaluate the fatigue life of a structure if the loading histogram is known, either statistically or based upon field data.

2.3.3 Rainflow Counting

Sign structures are subjected to varying wind load with time. Consequently, the stress histories of the critical details of the sign structures have variable amplitudes. In order to predict the life of a component subjected to a variable load history, it is necessary to reduce the complex history into a number of events which can be compared to the available constant amplitude test data for a given detail. Cycle counting is the process used to convert a complex load history into a number of constant amplitude events. A few of the methods that are used for counting stress ranges include the reservoir method, the rainflow method, the peak count, and the mean-crossing peak count method (Bannantine et. al., 1990). The rainflow method is commonly used in civil engineering applications and is convenient because it can be easily implemented through the use of a computer to perform the counting.

A rainflow counting method developed by Downing and Socie (1982) was used in the fatigue analysis procedure to process the stress history data of the specific structural sign details. This algorithm counts a history of peaks and valleys of stress time history in sequence which has been rearranged to begin and end with the maximum peak (or minimum valley). In the beginning of the counting process, three data points are read. Y is defined as the stress

range between the first and second data point and X is defined as the stress range between the second and third data point. The method then compares stress ranges X and Y. If X is larger than or equal to Y, a closed cycle is said to have occurred, and the peak and valley data points of Y are then eliminated before moving forward to form next group of X and Y. If X is smaller than Y, the method moves forward to read the next peak or valley data point, computes new ranges X and Y and repeats the process of comparing X and Y. Finally all the data points will be processed and all the closed stress cycles will be counted.

2.3.4 Fatigue Limits

There are three possible situations for the behavior of stress cycles in this investigation of sign structures. The first situation is that all cycles are above the CAFL. The second situation is that there are stress cycles both above and below the CAFL. The third situation is that all stress ranges are below the CAFL. For the first situation, it is clear that all of the stress cycles contribute to fatigue damage and must be considered in any fatigue life evaluation. For the third situation, it is clear that no fatigue damage will be accumulated in the structure. For the second situation, which is the case for the sign structures under wind loading in this research, a procedure is needed to determine the fatigue damage. Two such procedures investigated in this research are the straight-line S-N curve method and the VAFL method.

The variable amplitude fatigue limit (VAFL) (Moses et al, 1987) is used to distinguish the level below which damage will not occur for variable amplitude truck loading spectrums.

For highway bridges, the AASHTO LRFD Bridge Design Specification (AASHTO, 2004) stipulates that the VAFL is to be taken as one-half of the CAFL. The VAFL method continues the sloping straight line in the S-N curve down to one-half of the CAFL, and then extends horizontally. It is based on the assumption that all the stress cycles below the VAFL induce no fatigue damage, while all the stress cycles above the VAFL cause fatigue damage, which includes the impact of variable amplitude on the fatigue life. Even though the VAFL method is utilized in the AASHTO LRFD Bridge Design Specification (2004) to account for damage from truck loadings, it is also applied in this research to account for variable amplitude stress cycles experienced by sign structures.

The straight-line S-N curve assumes that the fatigue strength curve continues below the CAFL with the same constant slope of 3. It means that there is no fatigue limit existing and all stress cycles contribute to fatigue damage. It should be noted that the straight-line method will produce more conservative fatigue lives than both the CAFL method and the VAFL method.

Table 2.1 Constants for different fatigue detail categories (AASHTO, 2004).

Detail Catogory	M $(MPa)^3$	CAFL (MPa)
A	$82.0x10^{11}$	165
B	$39.3x10^{11}$	110
B’	$20.0x10^{11}$	82.7
C	$14.4x10^{11}$	69.0
C’	$14.4x10^{11}$	82.7
D	$7.21x10^{11}$	48.3
E	$3.61x10^{11}$	31.0
E’	$1.28x10^{11}$	17.9

Table 2.2 CAFL for different fatigue detail categories from sign structure design specification (AASHTO, 2001).

Detail Catogory	CAFL (MPa)
A	165
B	110
B’	83
C	69
D	48
E	31
E’	18
ET	8
K_2	7

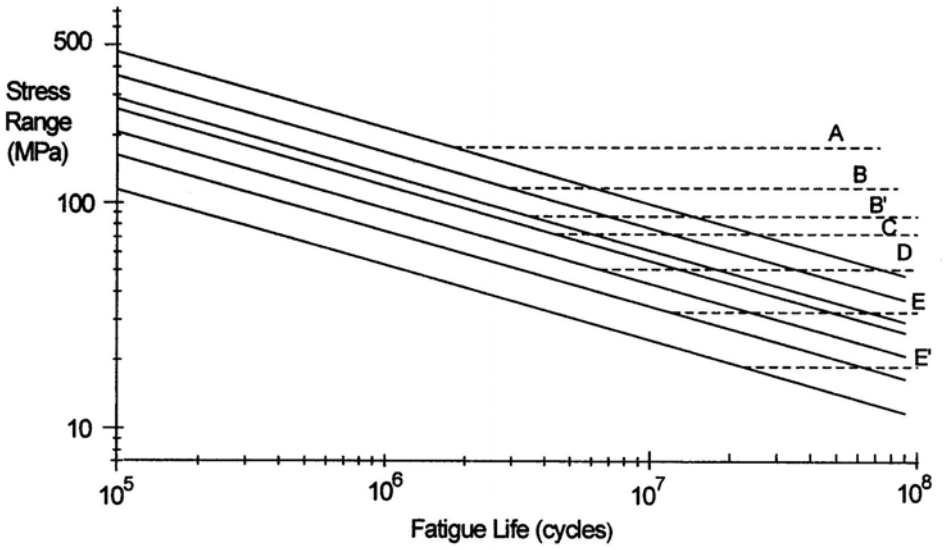

Fig. 2.1 S-N curves (Fisher et al. 1991).

CHAPTER 3

FINDINGS

Chapter 3 presents the specific findings of the research conducted to evaluate the fatigue lives of the critical details in sign structures, including double-mastarm cantilever sign structures, box-truss sign structures, monotube sign structures, tri-chord sign structures, and single-mastarm cantilever sign structures. Section 3.1 describes the finite element models of the sign structures developed based on selected prototype sign structures installed in Indiana. Section 3.2 presents wind speed distributions for six locations in Indiana, and a wind load simulation procedure developed to generate wind load time histories. Finally, a fatigue analysis procedure was used to predict the fatigue lives of sign structural details based on stress time history results from dynamic analyses performed with the generated wind load applied on the finite element models. The results are presented in Section 3.3.

3.1 Finite Element Modeling of Sign Structures

In this section, several types of sign structures, including double-mastarm cantilever sign structures, box-truss sign structures, monotube sign structures, tri-chord sign structures, and single-mastarm cantilever sign structures, are described and modeled for different connection details in ANSYS.

3.1.1 Modeling of Double-Mastarm Cantilevered Sign Structure

3.1.1.1 Prototype Sign Structure

The double-mastarm cantilever sign structure consists of a two-dimensional truss frame supported at one end by a single steel post. A typical double-mastarm cantilever sign structure is shown in Fig. 3.1. A cantilever structure IGDO-5 designed by Wascot Inc. was selected to be a prototype structure. It is located at Station 43+120 on Route I-64 East Bound in southern Indiana. The height of this structure is 9.602 m (31.5 ft), and its span is 7.620m (25 ft) with a sign panel area of 19.98 m^2. The sectional properties of the post, the chord and the strut are listed in Table 3.1.

3.1.1.2 Description of Finite Element Model

Several finite element models were developed for the prototype sign structure to investigate different structural details. They were used in the fatigue analysis procedure and the transient dynamic stress analyses discussed in Section 3.3. Finite element analyses were performed using the commercially available finite element program ANSYS (2002). The finite element models are described below.

To assist in the selection of a basic model, different ways of modeling the prototype sign structure with varying degrees of refinement were compared by examining the maximum stress at the post-to-base plate welded connection (Fig. 3.2). The decision on the appropriate model was made based on the convergence of the critical stress value and the computational

demand. The total number of elements for the basic finite element model was determined to be around 700. A schematic of the basic finite element model (Model A) used in the analyses for post-to-base plate connection detail of the IGDO-5 sign structure is shown in Fig. 3.3.

The chords and struts of the typical structure were modeled using BEAM4 elements with appropriate cross-sectional dimensions. The BEAM4 element is a uniaxial elastic line element with tension, compression, torsion, and bending capabilities, having six degrees of freedom at each node. The post was modeled using SHELL63 elements, which are elastic shells with both bending and membrane capabilities. Both in-plane and normal loads are permitted for SHELL63. The base plate was modeled using SOLID45 elements, which are three-dimensional solid elements and are defined by eight nodes having three degrees of freedom per node.

A spider bolt modeling technique was used to model the anchor rods. The main body of the bolt was modeled using a BEAM4 element. Both ends of the bolt were then connected to the nodes around the bolt hole using many very stiff BEAM4 elements to simulate the behavior of the bolt head and nut. It can transfer both tensile and bending loads and also has the benefit of simplicity. The boundary conditions of the model were that both ends of the anchor rods were constrained completely for all six degrees of freedom. The spider bolts are shown in Fig. 3.4.

A second model (Model B) with a chord to post connection detail as shown in Fig. 3.5 was also developed to investigate the chord-to-end plate socket weld connection and the vertical fillet weld in the built-up box. This model, which is shown in Fig. 3.6, focused on the portion between the chord and the post, which was not a region of focus in Model A. In this

model, the chord-to-post connection region was modeled with shell elements (Fig. 3.7). Most of the post was modeled with elastic beam elements to save computation effort. The remainder of the model, however, is similar to Model A.

Another model (Model C) of the hand hole detail (Fig. 3.8) was built to evaluate the fatigue life of the hand hole region. The only difference between Model C and Model A is the additional mesh added to simulate hand hole detail, as shown in Fig. 3.9.

3.1.2 Modeling of Single-Mastarm Cantilevered Sign Structure

3.1.2.1 Prototype Sign Structure

The single-mastarm cantilever sign structure consists of a single cantilever support post and a single cantilever arm. Both members are tapered. A typical single-mastarm cantilever sign structure is shown in Fig. 3.10. A single-mastarm cantilever structure GDO-1 designed by Maico Industries Inc. was selected to be the prototype structure. It is located on SR-19 in the Fort Wayne District in northeastern Indiana. The height of this structure is 6.4 m (21 ft), and its span is 12.2 m (40 ft) with a sign panel of 0.9 m by 1.5 m. The section dimensions of the post and the mastarm are listed in Table 3.2.

3.1.2.2 Description of Finite Element Model

An overall model was developed for the prototype single-mastarm cantilever sign structure, shown in Fig. 3.11. The mastarm, post, and base plate were modeled in the same manner as was done for Model A of the double mastarm structure described in Section 3.1.1.2.

3.1.3 Modeling of Box-Truss Sign Structure

3.1.3.1 Prototype Sign Structure

The box-truss sign structure consists of a welded three-dimensional space frame simply supported at each end by a two-post support frame. Fig. 3.12 shows a typical aluminum box-truss sign structure. A box-truss sign structure designed by Valmont Industries, Inc. was selected to be a prototype sign structure. It is located on I-65 at US-30 in Merriville, Indiana. The upright system and the truss system (including chords, diagonal struts and vertical struts) of the prototype structure were made of aluminum alloy 6061-T6 (E=69 GPa, density=2700 kg/m^3). The span of the sign structure is 28.2 m (92.5 ft) and the height is 7.9 m (25.8 ft). The areas of two sign panels are 16.9 m^2 (182 ft^2) and 19.4 m^2 (209 ft^2). The sectional dimensions of some major members are listed in Table 3.3.

3.1.3.2 Description of Finite Element Model

Two finite element models were developed for the box-truss prototype sign structure to investigate different structural details. They were intended to be used in the transient dynamic stress analyses. The details of the finite element models are described below.

A basic finite element model (Model A) for the box-truss sign structure is shown in Fig. 3.13. The entire space frame of the prototype box-truss sign structure was modeled using beam elements with appropriate cross-sectional dimensions. The posts in the end frames were modeled using shell elements. The lateral bracing members in the end frames, however, were

modeled using beam elements. The base plate was modeled using solid elements. The spider bolt modeling technique was used to model the anchor rod detail.

Another model (Model B) of the hand hole detail, as shown in Fig. 3.14, was built to specifically evaluate the fatigue life of this region. The only difference between Model B and Model A is the mesh refinement necessary to add the hand hole detail.

3.1.4 Modeling of Monotube Sign Structure

3.1.4.1 Prototype Sign Structure

A monotube sign structure consists of a horizontal chord supported by a steel post at each end. Fig. 3.15 shows a typical monotube sign structure; a similar sign structure was selected to be the prototype sign structure. The span of the prototype sign structure is 25.9 m (85 ft). The height is 7.3 m (24 ft). The areas of two sign panels are 16.9 m^2 (182 ft^2) and 19.4 m^2 (209 ft^2). The sectional dimensions of some major members are listed in Table 3.4.

3.1.4.2 Description of Finite Element Model

Two finite element models were developed for the monotube prototype sign structure to investigate different structural details. They were used in the transient dynamic stress analyses. The finite element models are described below.

A basic finite element model (Model A) for the monotube sign structure is shown in Fig. 3.16. It is developed with the same techniques used in the modeling of the double-mastarm cantilever sign structure as described in the previous section, except that the

mastarm–to-post connection was modeled to be a hinge that can rotate about the axis perpendicular to the ground -- all other degrees of freedom were constrained. Another model (Model B) with a hand hole detail, as shown in Fig. 3.17, was also built.

3.1.5 Modeling of Tri-Chord Sign Structure

3.1.5.1 Prototype Sign Structure

The tri-chord sign structure consists of a welded three-dimensional space frame simply supported at each end by a post. There are three chords in the space frame. Fig. 3.18 shows a typical tri-chord sign structure. A tri-chord sign structure located at Station 5+050 at the intersection of 96th Street and Interstate 70 in Indianapolis, IN was selected to be a prototype sign structure. The span of the sign structure is 48 m (157.5 ft) and the height is 7.53 m (24.7 ft). Two sign panels (both are 4.2 m by 1.9 m) are attached to this tri-chord sign structure. The sectional dimensions of some major members are listed in Table 3.5.

3.1.5.2 Description of Finite Element Model

Two finite element models were developed for the tri-chord prototype sign structure to investigate different structural details. They were used in the dynamic stress analyses. The finite element models are described below.

A basic finite element model (Model A) for the tri-chord sign structure is shown in Fig. 3.19. It is developed with the same techniques used in the modeling of the box-truss sign structure as described in Section 3.1.3.2. However, the end of the truss frame was modeled to

be a pin that can rotate about all three axes because the chord is only constrained by u-bolts to the posts at the end of the space frame. Another model (Model B) of the hand hole detail, as shown in Fig. 3.20, was also built based on Model A with additional elements added to simulate the hand hole detail.

3.2 Wind Speed Distribution and Wind Load Simulation

In this section, wind speed distributions at six locations in Indiana obtained via the maximum likelihood method are presented. In addition, a wind simulation procedure based on a wideband spectrum was developed and applied to generate dynamic loading for the four different prototype sign structures.

3.2.1 Wind Speed Distribution for Locations in Indiana

As presented in the previous section, a Weibull distribution was selected to describe the wind speed distribution in Indiana. However, the parameters of k and c will be different for different wind environments and need to be calculated from local wind speed data. The maximum likelihood method (Stevens and Smulders, 1979) was used to perform these calculations. Hourly wind speed data time series for the last fifteen years were obtained from the National Climatic Data Center (NCDC) for the following locations in the State of Indiana: Indianapolis (IND), Evansville (EVV), South Bend (SBN), and Fort Wayne (FWA); only five years of data were obtained for Lafayette (LAF) and Bloomington (BMG) due to limited

availability. As shown in Fig. 3.21, it is significant to note that these cities are located in the northern, central, and southern regions of the state, thus providing a wide range of geographic locations and conditions. The size of the database is large enough to evaluate k and c accurately. The hourly wind speed is recorded on the basis of a 2-minute average just prior to the observation time at the airport of that location.

The Weibull parameters k and c are listed in Table 3.6 for the six different locations in Indiana. The wind speed distribution curves for the locations in Indiana are shown in Fig. 3.22 and Fig. 3.23. Note that Indianapolis, South Bend and Fort Wayne have larger c values than Evansville and Bloomington. It can be seen in Fig. 3.22 that the main portion of the wind probability curves for Indianapolis and Fort Wayne are shifted right to relatively higher wind speeds as compared with the curve of Evansville. In Fig. 3.23, the main portion of the wind probability curves for South Bend are also shifted right to relatively higher wind speeds as compared with the curve of Bloomington. This implies that it is more likely for relatively higher wind loading to occur in Indianapolis, Fort Wayne and South Bend.

3.2.2 Wind Load Simulation

Wind loads are generated for use as input to the dynamic structural analyses, which are described in Chapter 5. In this section, a wind load simulation procedure is developed and applied for four types of sign structures.

3.2.2.1 Wind Load Simulation Procedure

A natural wind-induced force time history for a certain time span is needed to perform a dynamic finite element analysis. The analysis results will then be used to obtain a stress time history for the fatigue damage evaluation. In this section, the details for time-history simulation of the natural wind-induced forces will be described and the results presented.

A number of methods for simulating time histories for wind loading have been developed and can be generally classified into (1) fast Fourier transform (FFT) based types and (2) autoregressive moving average (ARMA) based approaches. The first method has been applied widely in engineering applications due to its simplicity and efficiency.

The FFT method has been chosen to represent wind speed fluctuation around a given mean wind. A series of discrete frequencies are chosen at specified intervals over a frequency range that includes most of the response components caused by the wind load in the sign structures. A sinusoidal variation in time is then assumed at each of these frequencies. So, at each of these frequencies, the wind velocity will have a narrow band oscillation around the mean wind speed. The wind velocity time series is expressed as a summation of these discrete frequencies (Bobillier et al., 2001):

$$V(t) = \sum_{i=1}^{N} v_i \cos(\omega_i t + \varphi_i) + V_{mean}$$

in which N = the selected number of discrete frequency components over the spectrum width for the simulation, v_i = velocity amplitude at each frequency, ω_i = circular frequency, φ_i = random phase angle, V_{mean} = the selected mean wind speed for this simulation and t = time. (In this study, t is selected to vary between 0 to 600 seconds because a time span of 10

minutes has been chosen to be a representative time length for the simulation.) In the equation above, the velocity amplitude is defined as:

$$v_i = \sqrt{2S(\omega_i)(\Delta\omega_i)}$$

in which $S(\omega_i)$ = wind spectral energy density provided by the Kaimal spectrum and $\Delta\omega_i$ = circular frequency interval. In this research, an interval $\Delta\omega_i = \pi/300$ rad/sec was chosen. For a prototype double cantilever sign structure and a prototype monotube sign structure, frequencies up to 2 Hz need to be considered to include most of the contributions of different natural modes. In addition, frequencies up to 3 Hz and frequencies up to 5 Hz should be considered respectively for a tri-chord sign structure and a box-truss sign structure. (As seen in Chapter 5, these frequencies are large enough to include the first three modes of each prototype structure.) A time increment step was chosen to be 0.25 seconds so that two samples per second will be achieved in the wind speed simulation, which is the minimal sampling rate to capture wind speed components at a frequency of 2Hz. Since the simulation time length is 600 seconds, the discrete frequency interval was chosen to be 1/600 Hz ($\pi/300$ rad/sec for circular frequency interval).

The wind speed time history can then be converted into a wind force time history. The time-varying wind force applied to the sign is given by the formula:

$$F_{wind}(t) = \frac{\rho}{2} V(t)^2 A_{sign} C_D$$

where ρ= density of air (1.25kg/m^3), C_D = drag coefficient (= 1.1) for a sign panel, and A_{sign} = area of the sign panel of the prototype sign structure.

The wind speed can fluctuate over a broad range. However, a wind speed maximum can be selected above which the probability of occurrence is negligible, i.e. smaller than

0.0001. This defines the relevant wind speed range. The wind speed range in the State of Indiana is assumed to vary from 0 m/s to 30 m/s. This range was divided into 15 subranges with an interval of 2 m/s. A wind speed time history was simulated for each of the subranges and then converted into a wind force time history with the equation formulated above. The mean wind speed of each simulated wind speed time history was selected to be the median value of that subrange. This process was repeated to generate the time-varying wind forces developed on the different components of the sign structures.

The wind loading can vary significantly over the surface of the entire sign structure. But it is impractical to simulate a wind loading for each small area. An approximate method is to choose a representative location with a relative large area on which to generate a wind force. If wind load pressure is assumed to be constant over an area, the wind load is considered to be correlated and a single concentrated load can be applied to that area to simulate the load effect. If wind load pressure is assumed to be non-constant over an area, the wind load is considered to be uncorrelated and multiple concentrated loads can be applied to different portions of that area to simulate the load effect.

It should be noted that it is assumed in this research that the wind blows in a direction perpendicular to the plane of the sign structure. This assumption will simplify the simulation procedure and makes the wind loading more critical than the situation in the field. In a related research, Foley et al. (2004) took a different approach by including the direction of natural wind and treating it as a random variable independent of natural wind speed.

3.2.2.2 Application of Wind Load Simulation

(1) Double-mastarm cantilever sign structure.

For each double-mastarm cantilever sign structure, wind-induced forces were produced for three locations on the prototype sign structure: one is generated for the sign panel (the height of the center of the sign panel is assumed to be representative); the other two are generated at different heights on the post (z=2.5m, 6.9m), with each of them assumed to be a correlated load over the bottom or the top portion of the post.

Three typical simulated wind induced force time-histories for the sign panel at wind speeds of V_{mean}= 5m/s, 11m/s, and 15m/s at the center of the sign panel are shown in Fig. 3.24, Fig. 3.25 and Fig. 3.26 respectively. As expected, the magnitudes of the peak load and the mean load were significantly increased with the rise of mean wind speed. The wind forces developed via the simulation were later applied in the transient dynamic finite element analysis discussed in Chapter 5.

(2) Box-Truss Sign Structure.

The following natural wind loads were generated to be used in the dynamic analysis of the box-truss model: load on the sign panels, load on the posts and load on the chords. The loads on the different sign panels are uncorrelated. Also, the loads on the top and the bottom chords are uncorrelated. Each post was loaded with two uncorrelated loads: one on the top half and another on the bottom half. It should be noted that under strong wind conditions, the loads can be correlated over a large area of adjacent structure components, such as two sign

panels. However, this is not a frequent situation and was not considered in this research.

According to the modal analysis results to be shown in Section 3.3.2.1, the second and third modes of the box-truss model are above 2 Hz. In order to excite the modes up to 5 Hz, the time length of each load step in the wind generation procedure described in a previous section was reduced from 0.25 seconds to 0.1 seconds. The time span of the simulated wind load events was changed from 10 minutes to 5 minutes to reduce the computation time of dynamic analyses. All the wind loads for the box-truss sign structure were generated using the procedure modified with the changes above.

(3) Monotube Sign Structure.

Three types of natural wind loads were generated to be used in the dynamic analysis of the monotube sign structure: load on the sign panels, load on the posts and load on the mastarms.

If a natural wind load is applied at the center of a sign panel, the twisting mode (second mode, f = 1.384 as per Section 3.3.4.1) of the monotube sign structure can not be excited. Therefore, the wind load simulation procedure was modified in order to generate four loads with 99% correlation to be applied on a sign panel to excite the second mode. In the simulation, a random phase angle array was produced and used to simulate one load. Then one phase angle in every one hundred phase angles in that array was changed to obtain a new phase angle array for use in simulation of another wind load on that sign panel. By repeating this procedure, four wind loads with 99% correlation were produced for a time span of 10 minutes and applied on each sign panel.

The loads on the mastarm segments are also uncorrelated. Moreover, each support

post was loaded with two uncorrelated loads: one on the top half and another on the bottom half.

(4) Tri-chord Sign Structure.

Four types of natural wind loads were generated with the wind load simulation procedure to be used in the dynamic analysis of the tri-chord sign structure: load on the sign panels, load on the chords, load on the truss members and load on the posts.

Each sign panel was loaded with a concentrated load. Each segment of the space frame is loaded with three concentrated loads: two on the top and the bottom chords, and one on the truss members. Each support post was loaded with two uncorrelated loads: one on the top half and another on the bottom half. The time span of these loads is 10 minutes.

3.3 Fatigue Analysis and Sign Structure Life Expectancies

This section describes the analytical procedures used in the fatigue strength investigation and also presents the results of the fatigue analyses. Transient dynamic analyses were performed with the finite element models introduced in Section 3.1 to obtain the stress time-histories at structural details of interest. The fatigue lives of those structural details were then calculated according the stress time-histories with the fatigue analytical procedure described heretofore, and the results are presented and discussed.

3.3.1 Analytical Procedure

A fatigue analysis procedure performed to obtain estimated fatigue lives for certain details of sign structures is described in this section. It can be divided into the following steps:

(1) First, the stress distributions along the member adjacent to the local detail of interest were investigated in a static analysis with one of the finite element models described in Chapter 3. A location on the member where the stress was not affected by the local detail was selected to be a reference point, and a reference stress was obtained at that point. A nominal static stress at the local detail was then calculated based on the slope of the stress distribution curve away from the local detail. Then a stress raiser of the nominal stress over the reference stress was obtained as a ratio of these two values. For the members or structural components that were assumed to have a uniform stress distribution along the member or element length, e.g. the anchor rods, a stress raiser of 1.0 was used.

(2) The stress histories (Histories SA) at the reference location identified in Step (1) were obtained from transient dynamic analyses for different mean wind speeds (from 1m/s to 29 m/s in intervals of 2m/s).

(3) Nominal stress histories (Histories SB) at the local detail were obtained from Histories SA by multiplying the stress histories by the stress raiser.

(4) The rainflow counting method was used to convert each of the nominal stress histories (Histories SB) into a number of constant amplitude events (constant stress ranges

from 1 MPa to 468 MPa at an interval of 1 MPa).

(5) The portion of time in one-year for a given mean wind speed was calculated from the mean wind speed distribution. Based on this time quantity, the cycles of constant amplitude stress ranges for each mean wind speed from the cycle counting were then scaled from a representative 10-minute event up to the portion of time in a year for that mean wind speed.

(6) All the cycles at the same stress range were summed over all mean wind speeds to obtain the yearly total number of cycles for a certain stress range. This process was repeated for all of the stress ranges (1 MPa to 468 MPa) to obtain the stress histogram for a one-year period.

(7) For each stress range, the number of cycles to cause failure at that stress range (the life cycle number) was found from the appropriate S-N curve.

(8) Miner's rule was then applied. The damage for each stress range was calculated by dividing the yearly number of cycles of a particular stress range by the fatigue life cycle number of the given stress amplitude. The damage was then summed over all the stress ranges to obtain the total accumulated fatigue damage for a one-year period.

(9) The life expectancy (in years) of the specific detail was obtained by dividing 1 over the damage accumulated in one year.

This standard fatigue analysis procedure was utilized to evaluate the cyclic behavior of all sign structure details considered in this study.

3.3.2 Fatigue Analysis Results for Double-Mastarm Cantilevered Sign Structure

This section summarizes the results of dynamic finite element analyses and the calculations performed to estimate the fatigue lives of several different structural details susceptible to fatigue damage in the double-mastarm cantilever sign structures.

3.3.2.1 Modal Analysis

Modal analysis was performed for the prototype sign structure to obtain the basic deformation modes. Usually, the first mode contributes significantly to the structural deformation and the critical stresses, while the higher modes often have less influence.

Three significant modes were obtained from the modal analysis. The first mode is an out-of-plane vibration with a frequency of 0.592 Hz, as shown in Fig. 3.27. The second mode is an in-plane vibration with a frequency of 1.524 Hz, as shown in Fig. 3.28. The third mode is a twisting of the upper portion of the sign structure with a frequency of 3.282 Hz, as shown in Fig. 3.29.

3.3.2.2 Fatigue Analyses and Life Results for Connection Details

The stress time-histories for the connection details of the double-mastarm cantilever sign structure were obtained from transient dynamic analyses with the finite element models of this structure. Fatigue analyses were then performed to estimate the fatigue lives of seven important structural details of the double-mastarm cantilever sign structures. The results are presented below.

(1) Post-to-base plate socket weld connection.

The post-to-base plate socket weld connection (Fig. 3.2) is considered to be one of the most critical details susceptible to fatigue damage under wind load. Analyses were performed using Model A to obtain the stress history at this detail. The life expectancy was then calculated using the fatigue analysis procedure described in Section 3.3.1. This base plate detail has an E' fatigue stress category, with a corresponding constant-amplitude fatigue threshold of 18 MPa (2.6 ksi).

The loadings were generated by wind speed simulations for each of 15 different mean wind speeds at five different regions of the sign structure (one at the center of the sign panel, two on the top and the bottom chord, and two on the top and the bottom portion of the post). The wind pressure was applied uniformly over the entire sign panel. The post was divided into two areas and one wind force was generated for each area. A damping ratio ζ of 1% was used for the analysis.

The most critical stress at the post-to-base plate socket weld occurred at the node in the weld circle 90 degrees from the sign structure plane, primarily due to the significant bending moment at the base produced by the wind load. Following the fatigue analysis procedure, the stress time history of a node 90 degrees from the sign structure plane at a height of 1.12 m from the base plate was selected to be the reference stress time history. This stress time history was multiplied by 1.156 to obtain the nominal time history for the socket weld. The ratio of 1.156 was obtained by projecting the stress at the base plate weld with the method described in the fatigue analysis procedure. A typical reference stress history plot for

a mean wind speed of 5m/s is shown in Fig. 3.30. The maximum stress range for this mean wind speed is around 12 MPa, with about 350 total cycles of variable amplitude during this 600 second time span. This is consistent with the fact that the first mode (0.592 Hz) was dominant in the structural response.

The nominal stress history was processed using the steps in the fatigue analysis procedure defined in Section 3.3.1 to obtain the life expectancy for six different locations in Indiana. The stress range histogram for a one-year period is plotted in Fig. 3.31. It clearly shows that most of the cycles are in the low stress range regime. Fig. 3.32 depicts the percentage of fatigue damage caused by each of the stress range bins (a VAFL at one half of the CAFL was assumed). As shown in Fig. 3.32, most of the fatigue damage was caused by the medium stress ranges and some high stress ranges. The actual cycle numbers at the high stress ranges are small, but significant damage was induced due to the relatively high stress range value.

Based on the predicted stress range values, the predicted cyclic life results for VAFL are listed in Table 3.7. Fort Wayne, Indianapolis and South Bend were expected to be more critical to fatigue than the other sites according to the Weibull parameter results in Chapter 3. This assumption can be verified by the life expectancy results in Table 3.7, which show that the post-to-base plate socket weld connection detail has a relatively shorter fatigue life in Fort Wayne, Indianapolis and South Bend than at the other sites.

In addition, the fatigue lives of the post-to-base plate socket weld connection were calculated with a straight-line S-N method. These life expectancy results are also presented in Table 3.7. Moreover, as shown in Table 3.7, the percentage differences between fatigue lives

calculated with a straight-line S-N method and fatigue lives calculated with a VAFL vary between 13% and 20% when the life expectancies are less than 50 years. When the life expectancies are larger than 50 years, the percentage differences of fatigue lives are considerably greater. The variations in fatigue lives reflect the impact of fatigue damage caused by the stress cycles below the VAFL. In general, the longer the fatigue life, the higher the percentage of stress cycles in the low stress range.

Lastly, Table 3.7 also shows the percentage of the stress range loadings that exceed the CAFL. It was demonstrated by Moses et al. (1987) that if the stress range exceeds the CAFL more than 1 in 10,000 (0.01%) times, fatigue damage will occur. A strong correlation between high levels of exceedance and lower fatigue lives can be observed.

(2) Hand hole.

The hand hole detail (Fig. 3.33) is also considered to be a critical detail susceptible to fatigue damage under wind load. Fatigue cracks have been observed in a number of sign structures at the hand hole detail (Dexter, 2002). Analyses were performed using Model C to obtain the stress history at the hand hole. The hand hole detail is classified as a category E detail, which has a constant-amplitude fatigue threshold of 31 MPa (4.6 ksi).

The model was loaded in the same way described in the previous section. The damping ratio ζ was also assumed to be equal to 1%. Based on the static stress distribution analysis, the stress time history of a reference node oriented 90 degrees from the sign structure plane at a height of 0.67 m from the base plate was selected to be the reference stress time history. This was multiplied by 1.05, which is the stress raiser computed following

the method described in Section 3.3.1, to obtain the nominal stress time history for this detail. The life expectancies were calculated for six different locations in Indiana using the fatigue analysis procedure defined in Section 3.3.1. The stress range histogram for a time span of one year is shown in Fig. 3.34. Again, most of the cycles were in low stress range.

The life expectancy results for VAFL are listed in Table 3.7. It clearly can be seen that the post-to-base plate connection has a shorter life than the hand hole detail and is more susceptible to fatigue damage for a given wind environment. Again, the fatigue life of the hand hole detail is relatively shorter in Fort Wayne, Indianapolis and South Bend than other locations in Indiana. The fatigue lives of the hand hole detail were also calculated with a straight-line method. These fatigue life results are also presented in Table 3.7. When the life expectancies are larger, the percentage differences of fatigue lives tend to be greater. A similar conclusion can be made for this detail as for the base-plate weld detail: the percentage of stress cycles in low stress range is higher for the longer fatigue lives. Finally, Table 3.7 also shows the percentage of the stress range loadings that exceed the CAFL for hand hole. Similarly, it can be observed that the higher the level of exceedance, the lower the fatigue lives will be.

(3) Chord-to-end plate socket weld connection.

The chord-to-end plate socket weld connection (Fig. 3.35) is also sensitive to fatigue damage. Analyses were performed using Model B to obtain the stress history at this detail. The chord-to-end plate detail is classified as a fatigue stress category of E’ with a constant-amplitude fatigue threshold of 18 MPa (2.6 ksi).

The model was loaded in the same way described in the section for the post-to-base-plate weld connection. As before, a 1% damping ratio was used for the dynamic analysis. According to the static stress distribution analysis, the time history of a node located 90 degrees from the sign structure plane and 0.386 m above the top surface of the base plate in the chord was selected to be the reference time history and multiplied by the stress raiser 1.114 to obtain the nominal time history for this detail. The factor of 1.114 was calculated by projecting the stress along the post to the base plate weld. The life expectancies were calculated for six different locations in Indiana based on VAFL and the results are listed in Table 3.7. The stress range histogram for a time span of one year is shown in Fig. 3.36. This histogram is very similar to the histogram of the hand hole. However, it produced a much shorter life due to the lower fatigue resistance associated with an E' category. The post-to-end plate detail has a longer fatigue life than the post-to-base plate socket weld detail, but a shorter life than the hand hole detail. The fatigue life of the chord-to-end plate socket weld connection detail also shows the same sensitivity to geographic location as the previous details, being relatively shorter in Fort Wayne, Indianapolis and South Bend than other locations in Indiana.

The fatigue lives of the chord-to-end plate socket weld connection were also calculated with a straight-line S-N curve method. These fatigue life results are also presented in Table 3.7, along with the percentage of the stress range loadings that exceed the CAFL for the chord-to-end plate socket weld connection. Similar conclusions can be made about the relations between the life expectancies, the fatigue lives, and the levels of exceedance as were found for the socket weld and the hand hole.

(4) Vertical fillet weld in the built-up box.

The vertical fillet weld in the built-up box (Fig. 3.37) was checked at three different locations. The stress in the side-plate at the intersection with the post was checked with Category ET (CAFL = 8 MPa); the stress in the post wall (the punching shear stress) was checked with Category K2 (CAFL = 7 MPa); and the stress at the fillet weld where the side-plate intersects the flange plate was inspected with Category E' (CAFL = 18 MPa). According to the fatigue life calculation at the three locations, the fatigue lives based on the stress at the side-plate to flange-plate intersection were shorter than the fatigue lives based on the stress in the post wall and the stress in the side-plate. So the fatigue life of the built-up box should be dictated by the stress at the side-plate-to-flange-plate intersection. The calculated fatigue lives of this detail are listed in Table 3.7. It can be observed that the fatigue lives for the built-up box were found to be less than those computed for the chord-to-end plate connection and the hand hole.

The fatigue lives of the vertical fillet weld in the built-up box were also calculated with a straight-line S-N curve method. Table 3.7 shows the fatigue life results and the percentage of the stress range loadings that exceed the CAFL for the chord-to-end plate socket weld connection. The same observations as described for the hand hole detail were found between the life expectancies, the fatigue lives, and the levels of exceedance.

(5) Anchor rods.

The anchor rods are a Category D detail (CAFL is 48 MPa). The lives of this detail

were found to be longer than 1000 years following the fatigue analysis procedure when using the VAFL. Such fatigue lives are considered to be infinite.

(6) Strut to gusset plate weld connection.

The strut to gusset plate weld connection (See Fig. 3.38) is a Category E' detail (CAFL is 18 MPa). The lives of this detail were also found to be infinite.

(7) Gusset plate to chord weld connection.

The gusset plate to chord weld connection (See Fig. 3.38) has a CAFL of 30 MPa. The lives of this detail were also infinite.

3.3.2.3 Sensitivity of Fatigue Lives to Load Simulation

A number of factors can cause variations in fatigue strength of a sign structure. For example, variations in fatigue life for a given fixed loading can occur as a result of material and fabrication effects. Moreover, variations in cyclic response can also be the result of variations in loading for a given detail geometry.

Material and fabrication factors are inherent in the fatigue design SN curves. The fatigue design curves in the AASHTO LRFD Bridge Specification (2004) are based on fatigue data from a number of different fatigue testing programs. According to a summary report representing most of the available fatigue test data for various details (Keating and Fisher, 1985), the COV of cyclic fatigue lives from the testing for category E' details was 13.2% as shown in Table 3.8. The COV information for other detail categories is also shown

in Table. 3.8.

Variations in load effects will also occur. All the fatigue lives obtained for the sign structures are based on one set of simulated natural wind loads. To evaluate the sensitivity of the simulation procedure, additional analyses were conducted to determine the variation in the fatigue lives with respect to different sets of simulated loads. If the sensitivity is high, then a large number of repeated dynamic analyses with different simulated loads may be needed to obtain statistically reliable fatigue lives.

In this investigation, twenty-nine additional simulations (labeled simulation 1 to simulation 29) were performed to produce natural wind loads. The cyclic fatigue lives for the post-to-base plate socket weld detail, which is a category E' detail with a CAFL of 18 MPa, were obtained for these new loads with the VAFL method and the results are listed together with the original simulation (simulation 0) in Table 3.9. Statistical parameters, such as the mean and coefficient of variation (COV), were calculated for the cyclic fatigue lives. It was found that the COVs ranged from 11.88% to 16.50% for different sites as shown in Table 3.9.

The COV of the cyclic lives computed for sign structures is due to the variation in random wind loading, and it does not include variations caused by material and fabrication effects. Based on the information in Table 3.9, it appears that the variation due to loading is comparable to the variation due to material and fabrication effects noted in Table 3.8.

This research only addresses the variation of cyclic lives due to loading. In reality, both the loading and the material affect the cyclic lives. Many other factors can also impact the cyclic life: for example, the damage arising from transportation of the structures, collisions with vehicles, and corrosion, to name a few. The study on variation of cyclic lives

due to combined effects of material, loading, and other factors is beyond the scope of this research.

3.3.3 Fatigue Analysis Results for Box-Truss Sign Structure

This section introduces information about a prototype box-truss sign structure and its finite element model. The results of dynamic analyses are then presented. Finally conclusions are made according to the results of the dynamic analyses.

3.3.3.1 Modal Analysis

Modal analysis was performed for the box-truss prototype sign structure model, and the first three modes were obtained. The first mode (shown in Fig. 3.39) is a lateral vibration of the whole structure with a frequency of 1.84 Hz. The second mode (shown in Fig. 3.40) is an out-of-plane vibration with a frequency of 3.72 Hz. As shown in Fig. 3.41, the third mode is an in-plane vibration with a frequency of 4.48 Hz.

To check the modal analysis results, a simple model of the box-truss was built with only beam elements (shown in Fig. 3.42). Fixed joints were assumed at the base connection of the structure. The first three modes were obtained for comparison. The first mode is the lateral vibration of the whole structure with a frequency of 2.13 Hz. The second mode is an out-of-plane vibration with a frequency of 4.24 Hz. The third mode is an in-plane vibration with a frequency of 4.97 Hz. The simple modal analysis results are close enough to that of the original model to verify the previous modal analysis results. The reason for slight increase in

frequencies is that the posts were modeled with beam elements rather than shell elements, so the stiffness of the structural system was increased.

3.3.3.2 Fatigue Analyses and Life Results for Connection Details

The dynamic finite element analyses and the fatigue analyses were performed to estimate the life expectancies of several structural details of the box-truss prototype sign structures. The results are presented below.

(1) Post-to-socket weld connection.

This detail is shown in Fig. 3.43. The transient dynamic analyses of Model A were performed to obtain the stress time histories at the post-to-socket weld connection (aluminum E' detail, CAFL= 7 MPa). A reference node was selected to be a node at a 90^0 angle from the sign plane and 1.32 m above the base plate. Following the steps in the fatigue analysis procedure, the reference stress time history was multiplied by 1.19 to obtain the nominal stress time history. The factor of 1.19 was calculated from the projection of stress along the post to the post-to-socket weld location. The stress data was then analyzed following the fatigue analysis procedure described to obtain the life expectancies for this detail. Fig. 3.44 is the histogram of one year for this detail at Indianapolis (IND). The lives of this detail were found to be infinite.

(2) Anchor rod.

A typical anchor rod detail is shown in Fig. 3.43. Four anchor rods with a 38 mm (1.5

in) diameter are used to attach the base plate to the foundation. The transient dynamic analyses of Model A were performed to obtain the stress time histories at the anchor rod detail (steel D detail, CAFL=48 MPa). A histogram (Fig. 3.45) of one year for this detail at IND was obtained following the fatigue analysis procedure. The fatigue lives of the anchor rod detail were found to be infinite when using VAFL.

(3) Hand hole.

A typical hand hole detail is shown in Fig. 3.46. Transient dynamic analyses of Model B were performed to obtain the stress time histories at the hand hole weld connection (aluminum D detail, CAFL=17 MPa). A reference node was selected to be a node at a 90^0 angle from the sign plane and 1.34 m above the base plate. This position corresponds to a location that is 0.8 m above the hand hole weld toe. The stress cycle histogram of one year for this detail at IND is shown in Fig. 3.47. The fatigue lives of the hand hole were found to be infinite for VAFL.

(4) U-bolt in chord-to-post connection.

A common U-bolt detail is shown in Fig. 3.48. The U-bolt is used to secure and hold the truss members to the vertical post. A typical diameter of the U-bolt is 19.1 mm (3/4 in). The transient dynamic analyses of Model A were performed to obtain the stress time histories at the post-to-socket weld connection. The U-bolt was modeled with elastic beam elements to obtain the axial stresses in bolts. For the fatigue resistance, a category D behavior for steel was used, along with a VAFL limit of 24 MPa. Based upon the fatigue analysis procedure, the

fatigue lives of the U-bolt in the chord-to-post connection were predicted to be infinite when using the VAFL method.

(5) Chord-to-transverse-plate weld connection.

A typical chord-to-transverse plate connection detail is shown in Fig. 3.49. A fillet weld is used to attach the chord members to an end plate, and the end plates are then bolted together with six high-strength bolts. The transient dynamic analyses of Model A were performed to obtain the stress time histories at the chord-to-transverse-plate weld connection. The critical detail for this connection is assumed to be chord to end plate fillet weld rather than the high-strength bolts. The welded connection is a category E' (aluminum) detail, with a CAFL = 7 MPa. The fatigue lives were calculated with the VAFL method to be 123 years for IND, 728 years for EVV, 153 years for LAF, 153 for SBN, 1910 for BLM and 71 years for FWA. These fatigue lives all exceed 50 years, so no fatigue problem is expected during the service life of the structure.

(6) Diagonal-truss-to-chord weld connection.

A diagonal truss-to-chord connection detail is shown in Fig. 3.50. There are two types of weld connections at the joint: a tube-to-tube fillet welded connection and a slotted tube-to-gusset fillet welded connection. A static finite element analysis was performed with the box-truss model to determine the most critical element in the truss joint. It was found that the most critical location in the truss members was a fillet welded diagonal-truss-to-chord weld connection (aluminum ET detail, CAFL is 3 MPa) at the end of the box-truss space

frame. The transient dynamic analyses of Model A were performed to obtain the stress time histories at this detail. The stress data were then analyzed following the fatigue analysis procedure. The fatigue lives of the diagonal-truss-to-chord weld connection were found to be infinite for VAFL.

It should be noted that fatigue cracking at fillet welded diagonal-truss-to-chord connections has been reported in other states. Based upon the analysis, it appears that such cracking may be due to factors other than typical fatigue resistance. Poor handling or poor weld quality during fabrication may explain the cracking observed.

(7) Horizontal-brace-to-post weld connection.

This detail is shown in Fig. 3.51. Based on a static analysis, it was decided that the most critical location in the horizontal lateral braces between the posts was a horizontal-brace-to-post connection (aluminum ET detail, CAFL is 3 MPa) at the bottom of the post. Following the fatigue analysis procedure, the fatigue lives of the horizontal-brace-to-post weld connection were calculated to be infinite for VAFL.

(8) Diagonal-brace-to-post connection.

A typical diagonal brace-to-post connection detail is shown in Fig. 3.51. According to a static analysis, the most critical location in the diagonal lateral braces between the posts was a diagonal-brace-to-post weld connection (aluminum ET detail, CAFL is 3 MPa) at the top of the post. It is reasonable because there is more deformation at the top of the post than at the bottom of the post when the sign structure is under natural wind load. A similar analysis

procedure as the previous detail was then applied. The fatigue lives of the diagonal-brace-to-post weld connection were found to be infinite for VAFL.

3.3.4 Fatigue Analysis Results for Monotube Sign Structure

This section describes dynamic analyses of a prototype monotube sign structure. It is a steel structure. The results of dynamic analyses are presented. Conclusions are then made according to the results of the dynamic analyses and the fatigue analyses.

3.3.4.1 Modal Analysis

The first three modes for the monotube prototype sign structure model were obtained by modal analysis. The first mode is an out-of-plane vibration of the structure with a frequency of 1.19 Hz (as per Fig. 3.52). The second mode is the twisting of the mastarm with a frequency of 1.384 Hz (as per Fig. 3.53). The third mode is an in-plane vibration with a frequency of 1.507 Hz (as per Fig. 3.54).

3.3.4.2 Fatigue Analyses and Life Results for Connection Details

The life expectancies of several structural details of the monotube prototype sign structures were estimated with the fatigue analysis procedure, and the results are presented below.

(1) Post-to-socket weld connection.

A post-to-base plate connection detail is shown in Fig. 3.55. An aluminum post is fillet welded to a cast aluminum base plate socket. The transient dynamic analyses of Model A were performed to obtain the stress time histories at the post-to-socket weld connection. The weld detail is classified for fatigue as category E' with a corresponding CAFL of 18 MPa. The fatigue lives of this detail were found to be infinite under natural wind loading – the shortest life among all sites is 820 years for IND. The histogram of this detail at IND is shown in Fig. 3.56.

(2) Anchor rod.

A common anchor rod detail is shown in Fig. 3.57. The diameter of the anchor rods is 44.5 mm (1.75 in). The transient dynamic analyses of Model A were performed to obtain the stress time histories at the anchor rod detail. It is a category D detail with a CAFL of 48 MPa. A histogram (Fig. 3.58) of one year for this detail at IND was obtained following the fatigue analysis procedure. The fatigue lives of the anchor rod detail were calculated to be infinite for VAFL.

(3) Hand hole.

This detail is shown in Fig. 3.59. The transient dynamic analyses of Model B were performed to obtain the stress time histories at the hand hole weld connection. It is a category D detail with a CAFL of 48 MPa. The stress cycle histogram of one year for this detail at IND

is shown in Fig. 3.60. The fatigue lives of the hand hole were predicted to be infinite for VAFL.

(4) Mastarm-to-transverse-plate weld connection at middle span.

This detail is shown in Fig. 3.61. The transient dynamic analyses of Model A were performed to obtain the stress time histories at the mastarm-to-transverse-plate weld connection. It is a category E' detail with a corresponding CAFL of 18 MPa. The histogram for this detail at IND is shown in Fig. 3.62. This connection was also found to have an infinite fatigue life under VAFL.

(5) Monotube-to-post pin connection.

A typical monotube-to-post pin connection detail is shown in Fig. 3.63. The pin connection under shear at the end of the monotube sign structure was evaluated using the dynamic analysis. Both the fillet weld under shear and the base material under shear are classified to be Category E by AASHTO LRFD Bridge Design Specification(2004). The areas to carry the wind-induced shear were calculated for different locations. The effective shear area for the monotube to end plate fillet weld connection was 0.00416 m^2. The shear area for the base material of the monotube was 0.00419 m^2. The effective shear area for the shear tab to post fillet weld connection was 0.00218 m^2. Therefore, the shear tab to post fillet weld detail is the most critical detail among these several details because its shear area is the smallest. The fatigue lives of this weld detail were found to be infinite under natural wind loading. The histogram of this detail at IND is shown in Fig. 3.64.

3.3.5 Fatigue Analysis Results for Tri-Chord Sign Structure

This section includes the following contents: description of a prototype tri-chord sign structure and its finite element model, the results of dynamic analyses, and conclusions about fatigue damage evaluation of the tri-chord prototype sign structure.

3.3.5.1 Modal Analysis

Modal analysis was performed for the tri-chord sign structure model and the first three modes were obtained. The first mode is an out-of-plane vibration with a frequency of 1.209 Hz (Fig. 3.65). The second mode is an in-plane vibration with a frequency of 1.92 Hz (Fig. 3.66). The third mode is the lateral vibration of the whole structure with a frequency of 2.747 Hz (Fig. 3.67).

3.3.5.2 Fatigue Analyses and Life Results for Connection Details

The wind-induced fatigue damage on four different connection details of the tri-chord prototype sign structures is evaluated. The connection details are introduced and fatigue lives are calculated.

(1) Post-to-base-plate weld connection.

This detail is shown in Fig. 3.68. The transient dynamic analyses of Model A were

performed to obtain the stress time histories at the post-to-socket weld connection (E' detail, VAFL = 9 MPa). Fatigue analysis procedure was performed to obtain the fatigue life of the base weld. The fatigue lives of the base weld were calculated to be 574 years for IND, 433 years for Fort Wayne, 622 years for South Bend, 764 years for Lafayette, and longer than 1000 years for Bloomington and Evansville. So all the lives are longer than the design life of the sign structure, which is 50 years according to Table 3.3 in the AASHTTO sign structure design specification (2001). The histogram is shown in Fig. 3.69 for IND.

(2) Anchor rod.

An anchor rod detail is shown in Fig. 3.70. The diameter of the anchor rods is 38 mm (1.5 in). An eight anchor rod pattern was used. The transient dynamic analyses of Model A were performed to obtain the stress time histories at the anchor rod detail (D detail, VAFL = 24 MPa). A histogram (Fig. 3.71) of one year for this detail at IND was obtained following the fatigue analysis procedure. The fatigue lives of the anchor rod detail were calculated to be infinite for VAFL.

(3) Hand hole.

This detail is shown in Fig. 3.72. The transient dynamic analyses of Model B were performed to obtain the stress time histories at the hand hole weld connection (D detail, VAFL = 24 MPa). A reference node was selected to be a node at 90^0 face from the sign plane and 1.1 m above the base plate. The stress cycle histogram of one year for this detail at IND is shown in Fig. 3.73. The fatigue lives of the hand hole were predicted to be infinite for

VAFL.

(4) Chord-to-transverse-plate weld connection at middle span.

A typical chord-to-transverse plate connection detail is shown in Fig. 3.74. The transient dynamic analyses of Model A were performed to obtain the stress time histories at the chord-to-transverse-plate weld connection (E' detail, VAFL = 9 MPa). The stress data were then analyzed following the fatigue analysis procedure. The histogram for this detail at IND is shown in Fig. 3.75. The fatigue lives of the chord-to-transverse-plate weld connection were found to be infinite for VAFL.

3.3.6 Fatigue Analysis Results for Single-Mastarm Cantilever Sign Structure

This section discusses the research performed on single-mastarm cantilever sign structures. Finite element models developed for prototype single-mastarm cantilever sign structures are described and modal analyses are presented. Finally conclusions are made based on the results of the modal analyses.

3.3.6.1 Modal Analysis

This section summarizes the results of modal analyses for the single-mastarm cantilever sign structures. The first two deformation modes were obtained. The first mode is an in-plane vibration with a frequency of 0.1656 Hz, as shown in Fig. 3.76. The second mode

is an out-of-plane vibration with a frequency of 0.422 Hz, as shown in Fig. 3.77.

Modal analyses were also performed for two additional, similar single-mastarm cantilever sign structures with different arm lengths (9 m and 6 m). It was found that an in-plane vibration is always the first mode (0.259 Hz and 0.359 Hz). Consequently, it can be concluded that the in-plane vibration should make the most significant contribution to fatigue damage for the single-mastarm cantilever sign structures commonly used in Indiana.

The in-plane vibration of the single-mastarm cantilever sign structure is primarily excited by in-plane forcing consistent with galloping. So the assumption of natural wind gusts making the most contribution to the critical stress in sign structures is not valid for the single-mastarm cantilever sign structures. The analytical procedure described previously for the double-mastarm cantilever sign structure is not applicable to the analysis of the single-mastarm cantilever sign structure. If a fatigue analysis needs to be performed for the single-mastarm cantilever sign structure, the design method described in Section 11 of the AASHTO sign structure design specification (2001) should be used to evaluate the sign structure for infinite fatigue life. In that method, recommended equivalent static wind load effects (AASHTO, 2001) are applied to sign structure, and stresses due to these loads on all components, mechanical fasteners, and weld details must satisfy the requirements of their respective detail categories within the CAFL provided in Table 2.2.

3.3.7 Conclusions and Discussions

(1) Double-mastarm cantilever sign structure.

It can be observed that the details of the double-mastarm cantilever sign structure that produced the lowest fatigue lives, in ranked order from the shortest life to the greatest life, are: post-to-base plate socket weld connection, fillet weld in built-up box, chord-to-end plate socket weld connection, and the hand hole connection. The anchor rods, strut-to-gusset plate welded connection, and gusset plate-to-chorded weld connection of the double-mastarm sign structure all were found to have effectively infinite lives.

Note that the computed fatigue life for given details in a typical double-mastarm sign structure varied considerably at different geographic sites. For example, a sign structure being in service for a certain period of time is more likely to have fatigue damage in South Bend than in Bloomington. The variations in life were primarily due to significant differences in the wind environment at various sites.

Regarding the fatigue life results, it should be noted that no experimental work or field observation data are available to validate or calibrate the analytical predictions. The state of Indiana does not have an established sign structure inspection program at present. However, the research study reported herein was initiated to assist the Indiana DOT in developing a sign structure inspection program. The fatigue life results in Table 3.7 are provided to compare the relative length of fatigue lives for different structural details.

The fatigue lives calculated with the VAFL method and the straight-line S-N curve

method were notably different. The fatigue lives according to the straight-line S-N curves are conservative relative to the VAFL method. If the life expectancy was less than 50 years, the difference was found to be greater by 13% to 37% when a VAFL method was used in the damage prediction compared with the life predicted by simple extension of the S-N curve. This variation is due to the fact that small stress cycles contribute to a larger portion of fatigue damage.

A strong correlation between high levels of exceedance of the CAFL stress range level and lower fatigue lives can be observed for the four details included in Table 3.7. It indicates that the calculated fatigue lives are consistent with the exceedance with regard to fatigue damage.

(2) Single-mastarm cantilever sign structure.

According to the results from the modal analyses of single-mastarm cantilever sign structures, an in-plane vibration is the first mode. So galloping, rather than natural wind, may be the most critical loading to cause major fatigue damage to the single-mastarm cantilever sign structure. The fatigue analytical procedure described in Section 3.3.1 thus can not be applied to the single-mastarm cantilever sign structure. However, this structure is very flexible and has the potential to be susceptible to wind-induced fatigue damage. Until a new approach is developed to investigate the fatigue performance of the single-mastarm cantilever sign structures, the provisions outlined in the AASHTO sign specification (2001) can be used to evaluate the cyclic behavior.

(3) Box-truss sign structure, monotube sign structure, and tri-chord sign structure

According to the dynamic analyses and fatigue analyses results of the structural details in the box-truss sign structure, the monotube sign structure and the tri-chord sign structures, little wind-induced fatigue damage occurred. So it can be concluded that these three types of sign structure are not as critical as the double-mastarm cantilever sign structure. The chord-to-transverse-plate weld connection is more critical than the other major details in the box-truss sign structure, and the post-to-base-plate weld connection is more critical than the other details in the tri-chord sign structure.

However, by no means do the results indicate that there will be no wind-induced fatigue failures occurring in these sign structures. First, all the welds in this study were assumed to be qualified for the standards in AWS D1.1 (2004) or D1.2 (2003) and the AASHTO Sign Specification (2001). But in reality some defects are very likely to exist in the initial welds and induce significant local stress concentrations. If these discontinuities are large enough, they may significantly reduce the fatigue resistance of the welded connections. Under this circumstance, fatigue damage can accumulate at a greater rate and may cause failures of structure members within the service period of the sign structures. Second, all the investigations were mainly based on sign structure designs in Indiana following the new 1999 or 2001 sign structure design specification, which is widely considered to lead to conservative designs. So the results in this investigation can not be extended to the sign structures designed following the old sign structure design specification or to new sign structures not following the standard design practice of Indiana.

(4) Sensitivity of Fatigue Lives to Load Simulation.

Based on the results of the sensitivity investigation in Section 3.3.2.3, the COVs computed in the sensitivity investigation is comparable with in the COV from typical constant-amplitude fatigue testing. Therefore, the variation in the cyclic fatigue lives with respect to different sets of simulated loads is comparable to the variation that occurs as a result of material and fabrication effects.

Table 3.1 Sectional dimensions for double-mastarm cantilever prototype sign structure.

Name	Description	A (mm^2)	I (mm^4)
Post	Pipe, 457mm O.D., 13mm Thick.	18,133	447,200,000
Chord	Pipe, 273mm O.D., 9.3mm Thick.	7,704	67,052,204
Strut	Angle, 10mm x 76mm x 76 mm	1,420	755,991

Table 3.2 Sectional dimensions for single-mastarm cantilever prototype sign structure.

Member Name	Description
Post	O.D. at bottom: 457 mm. O.D. at top: 382 mm. Length: 6.4 m. Wall Thickness: 10.9 mm.
Arm	O.D. at bottom: 381 mm. O.D. at top: 288 mm. Length: 12.2 m. Wall Thickness: 10.9 mm.
Base Plate	724 mm square. Thickness: 76 mm.
Anchor Rod	Diameter: 76 mm. Length: 3.66 m.

Table 3.3 Sectional dimensions for box-truss prototype sign structure.

Member Name	Description
Post	Diameter: 254 mm. Wall Thickness: 9.5 mm.
Diagonal Brace in End Frame	Diameter: 114 mm. Wall Thickness: 6.4 mm.
Horizontal Brace in End Frame	Diameter: 76 mm. Wall Thickness: 4.8 mm.
Chord	Diameter: 121 mm. Wall Thickness: 6.4 mm.
Vertical Truss	Diameter: 51 mm. Wall Thickness: 6.4 mm.
Diagonal Truss	Diameter: 76 mm. Wall Thickness: 6.4 mm.

Table 3.4 Sectional dimensions for monotube prototype sign structure.

Member Name	Description
Post	O.D. at bottom: 330 mm. O.D. at top: 245 mm. Length: 7.3 m. Wall Thickness: 6.4 mm.
Middle Monotube	Diameter: 406 mm. Wall Thickness: 6.4 mm.
End Monotube	O.D. at bottom: 406 mm. O.D. at top: 293 mm. Wall Thickness: 4.6 mm.
Base Plate	457 mm square. Thickness: 51 mm.
Anchor Rod	Diameter: 44.5 mm. Length: 2.3 m.

Table 3.5 Sectional dimensions for tri-chord prototype sign structure.

Member Name	Description
Post	Diameter: 508 mm. Wall Thickness: 4.8 mm.
Base Plate	775 mm diameter circular plate. Thickness: 32 mm.
Anchor Rod	Diameter: 38 mm. Length: 1.4 m.
Chord	Diameter: 114 mm. Wall Thickness: 6.0 mm.
Vertical Truss	Diameter: 42.2 mm. Wall Thickness: 3.6 mm.
Diagonal Truss	Diameter: 48.3 mm. Wall Thickness: 3.7 mm.

Table 3.6 Weibull parameters for different locations in Indiana.

Location	IND	EVV	LAF	SBN	BMG	FWA
k	2.327	2.233	2.120	2.357	2.354	2.155
c	11.533	9.823	10.530	11.449	9.710	11.380

Table 3.7 Life expectancies (in years) at various locations for different details of a double mastarm cantilever sign structure.

Location		IND	EVV	LAF	SBN	BMG	FWA
Post-to-base plate socket weld connection	Straight-line S-N curve	27	61	35	30	74	22
	VAFL method	32	84	42	36	112	25
	Difference	18%	38%	19%	20%	52%	13%
	CAFL Exceedance	0.993%	0.292%	0.738%	0.884%	0.175%	1.236%
Hand Hole	Straight-line S-N curve	72	340	90	88	621	65
	VAFL method	86	548	106	108	1494	72
	Difference	19%	61%	18%	23%	141%	11%
	CAFL Exceedance	0.060%	0.009%	0.049%	0.047%	0.003%	0.107%
Chord-to-end plate socket weld connection	Straight-line S-N curve	58	140	75	63	180	49
	VAFL method	77	233	102	87	332	61
	Difference	33%	66%	36%	38%	84%	24%
	CAFL Exceedance	0.296%	0.081%	0.213%	0.240%	0.048%	0.395%
Welded built-up box	Straight-line S-N curve	44	105	56	47	135	36
	VAFL method	58	171	73	65	259	46
	Difference	34%	62%	30%	37%	91%	26%
	CAFL Exceedance	0.379%	0.106%	0.284%	0.333%	0.062%	0.494%

Table 3.8 COVs for cyclic fatigue lives of tested bridge weld connection details (Keating and Fisher, 1985).

Category	**A**	**B**	**B'**	**C**	**D**	**E**	**E'**	**Average**
COV	21.70%	14.10%	13.20%	15.30%	14.20%	9.70%	13.20%	14.5%

Table 3.9 Life expectations and statistical data for post-to-base plate socket weld connection with different simulated load.

Simulation Num	IND	EVV	LAF	SBN	BMG	FWA
0	32.4	83.9	42.0	36.4	112.4	24.7
1	39.0	95.4	50.9	43.3	124.7	31.1
2	31.3	81.6	40.9	35.1	110.5	24.4
3	42.2	104.8	54.7	47.2	136.8	32.9
4	29.4	72.3	38.5	32.6	95.1	23.6
5	34.9	77.1	44.9	38.6	92.9	27.9
6	30.4	74.4	38.4	34.5	92.0	22.0
7	24.2	56.1	31.7	26.7	71.3	19.9
8	33.7	80.4	43.7	37.6	101.5	26.6
9	34.4	80.5	44.6	38.2	101.0	27.5
10	34.4	80.5	44.6	38.2	101.0	27.5
11	26.2	63.5	34.3	29.0	82.9	21.2
12	37.4	96.9	48.8	41.9	130.6	29.1
13	32.1	69.3	41.7	35.0	84.3	26.7
14	27.1	62.9	35.2	29.9	79.4	21.8
15	29.7	69.5	38.6	32.8	88.0	23.9
16	33.8	77.5	44.0	37.3	97.0	27.5
17	31.6	80.6	41.3	35.4	107.3	24.7
18	30.7	76.2	39.8	34.4	98.7	23.8
19	33.9	81.1	44.4	37.5	105.1	27.5
20	34.1	82.6	44.4	37.8	107.8	27.1
21	38.0	94.2	49.6	42.4	123.3	30.0
22	33.2	82.4	43.3	36.9	108.7	26.2
23	37.5	86.9	48.4	41.6	108.1	29.7
24	36.6	91.2	47.0	41.1	117.8	27.7
25	32.4	73.9	42.0	35.8	91.3	26.1
26	32.6	85.1	42.3	36.7	114.9	24.9
27	26.1	58.9	33.8	28.8	72.7	21.0
28	31.3	68.7	40.5	34.3	83.6	25.6
29	28.8	65.2	37.7	31.6	81.9	24.0
Mean	32.6	78.4	42.4	36.3	100.7	25.9
STD DEVI	4.0	11.5	5.2	4.6	16.6	3.1
COV	12.40%	14.61%	12.34%	12.67%	16.50%	11.88%

Fig. 3.1 A typical double-mastarm cantilever sign structure.

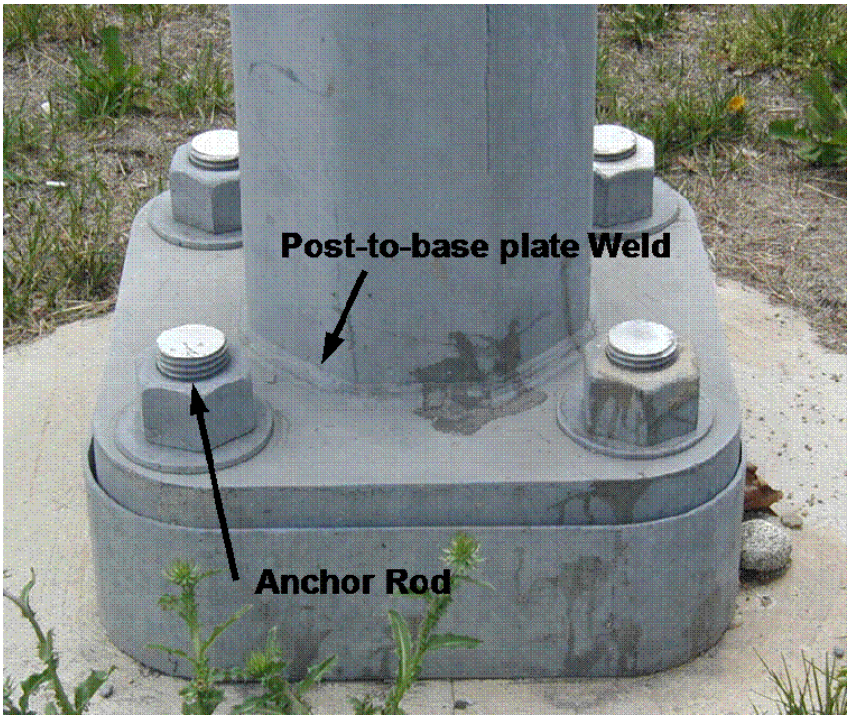

Fig. 3.2 Post-to-base plate detail.

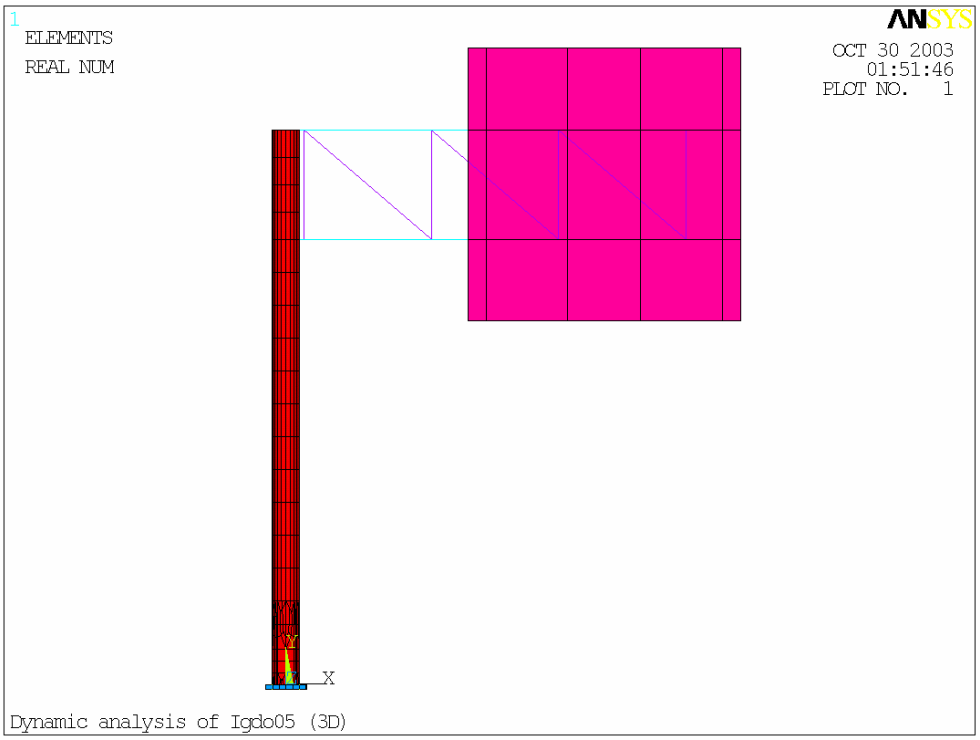

Fig. 3.3 Typical cantilevered sign structure model (Model A).

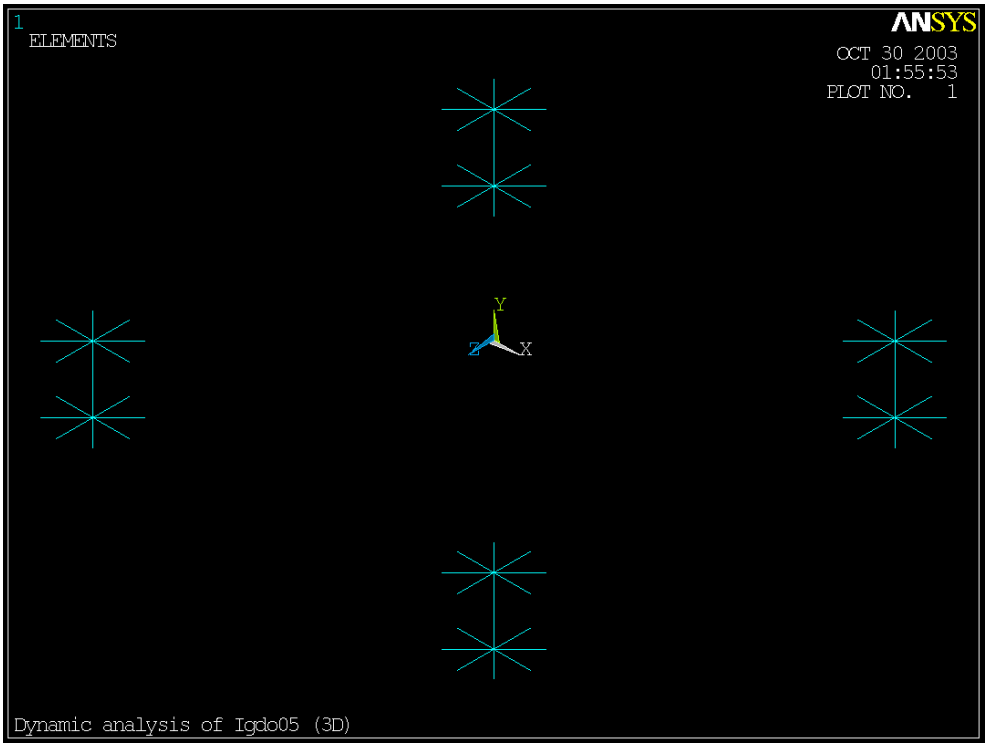

Fig. 3.4 Spider bolts (3D view).

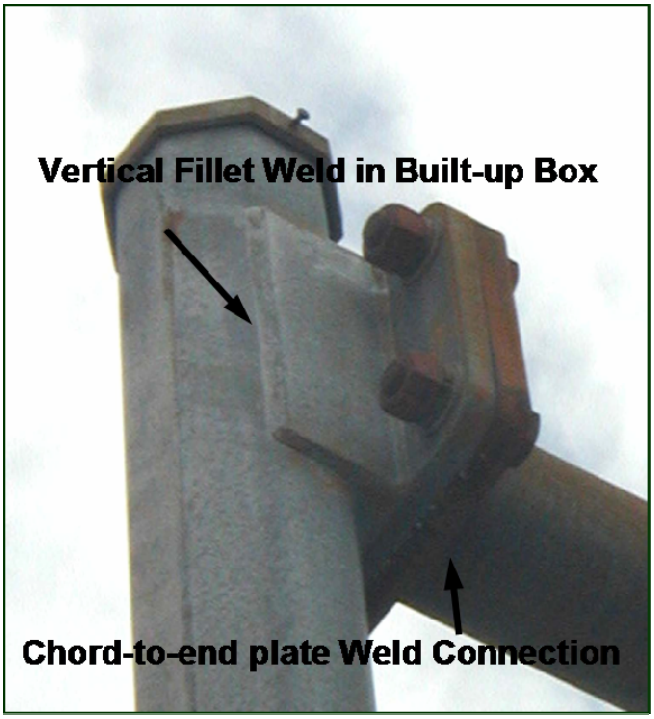

Fig. 3.5 Chord-to-post connection.

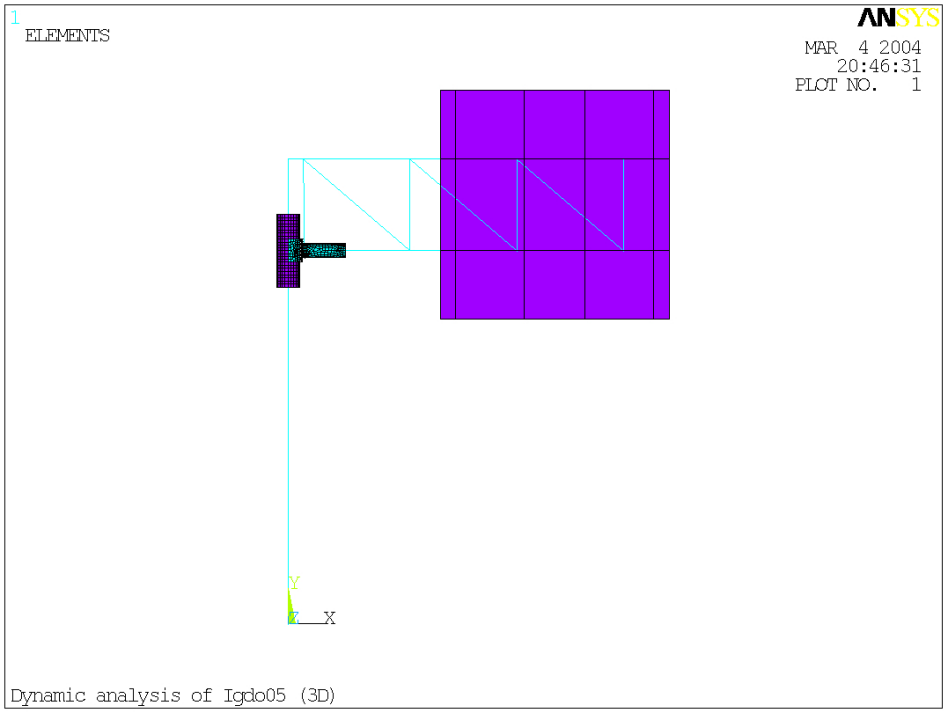

Fig. 3.6 Model with chord-to-post detail (Model B).

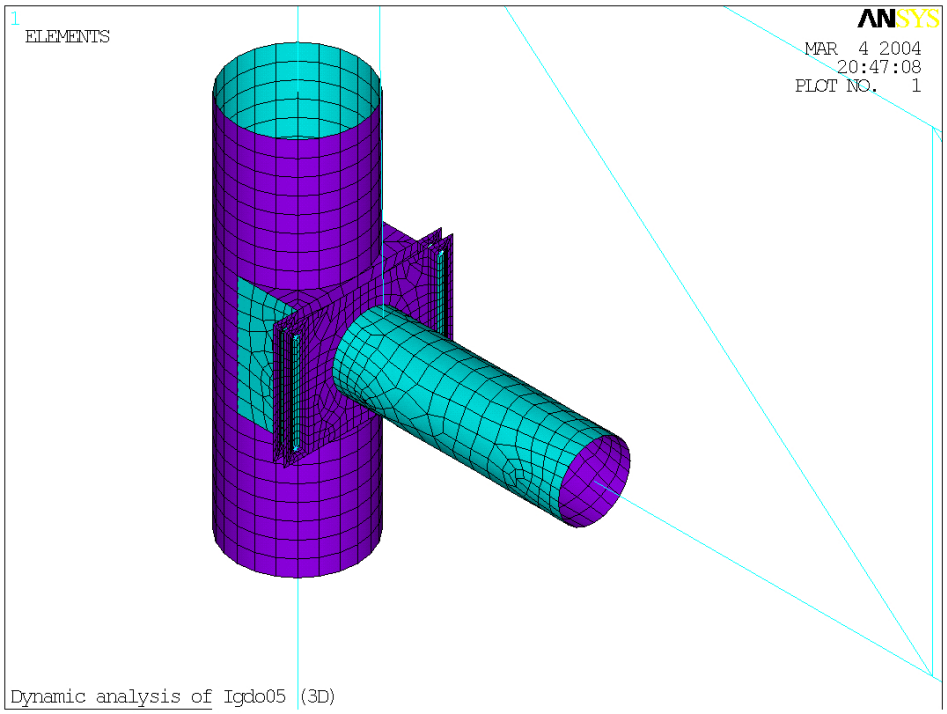

Fig. 3.7 Chord-to-post detail in Model B.

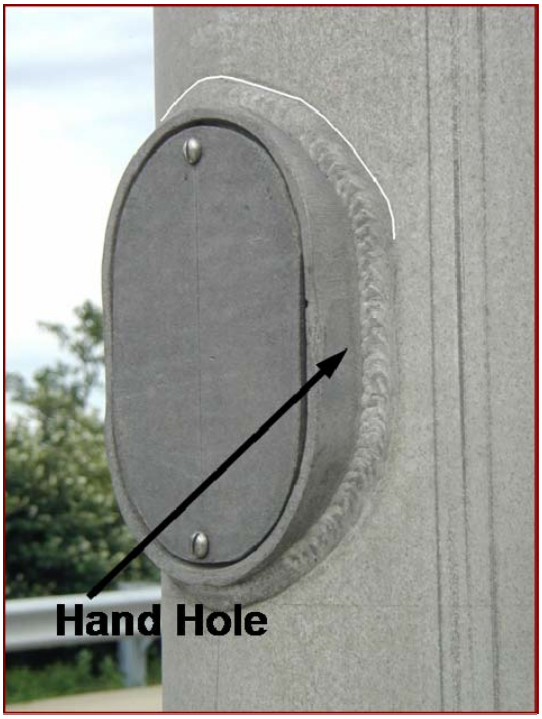

Fig. 3.8 Hand hole detail.

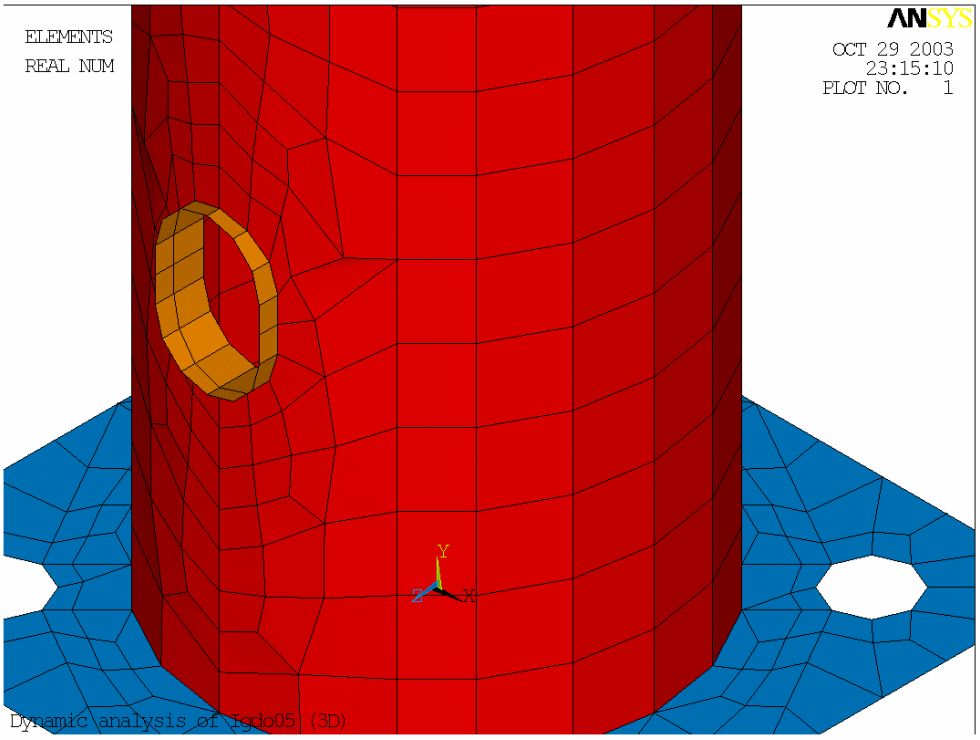

Fig. 3.9 Model with hand hole detail (Model C).

Fig. 3.10 A typical single-mastarm cantilever sign structure.

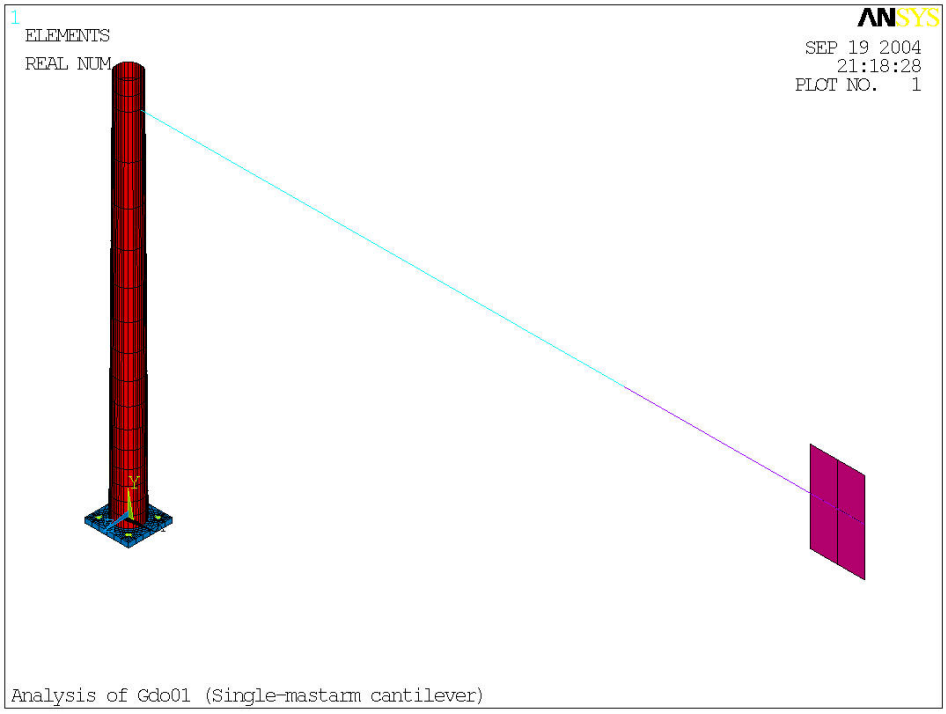

Fig. 3.11 A prototype single-mastarm cantilever sign structure model.

Fig. 3.12 A typical box-truss sign structure.

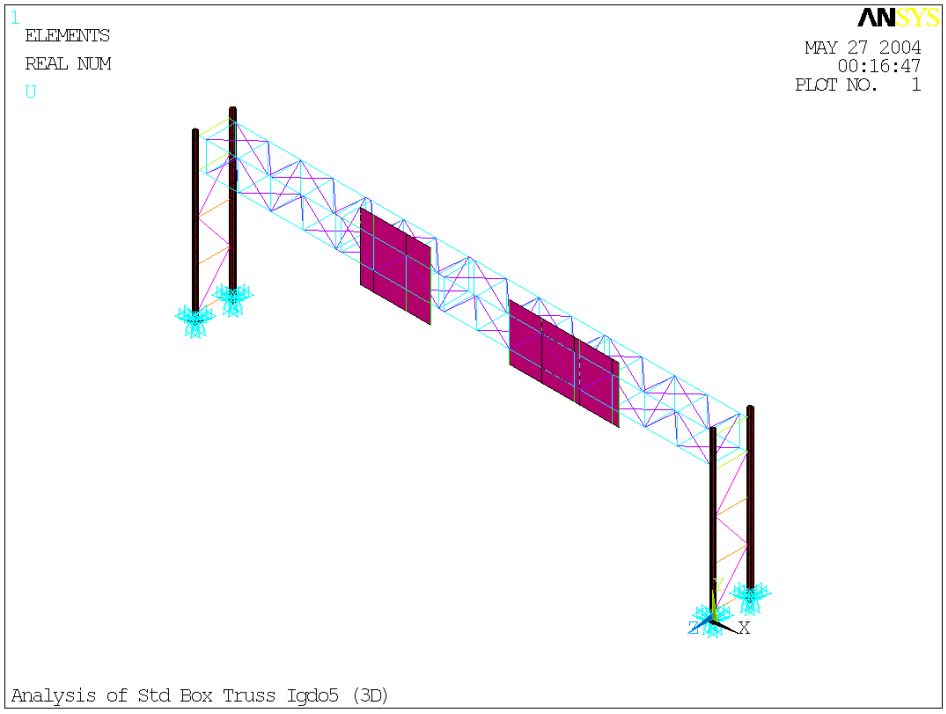

Fig. 3.13 Model A for box-truss sign structure.

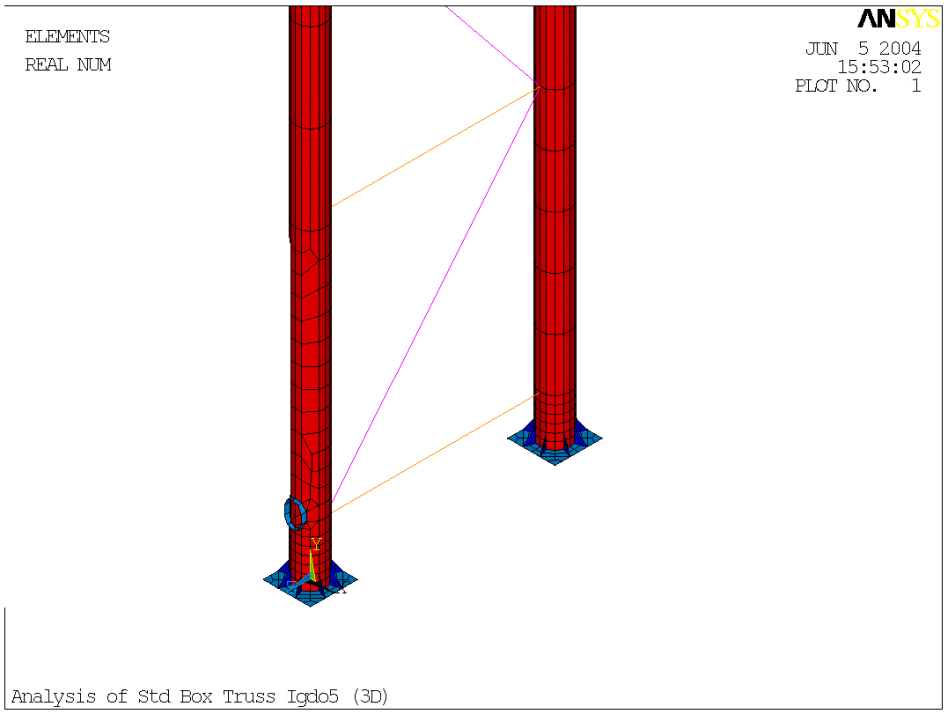

Fig. 3.14 Model B for box-truss sign structure.

Fig. 3.15 A typical monotube sign structure.

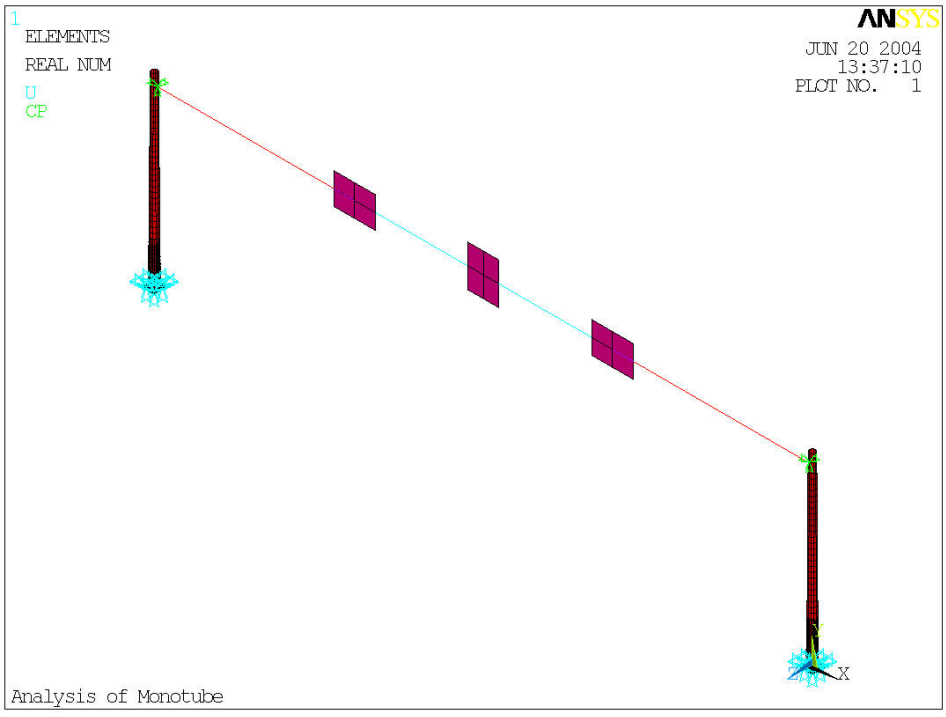

Fig. 3.16 Model A for monotube sign structure.

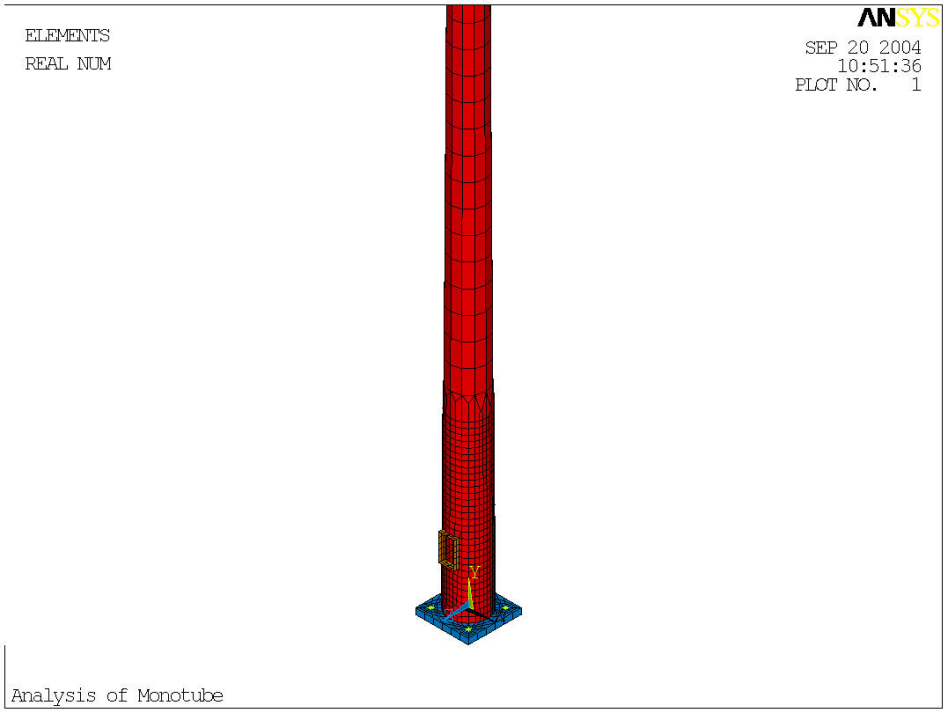

Fig. 3.17 Model B for monotube sign structure.

Fig. 3.18 A typical tri-chord sign structure.

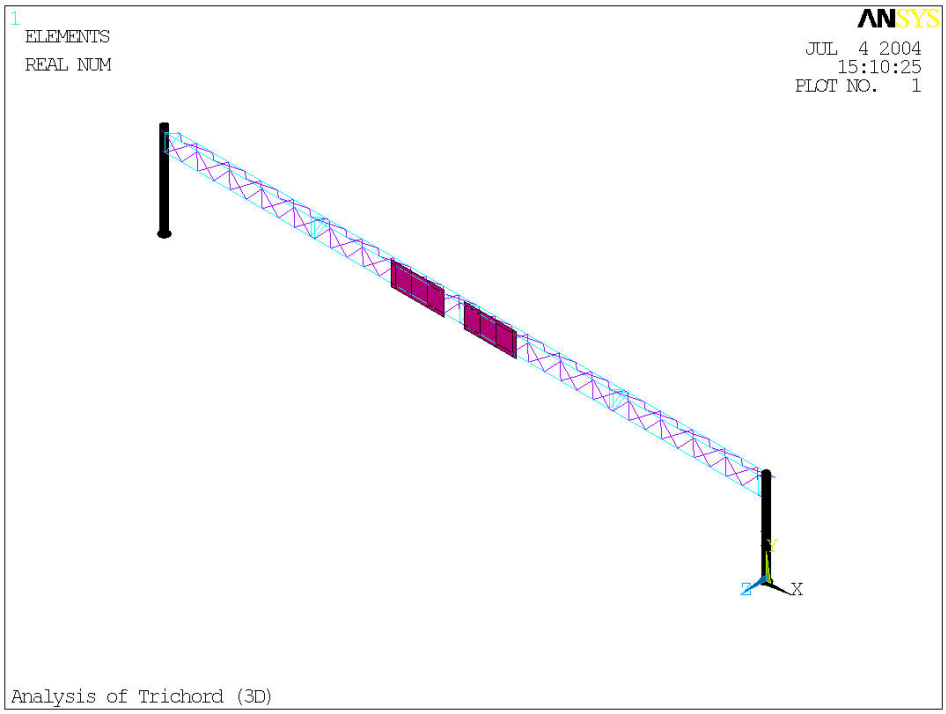

Fig. 3.19 Model A for the tri-chord sign structure model.

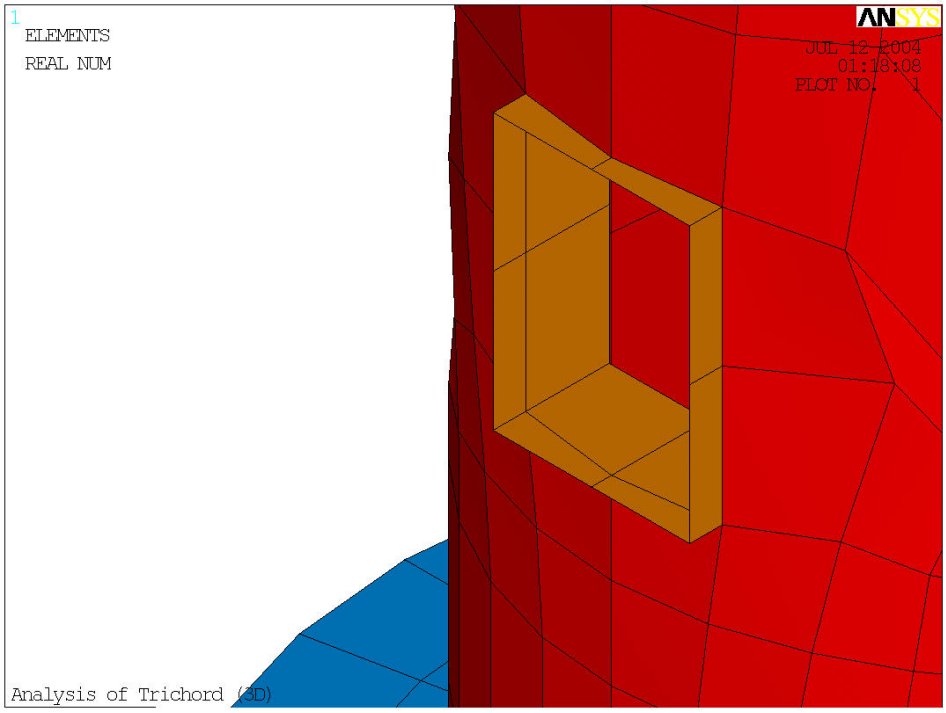

Fig. 3.20 Model B for the tri-chord sign structure.

Fig. 3.21 Selected locations in Indiana.

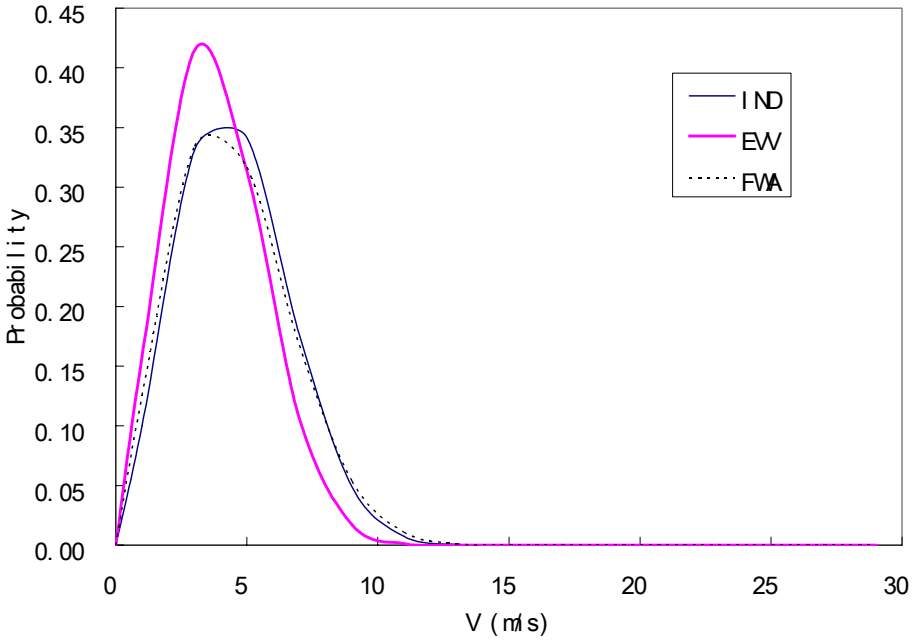

Fig. 3.22 Wind speed distribution curves (1).

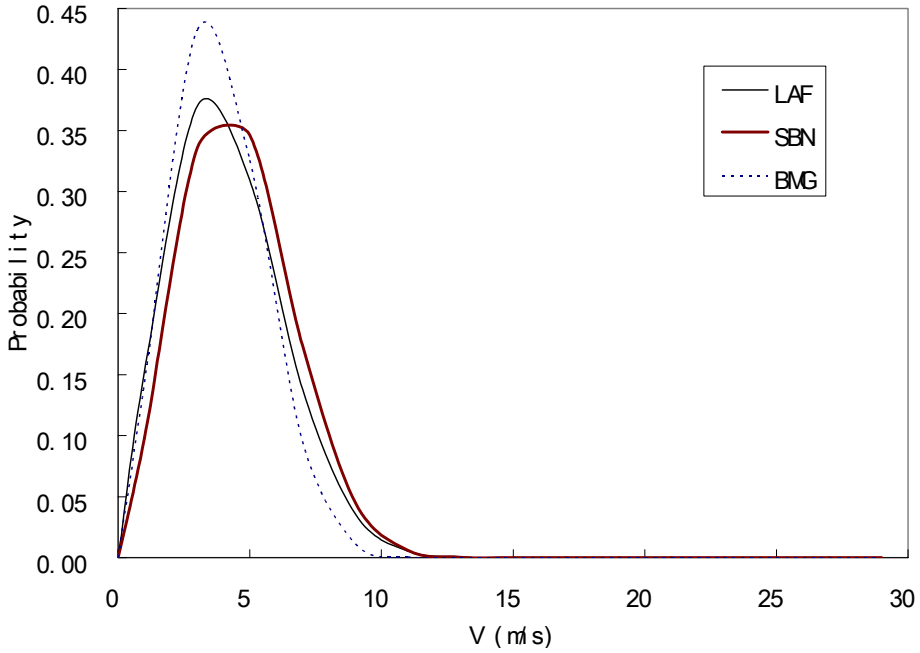

Fig. 3.23 Wind speed distribution curves (2).

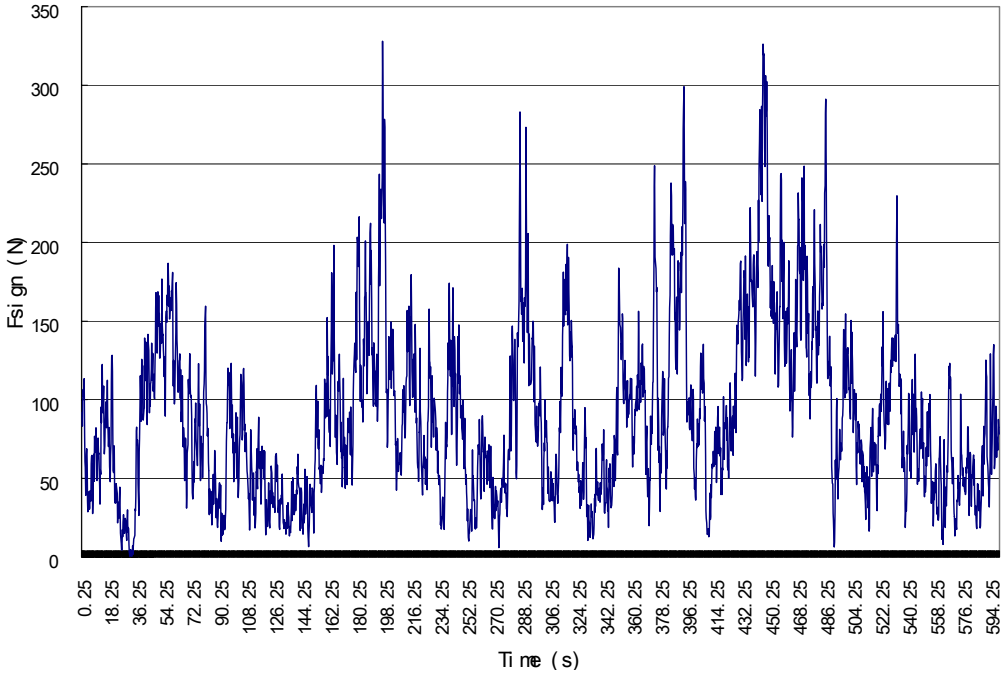

Fig. 3.24 Wind force time-history on the sign panel for V_{mean}=5 m/s at the center of the sign panel.

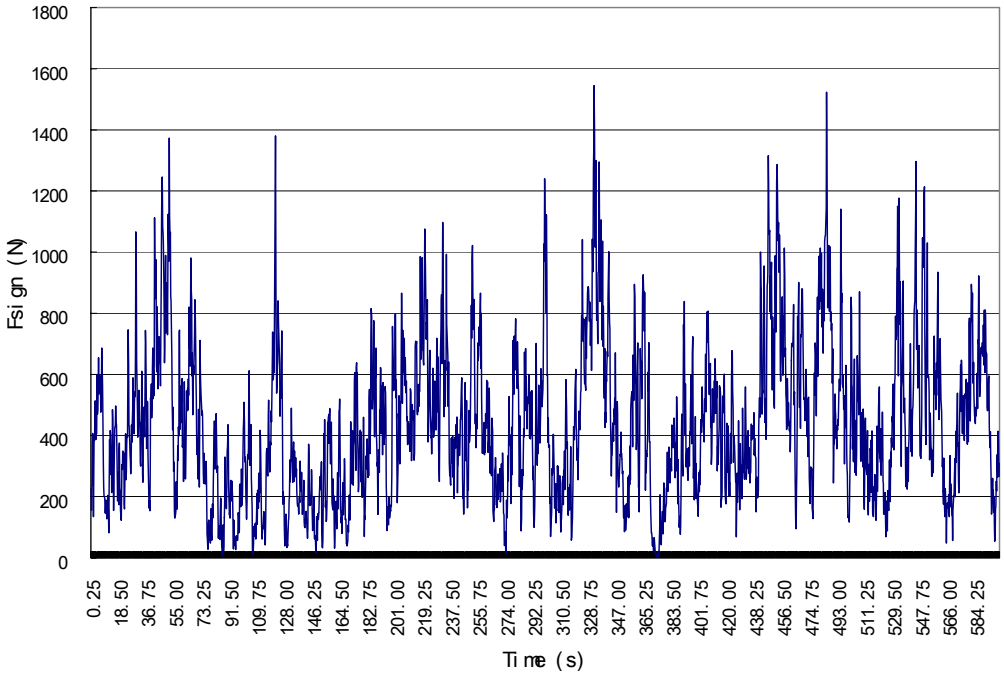

Fig. 3.25 Wind force time-history on the sign panel for V_{mean}=11 m/s at the center of the sign panel.

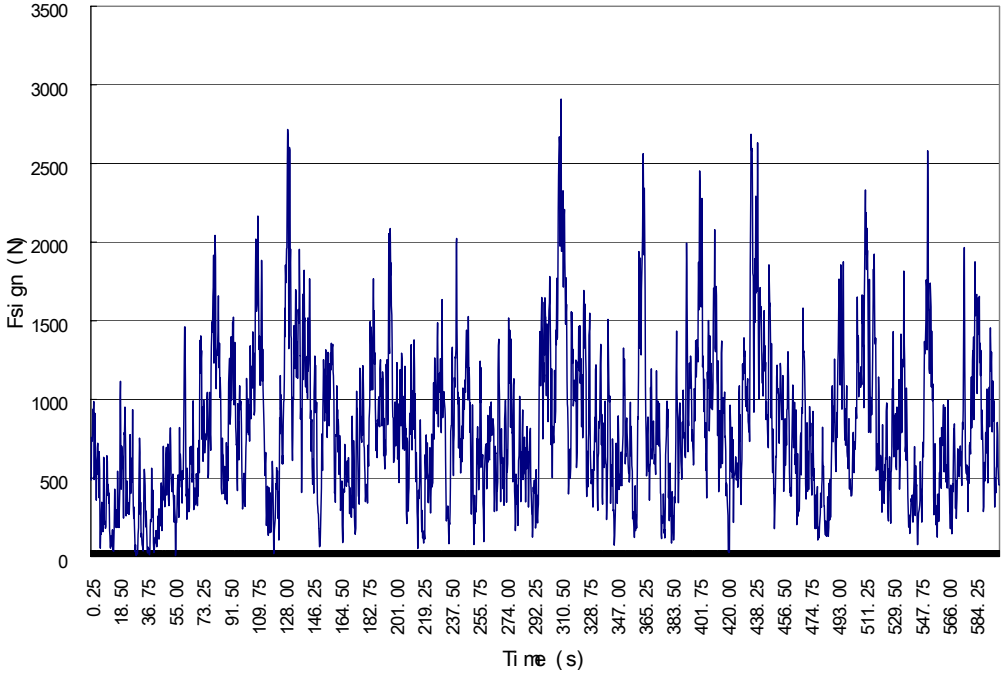

Fig. 3.26 Wind force time-history on the sign panel for V_{mean}=15 m/s at the center of the sign panel.

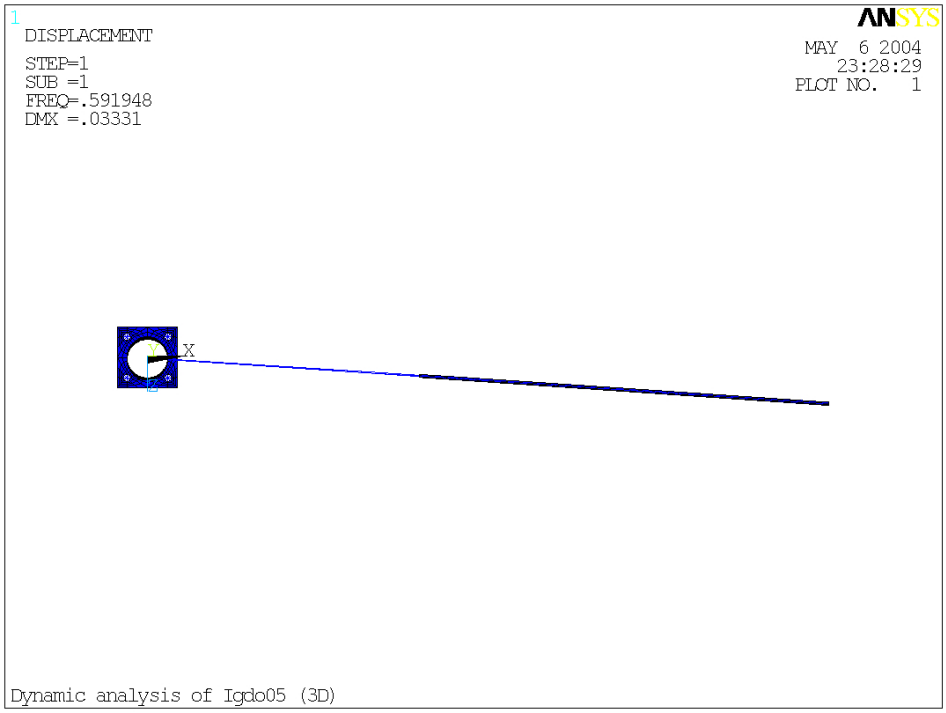

Fig. 3.27 First mode of the double-mastarm cantilever sign structure (top view).

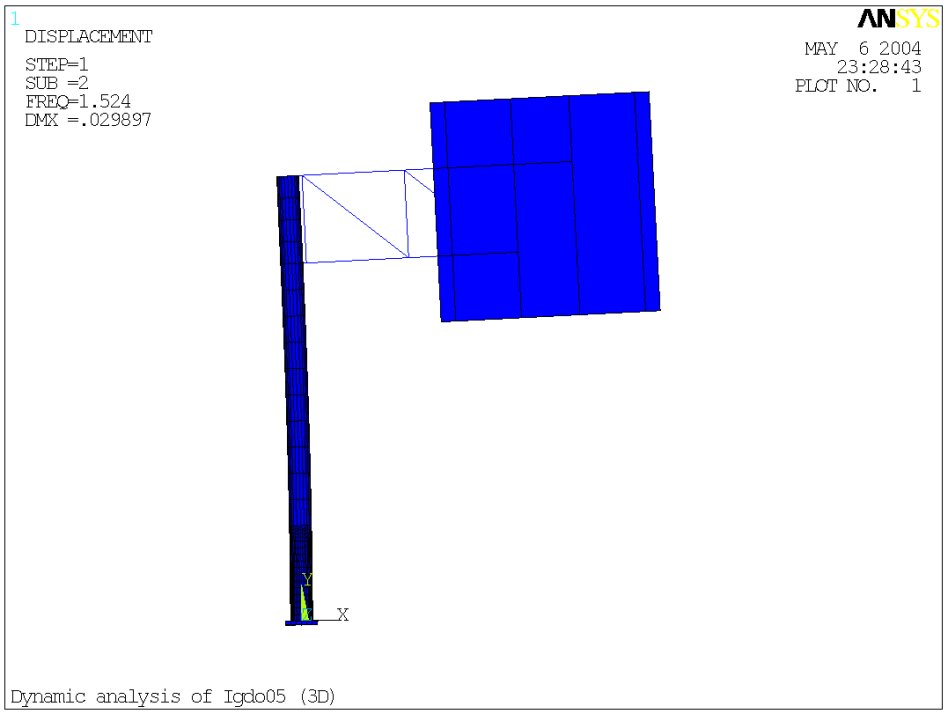

Fig. 3.28 Second mode of the double-mastarm cantilever sign structure.

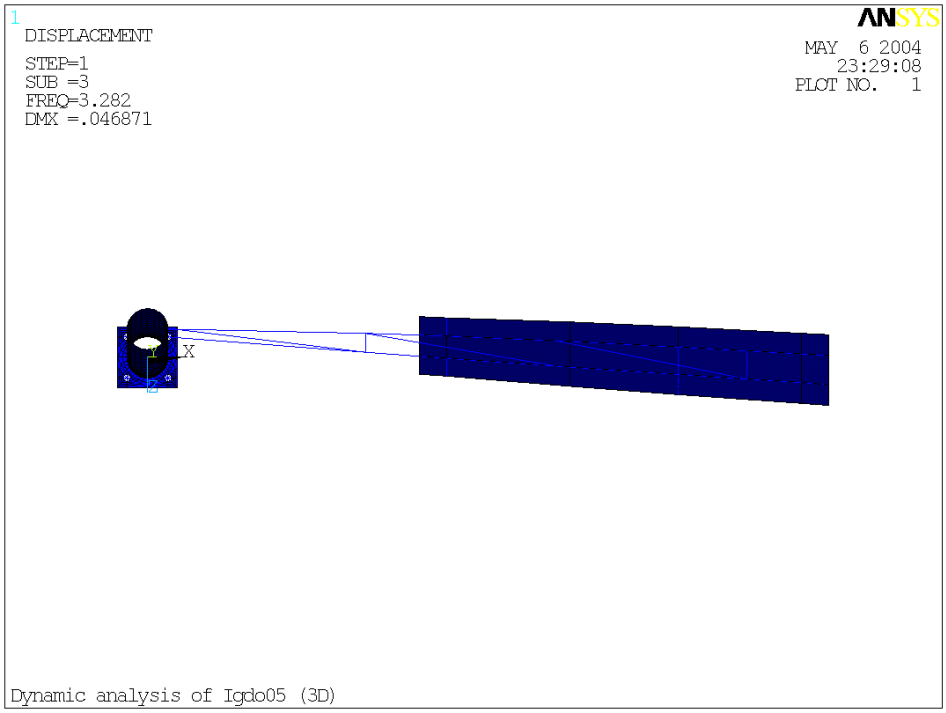

Fig. 3.29 Third mode of the double-mastarm cantilever sign structure (top view).

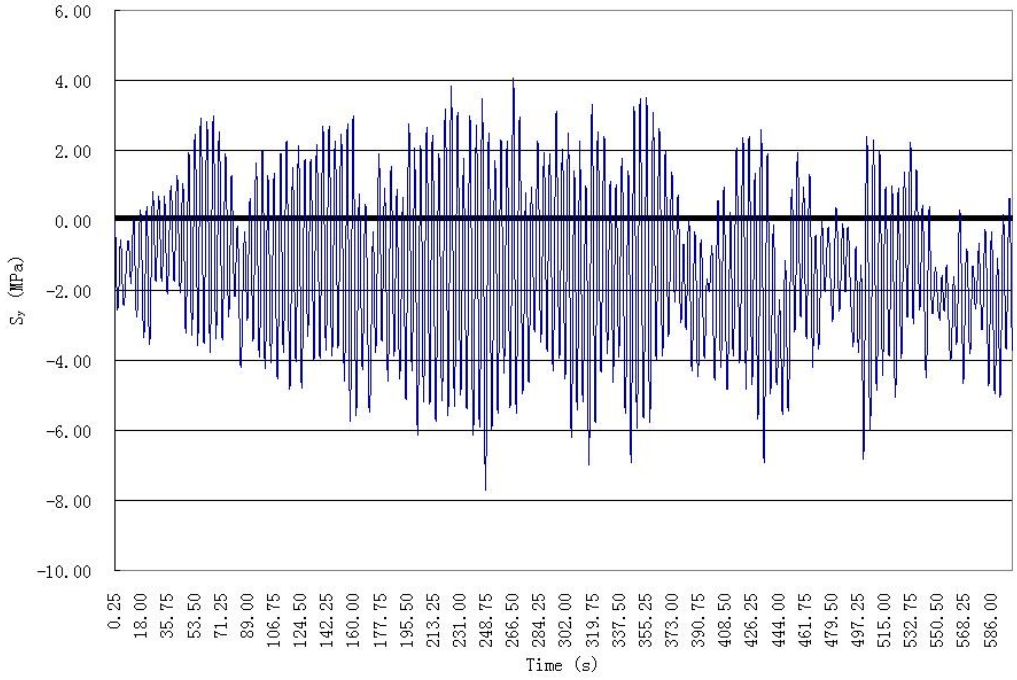

Fig. 3.30 Stress history at post-to-base plate connection for V_{mean}= 5 m/s.

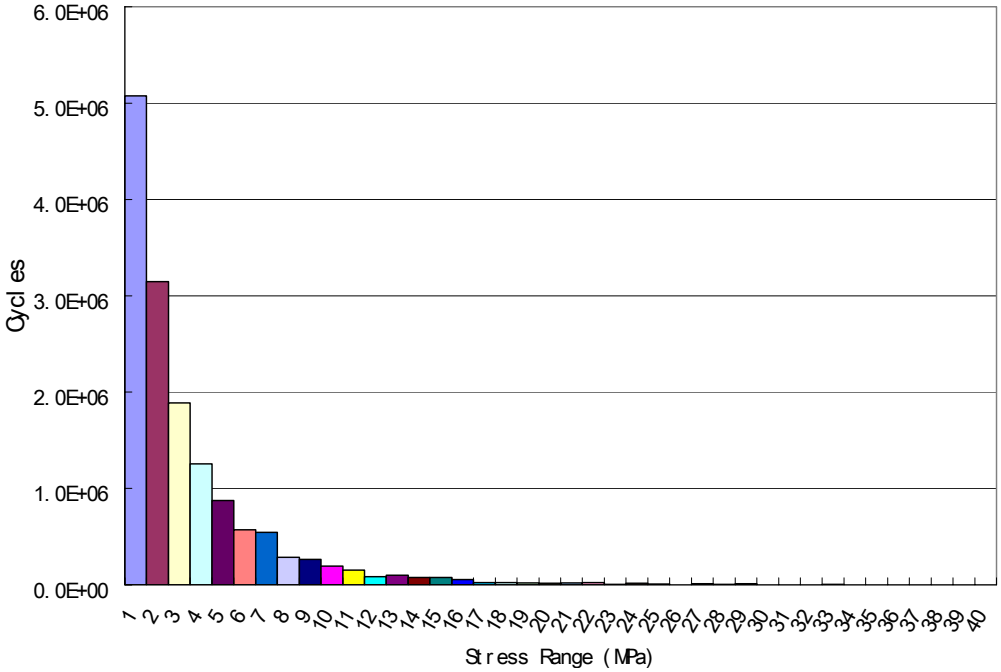

Fig. 3.31 Histogram of stress cycles for post-to-base plate weld connection.

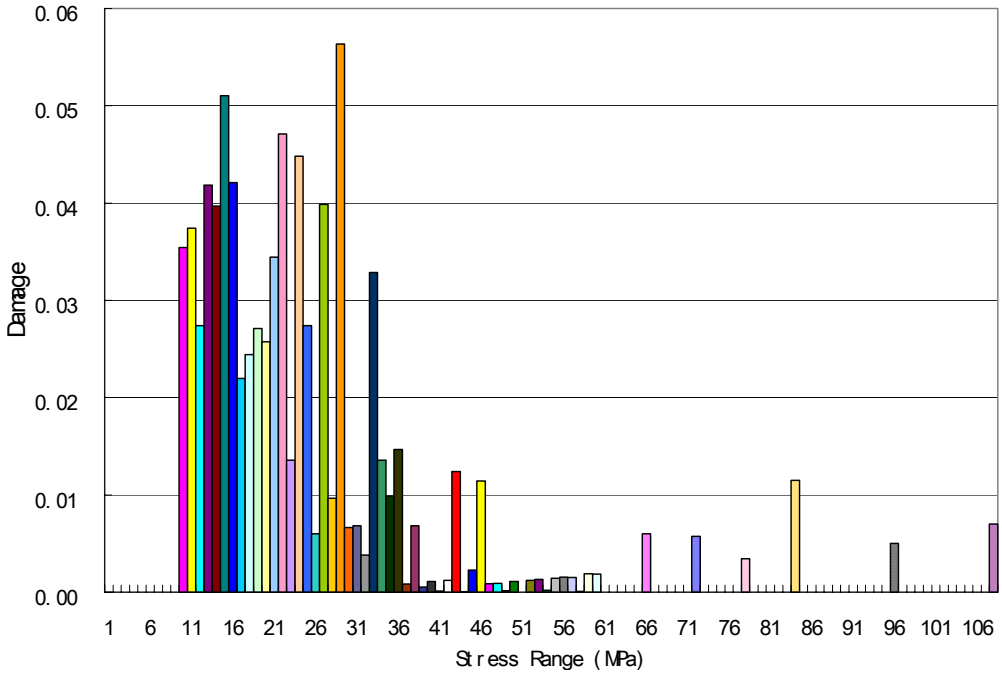

Fig. 3.32 Damage percentage for different stress ranges.

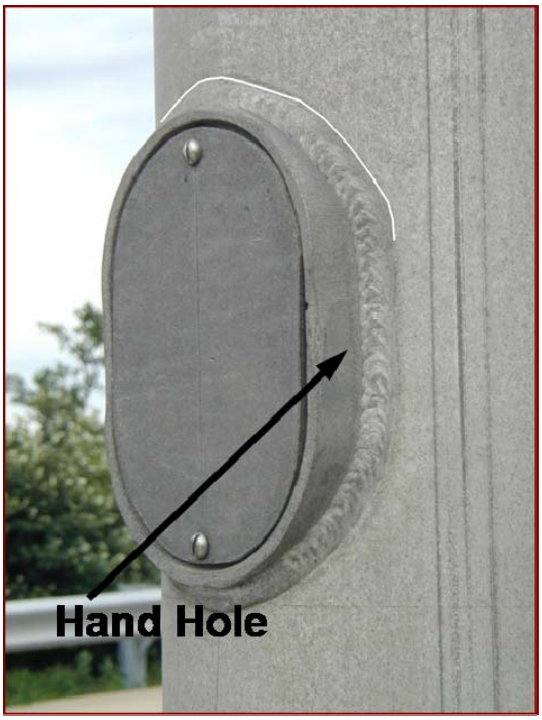

Fig. 3.33 Hand hole detail.

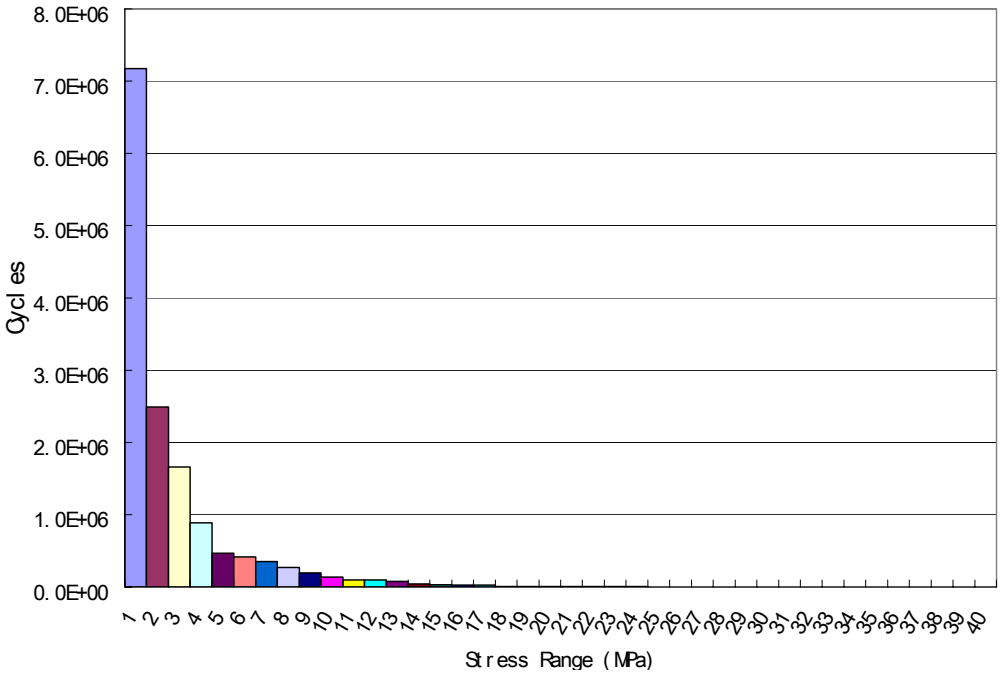

Fig. 3.34 Histogram of stress cycles for hand hole.

Fig. 3.35 Chord-to-post connection.

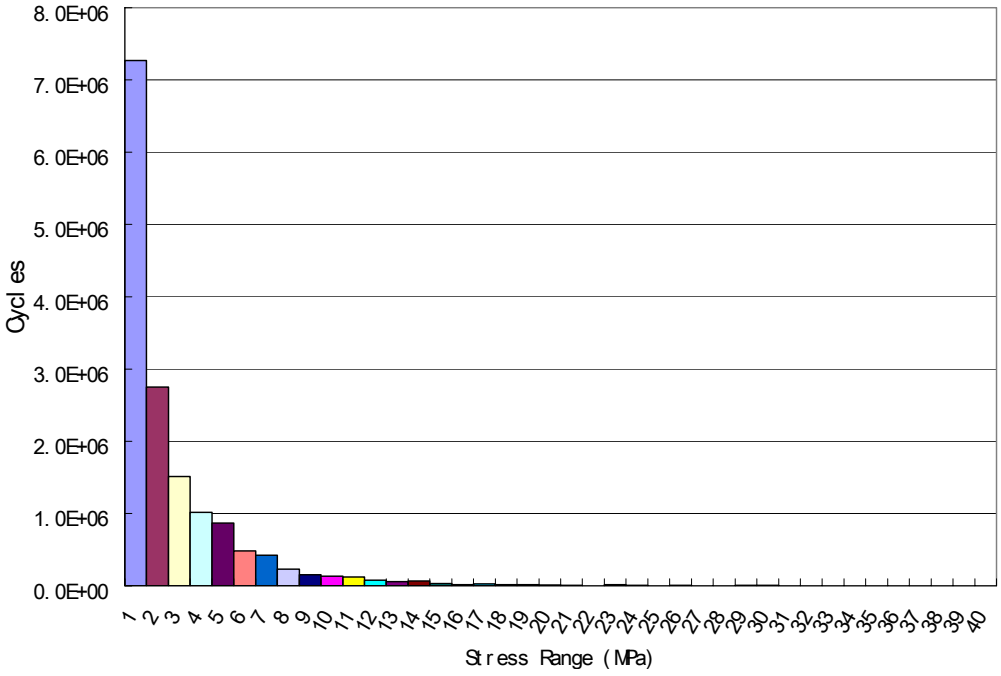

Fig. 3.36 Histogram of stress cycles for post-to-end plate connection.

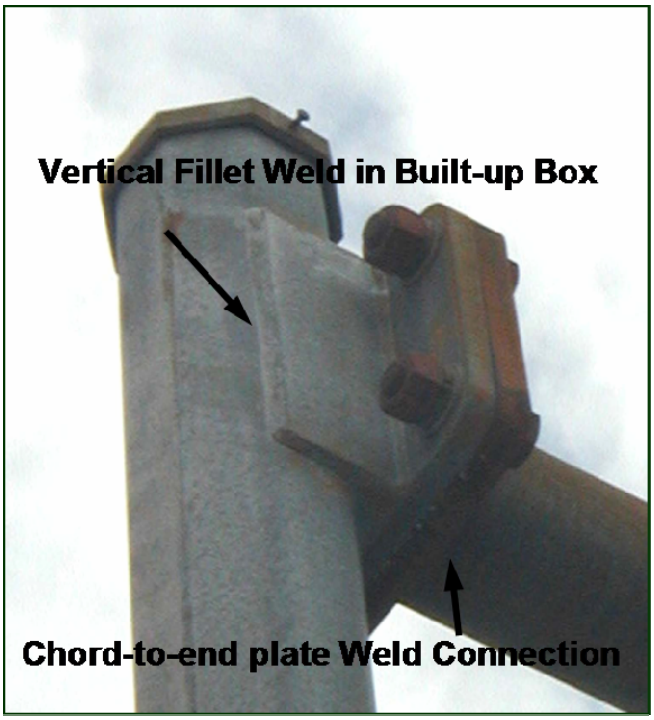

Fig. 3.37 Chord-to-post connection.

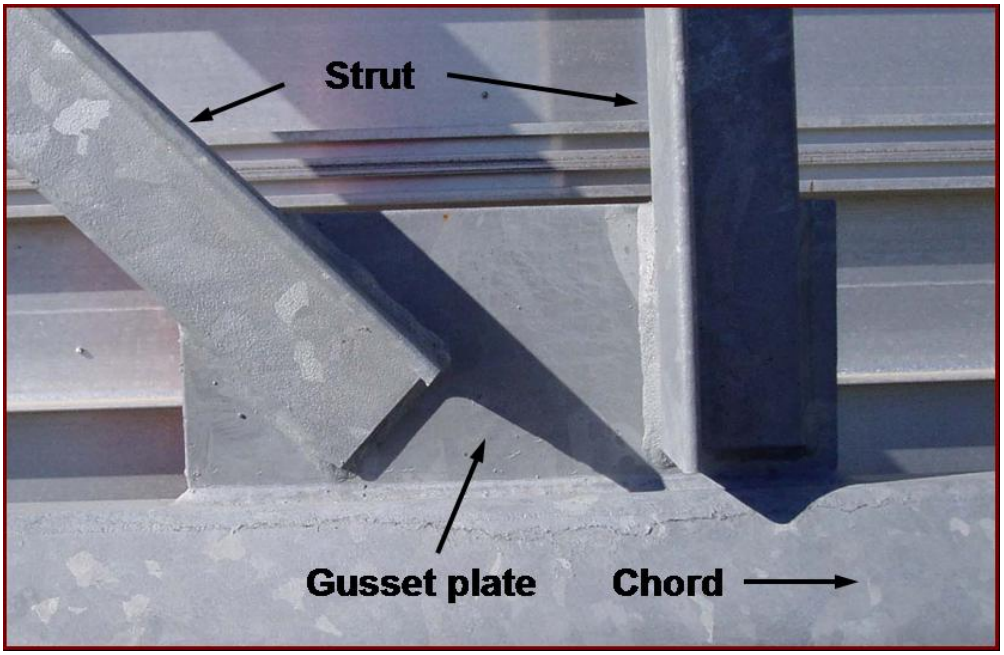

Fig. 3.38 Strut to gusset plate weld connection and gusset plate to chord weld connection.

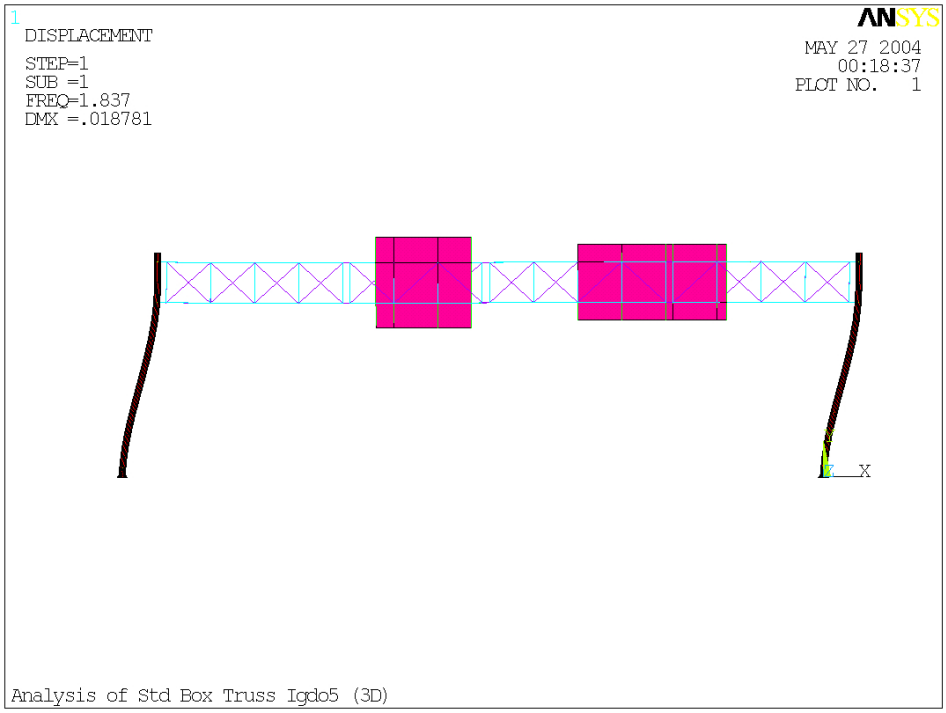

Fig. 3.39 First mode of the box-truss sign structure.

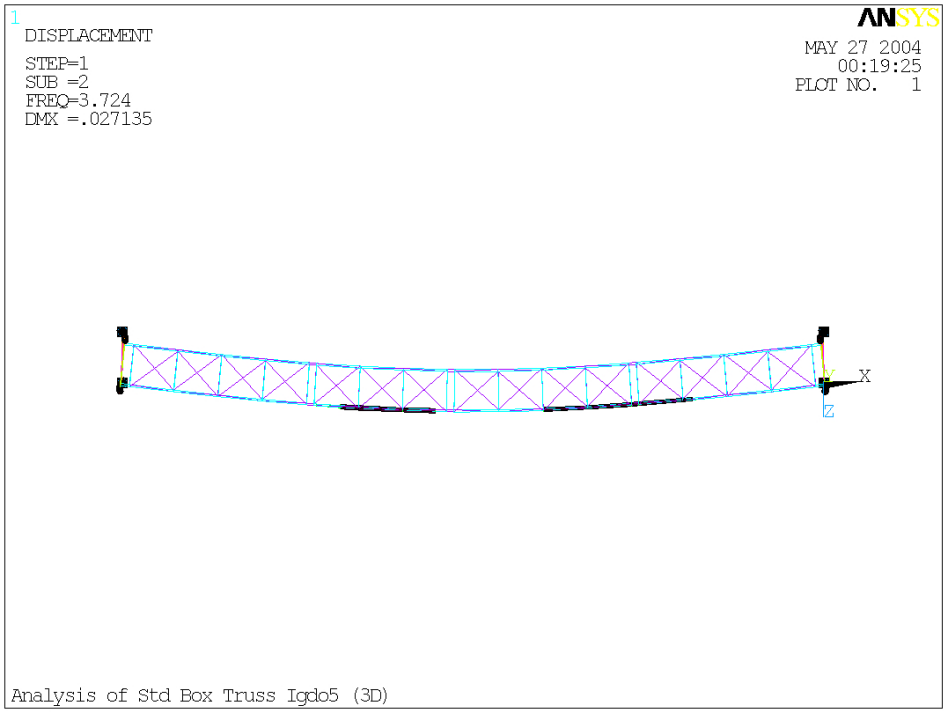

Fig. 3.40 Second mode of the box-truss sign structure.

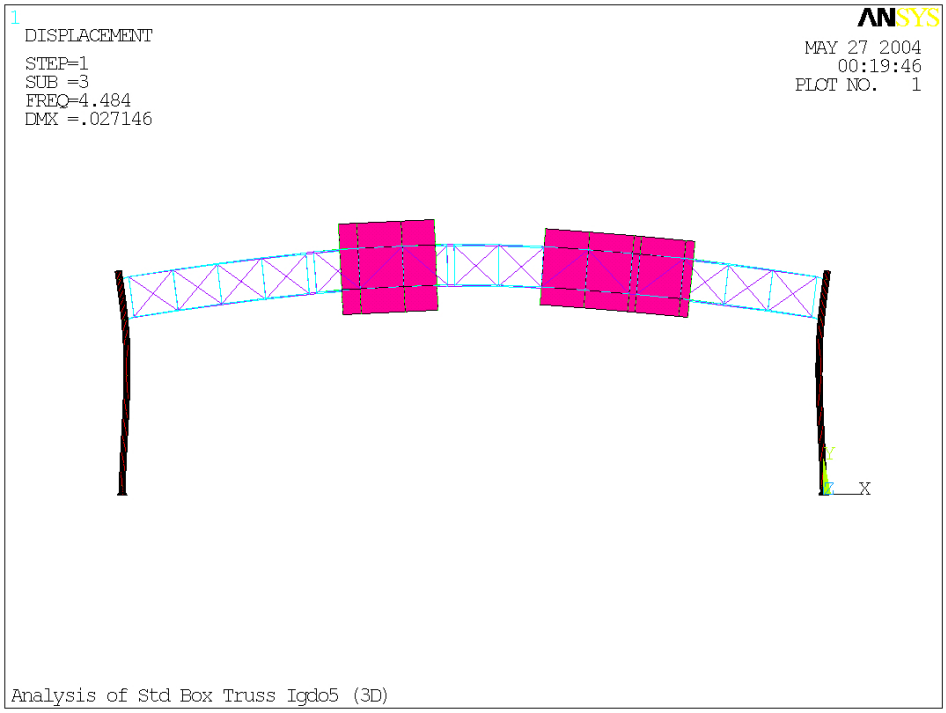

Fig. 3.41 Third mode of the box-truss sign structure.

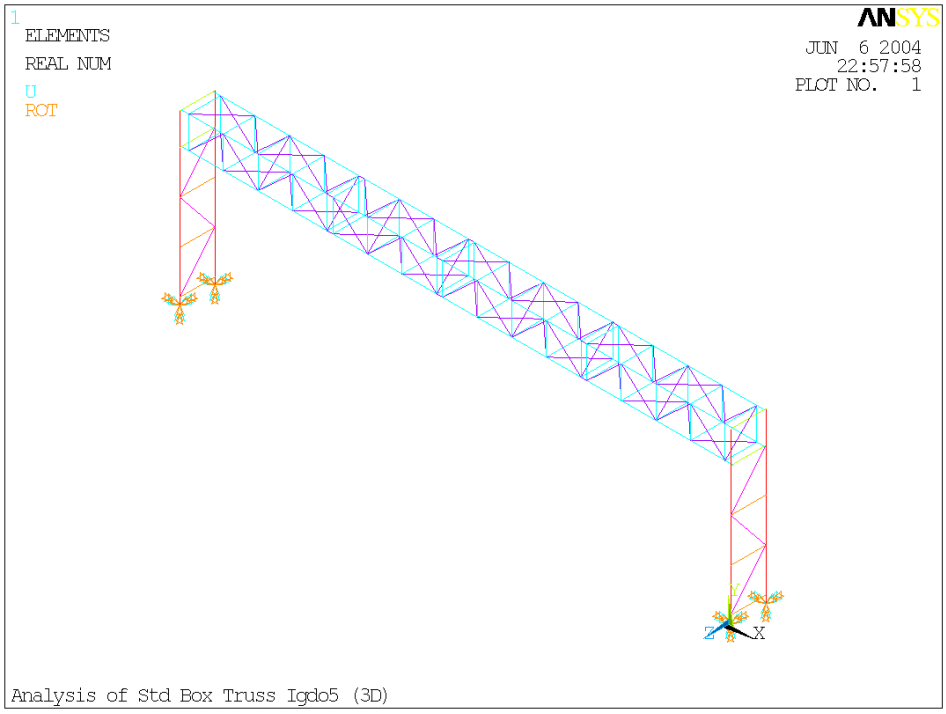

Fig. 3.42 A simple model of the box-truss sign structure.

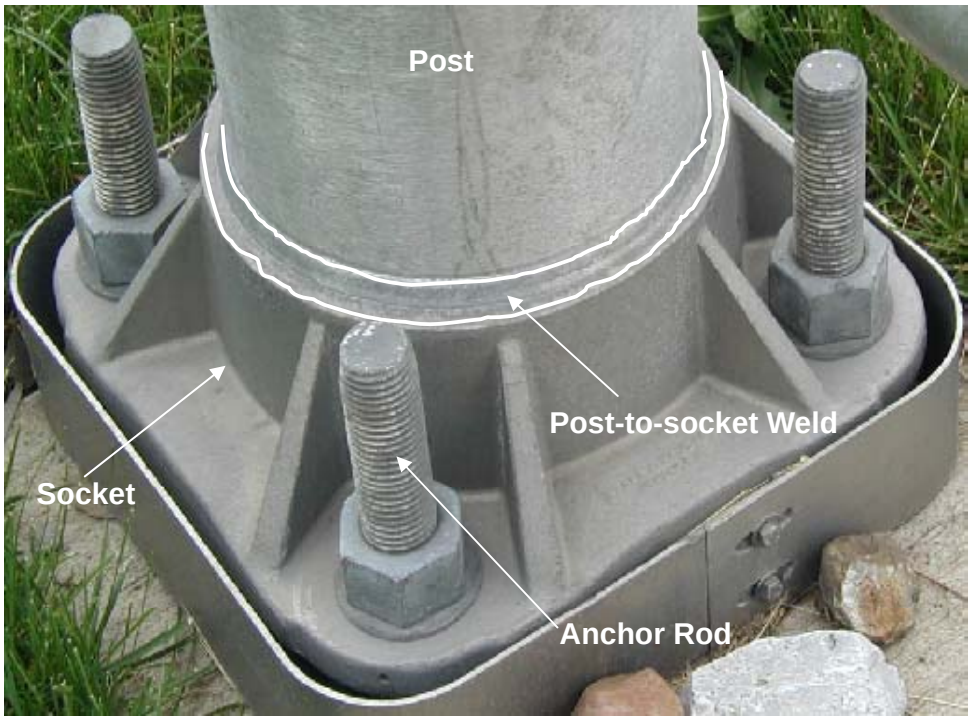

Fig. 3.43 Post-to-socket weld connection and anchor rod for the box-truss sign structure.

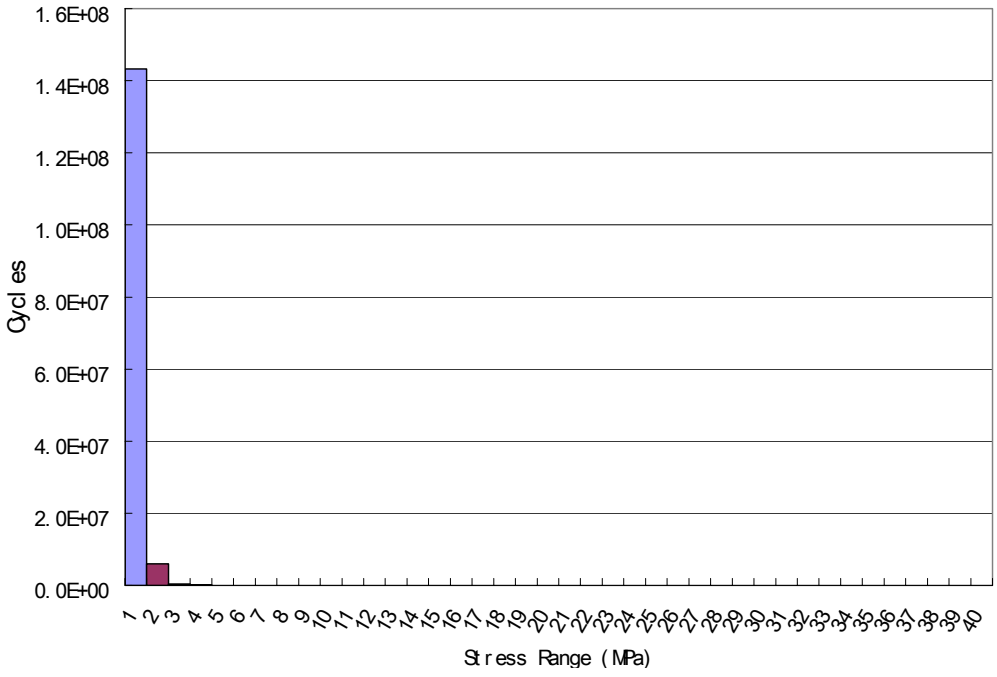

Fig. 3.44 Histogram for post-to-socket weld connection.

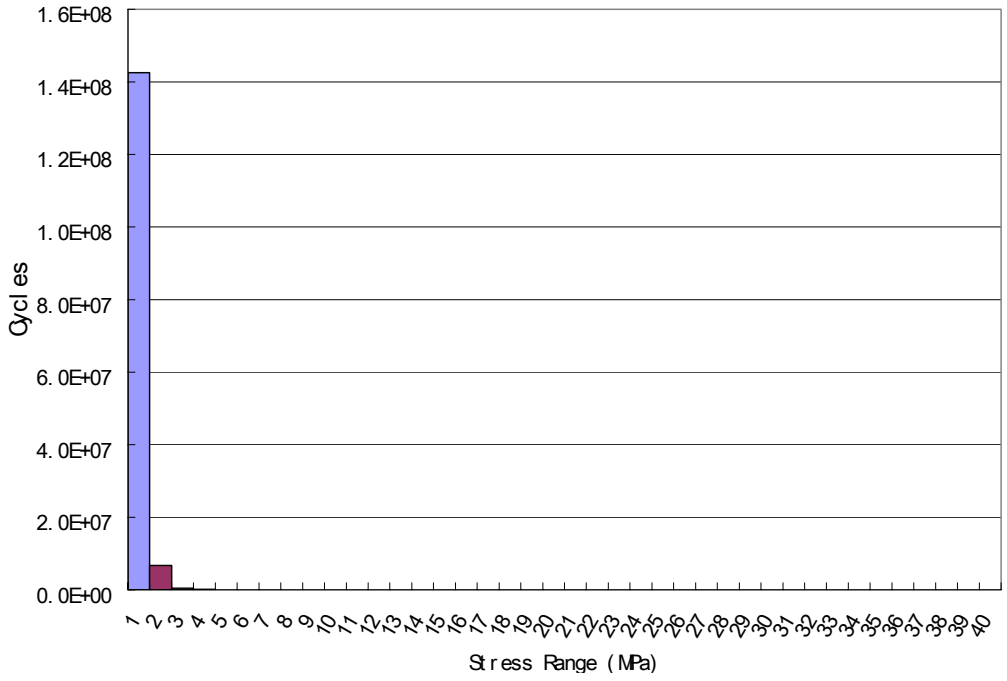

Fig. 3.45 Histogram for anchor rod.

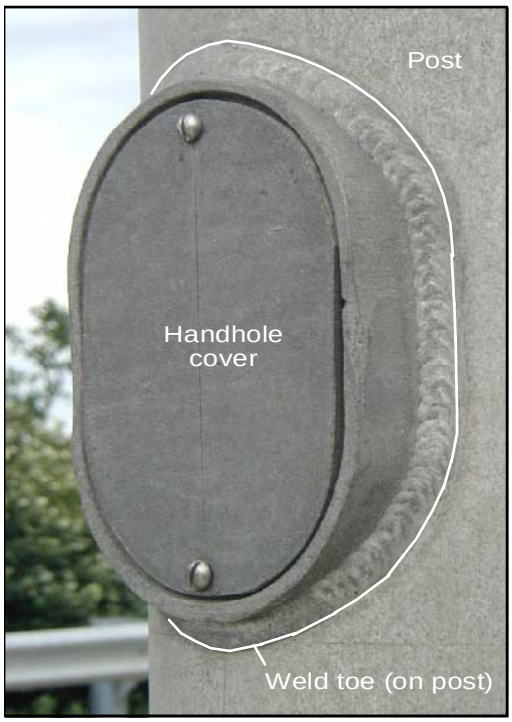

Fig. 3.46 Hand hole of a box-truss sign structure.

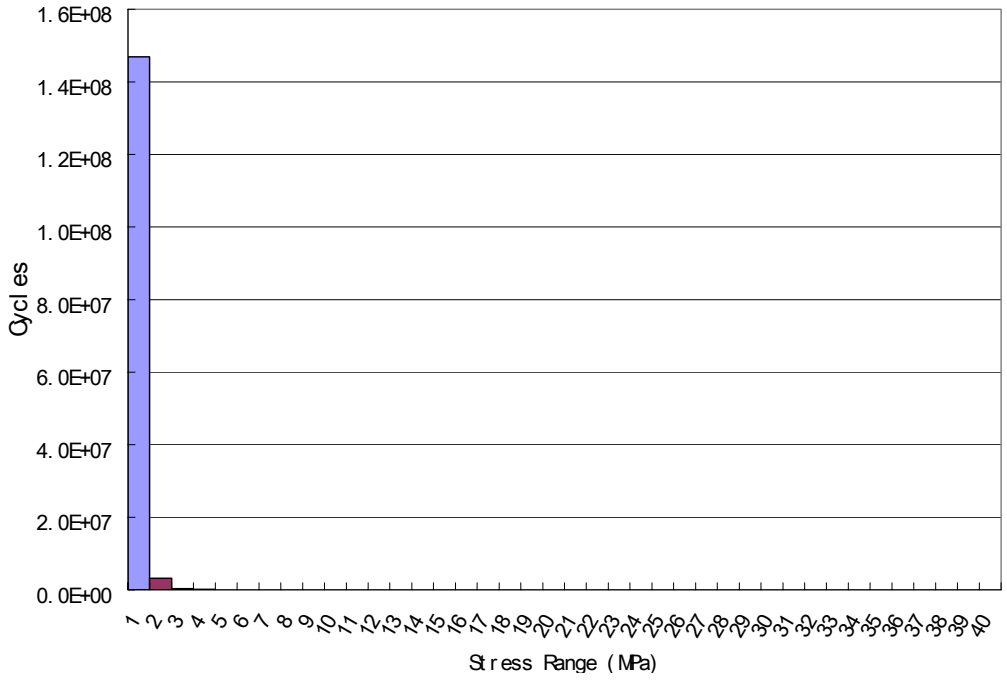

Fig. 3.47 Histogram for hand hole.

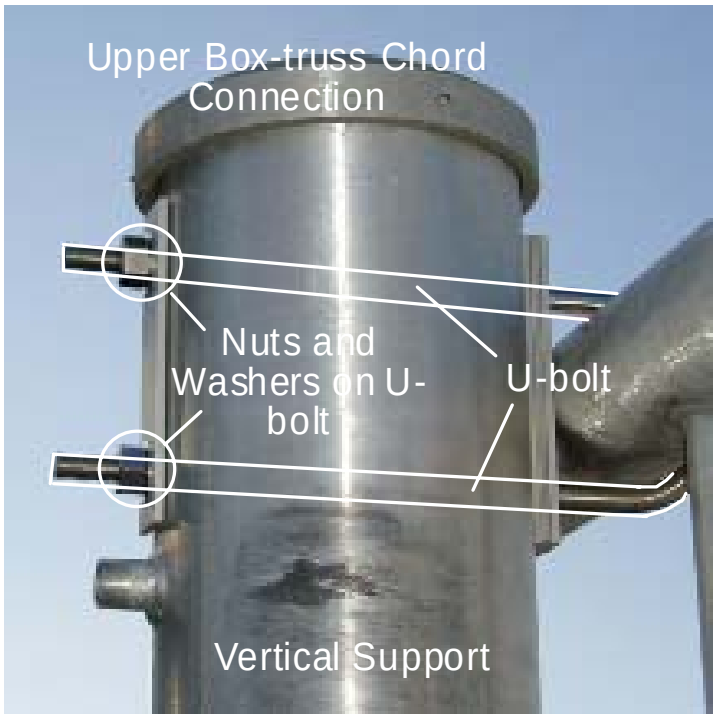

Fig. 3.48 U-bolt in chord-to-post connection for a box-truss sign structure.

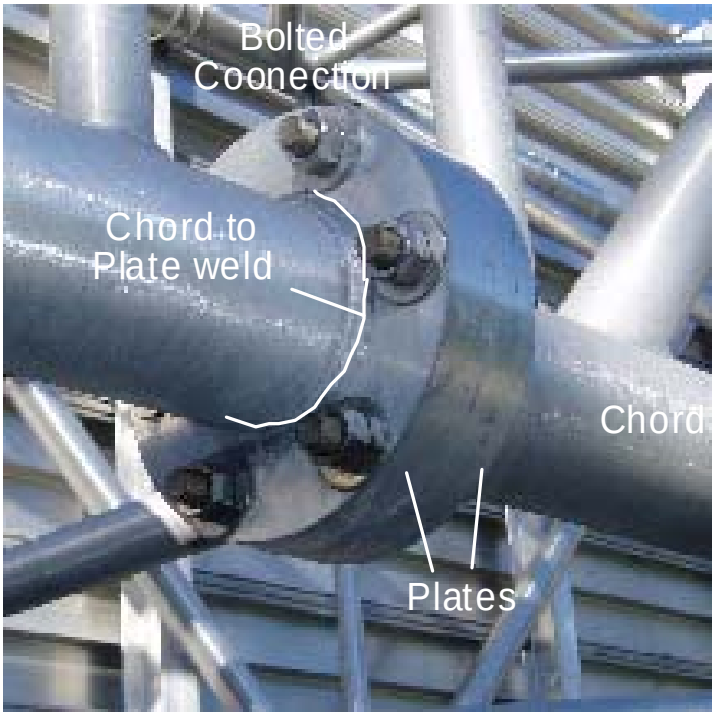

Fig. 3.49 Chord-to-plate weld connection for a box-truss sign structure.

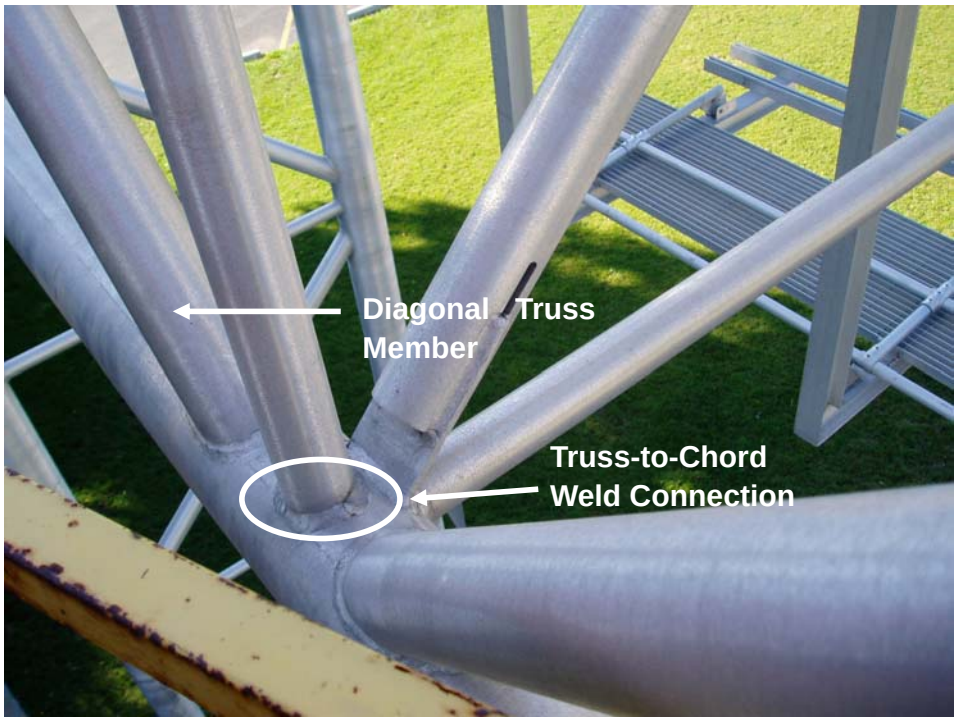

Fig. 3.50 Truss-to-chord weld connection for a box-truss sign structure.

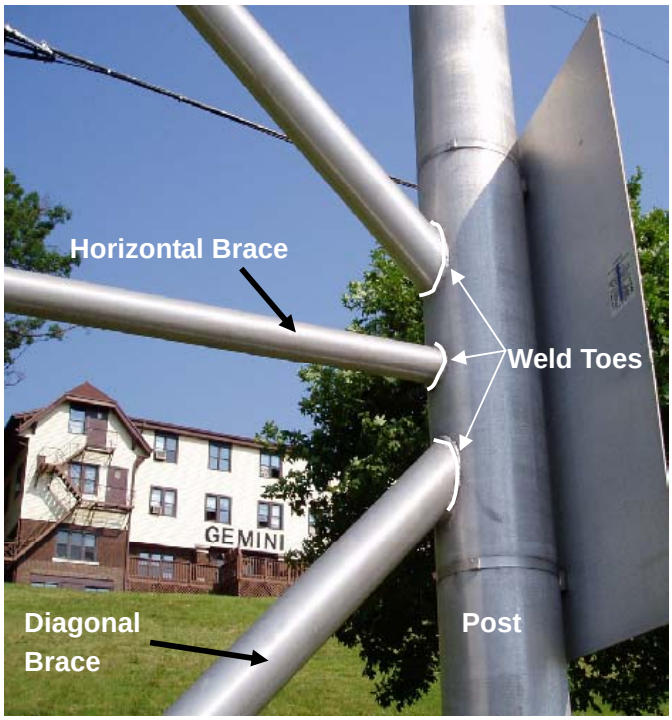

Fig. 3.51 Lateral-braces-to-post connection for a box-truss sign structure.

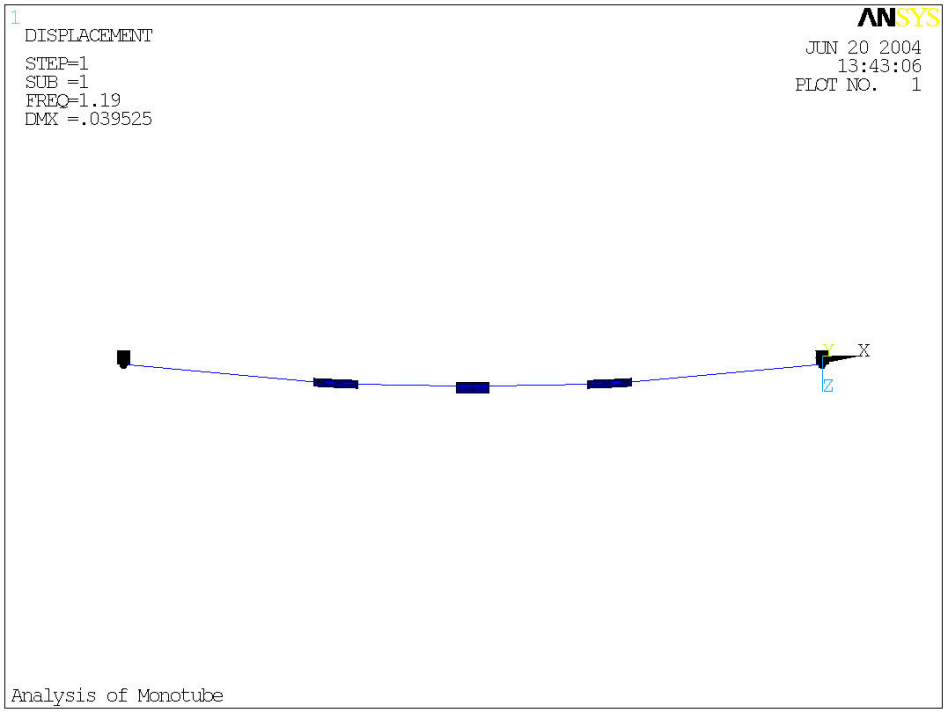

Fig. 3.52 First mode of the monotube sign structure.

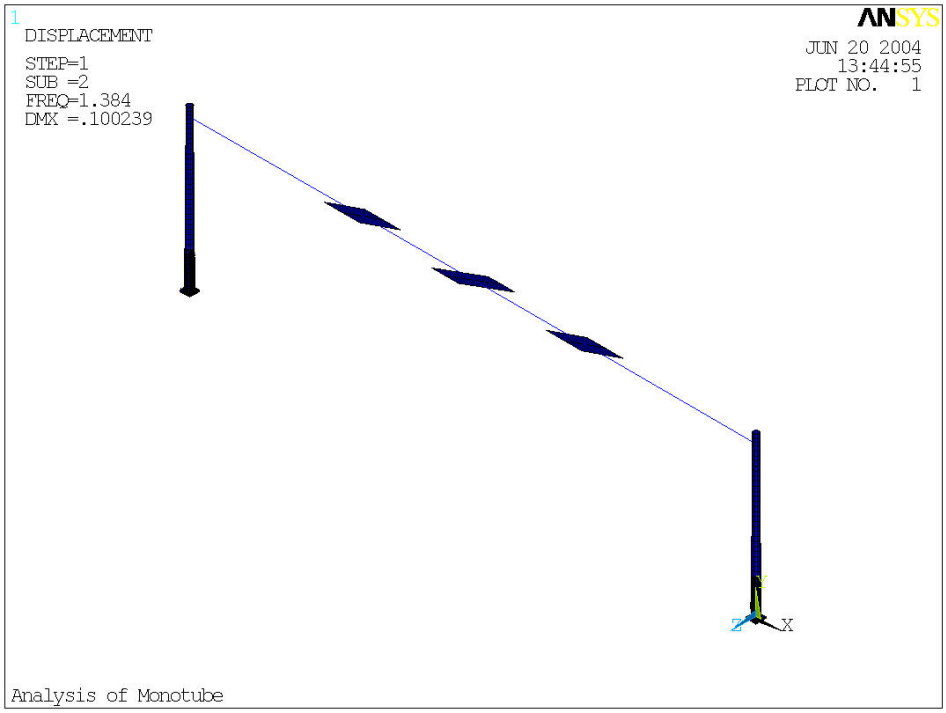

Fig. 3.53 Second mode of the monotube sign structure.

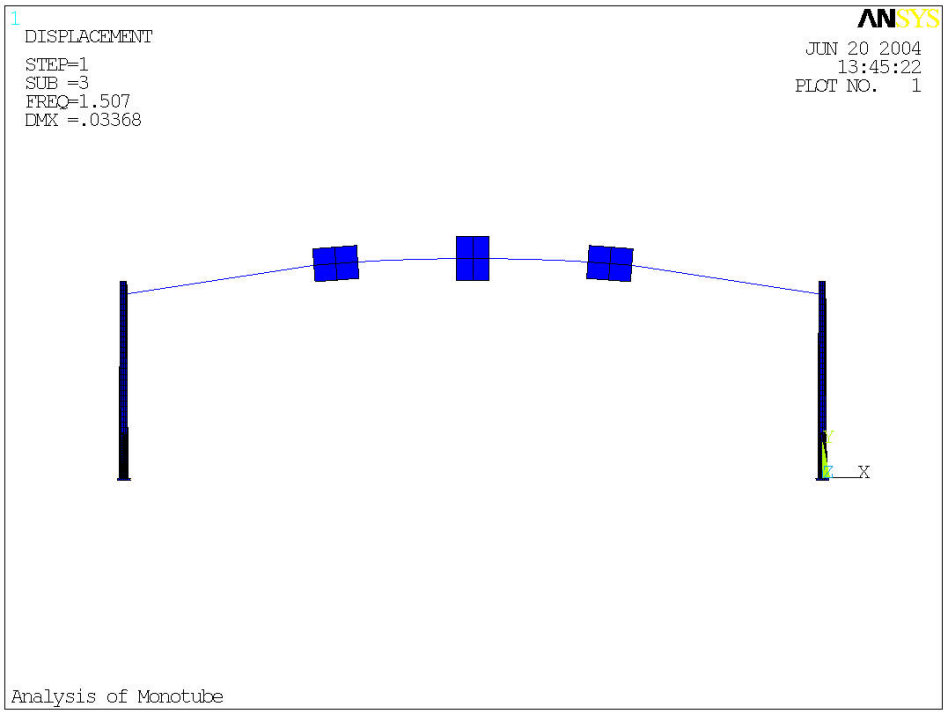

Fig. 3.54 Third mode of the monotube sign structure.

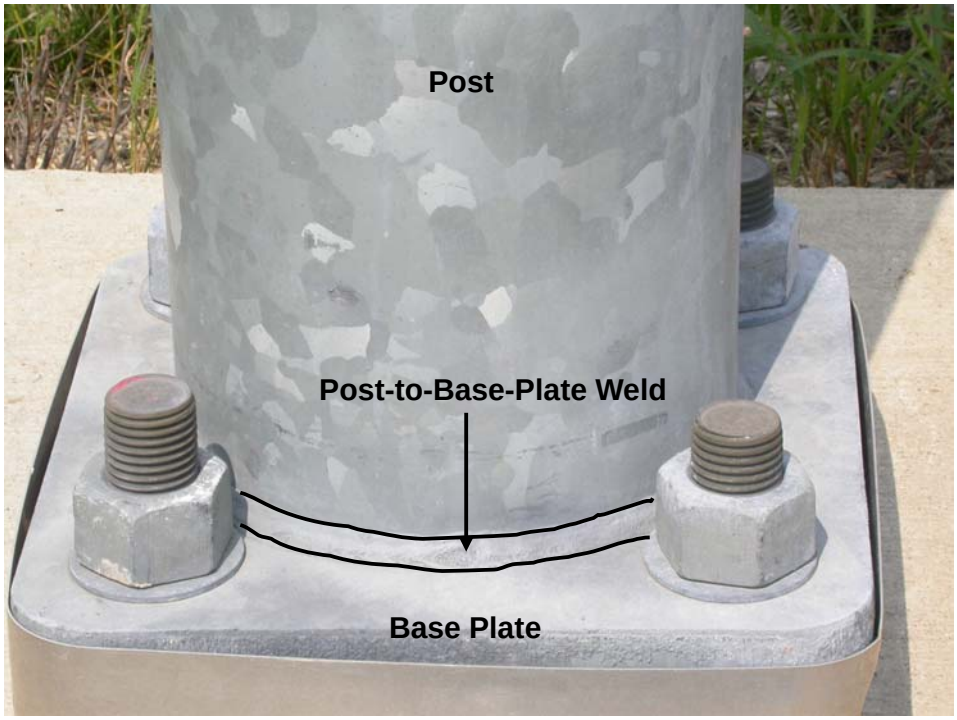

Fig. 3.55 Post-to-base-plate weld detail of a monotube sign structure.

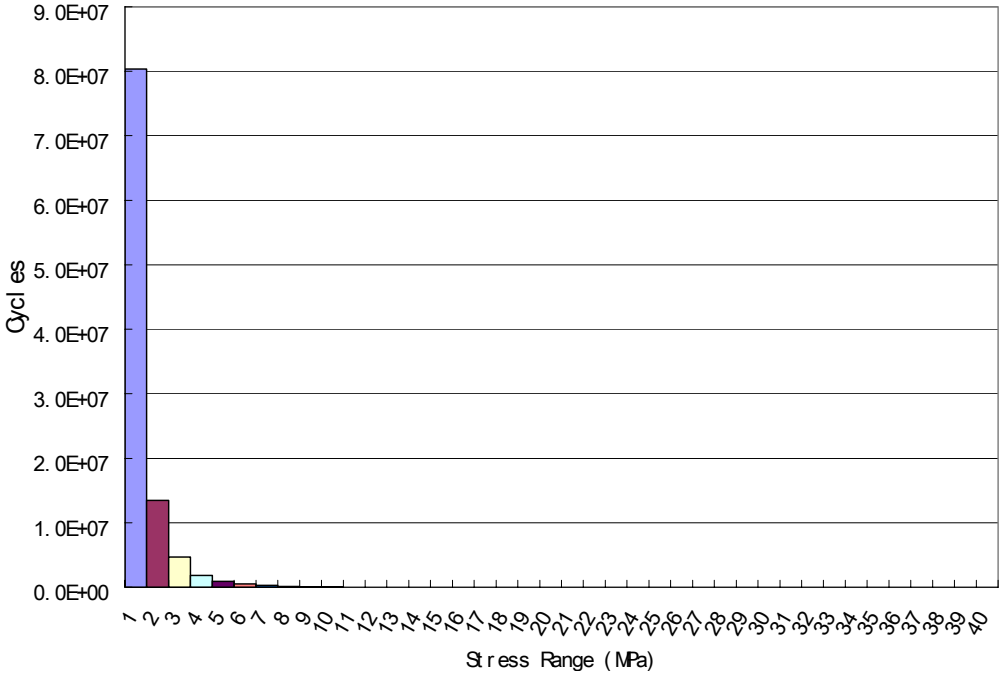

Fig. 3.56 Histogram for post to base plate weld connection.

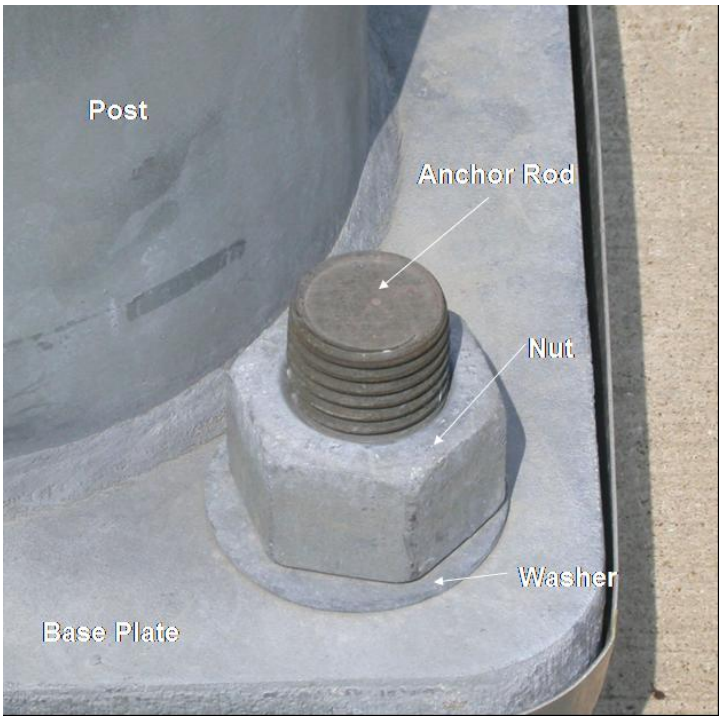

Fig. 3.57 Anchor rods detail of a monotube sign structure.

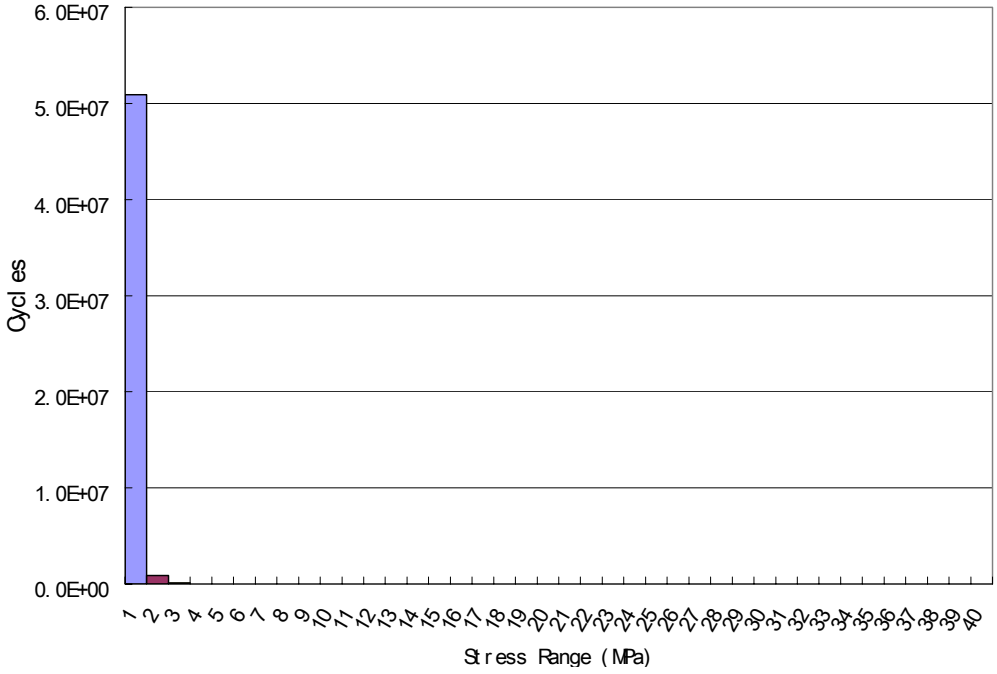

Fig. 3.58 Histogram for anchor rod detail.

Fig. 3.59 Hand hole of a monotube sign structure.

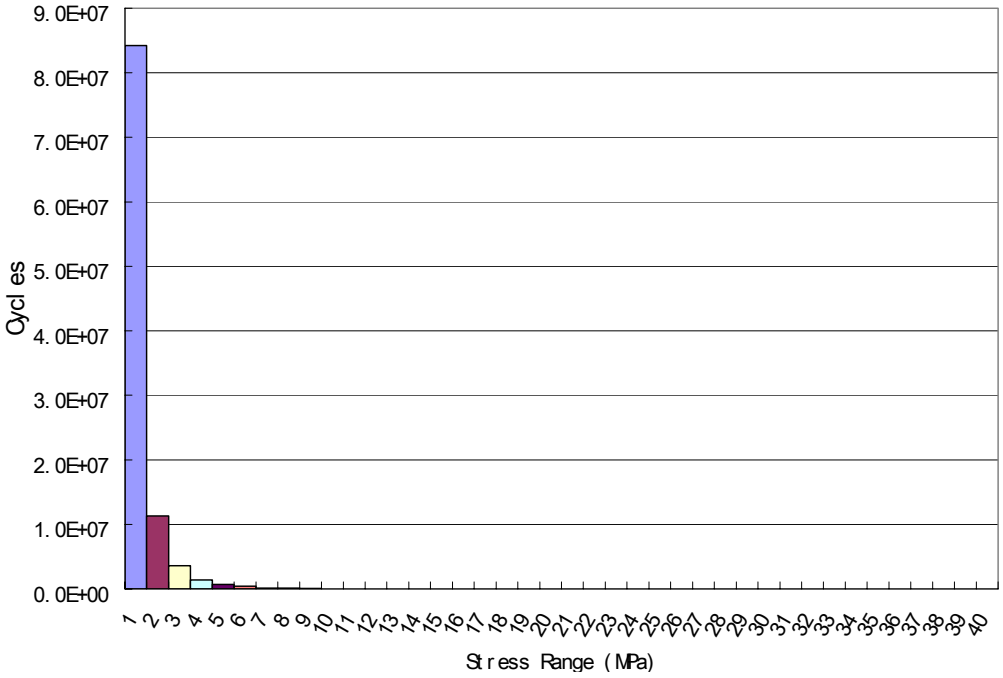

Fig. 3.60 Histogram for hand hole detail.

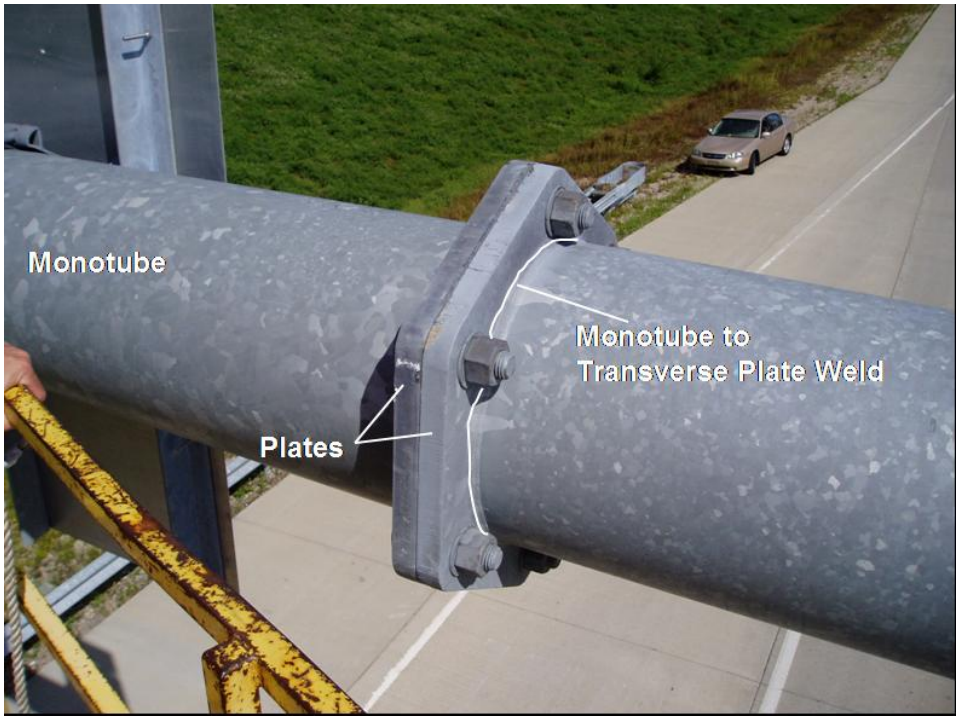

Fig. 3.61 Monotube-to-transverse-plate weld connection for a monotube sign structure.

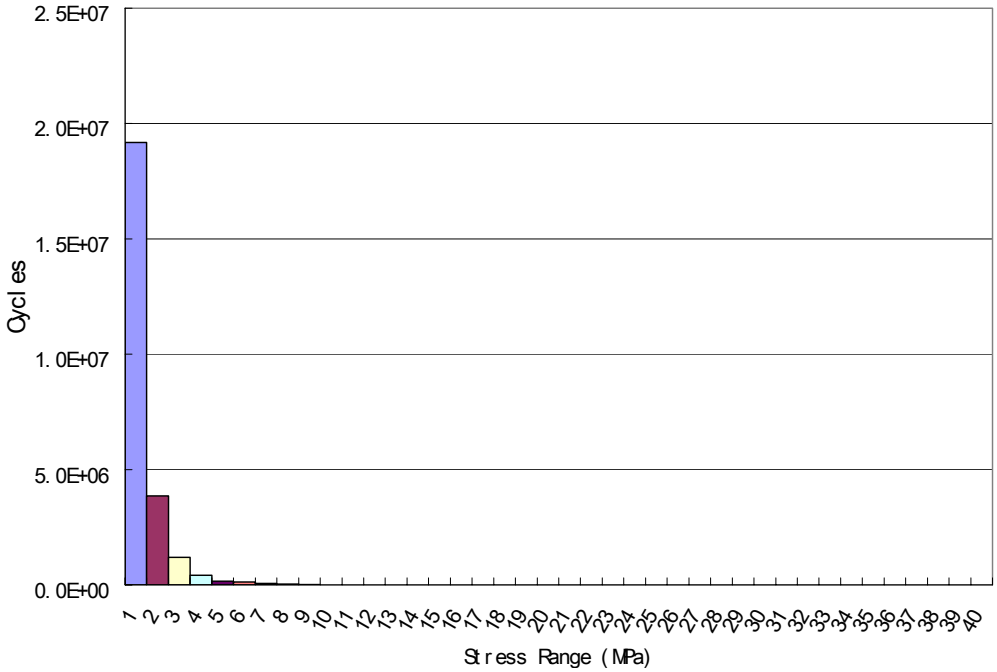

Fig. 3.62 Histogram for monotube to transverse plate weld detail.

Fig. 3.63 Monotube-to-post pin connection for a monotube sign structure.

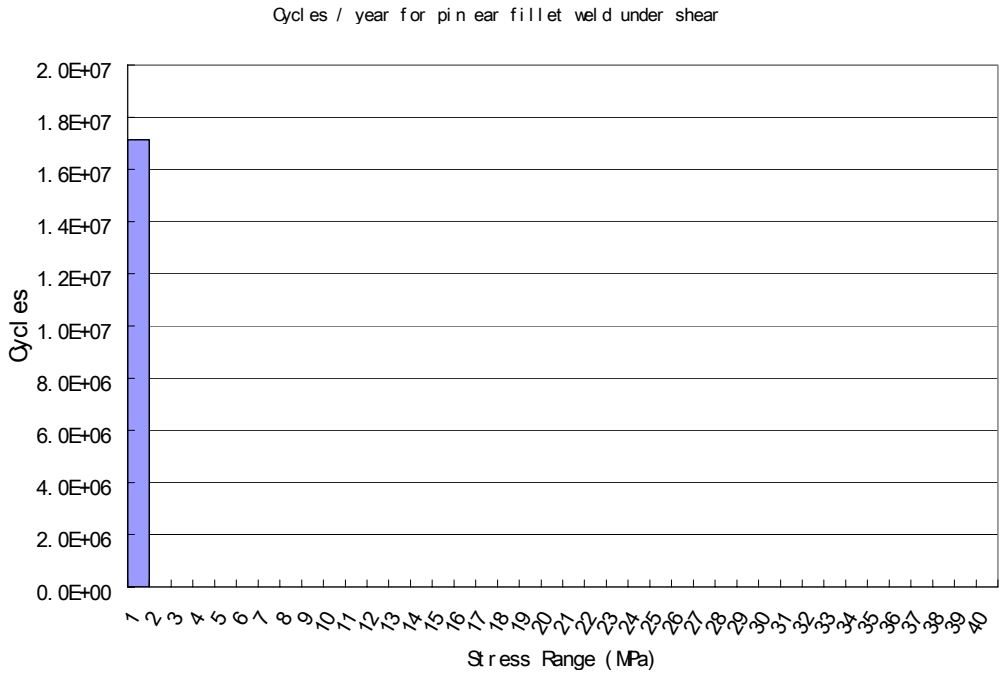

Fig. 3.64 Histogram for the ear to post weld connection.

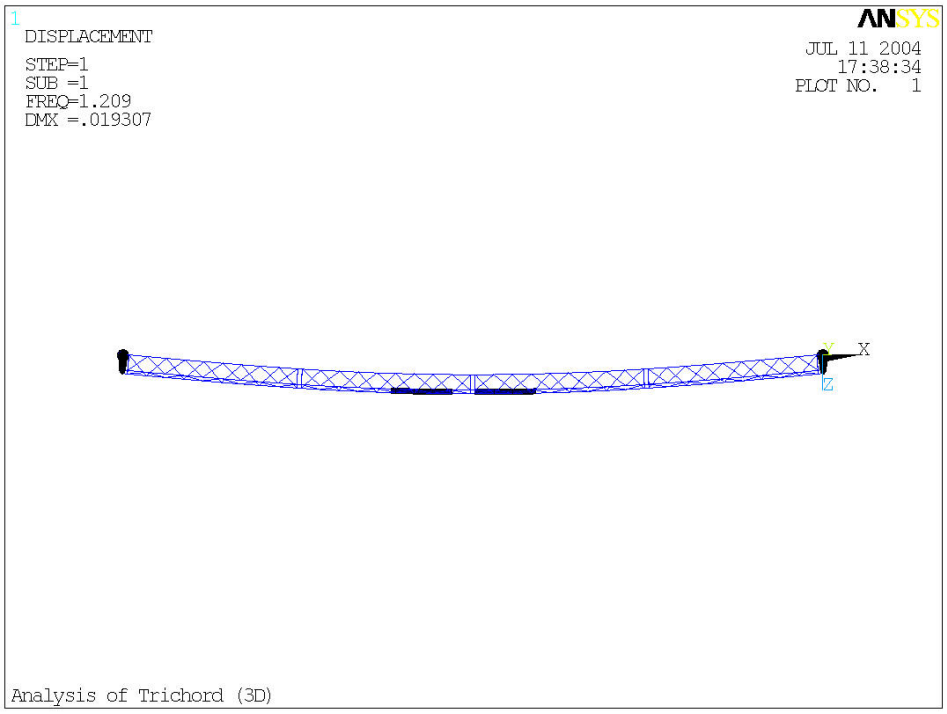

Fig. 3.65 First mode for the tri-chord sign structure.

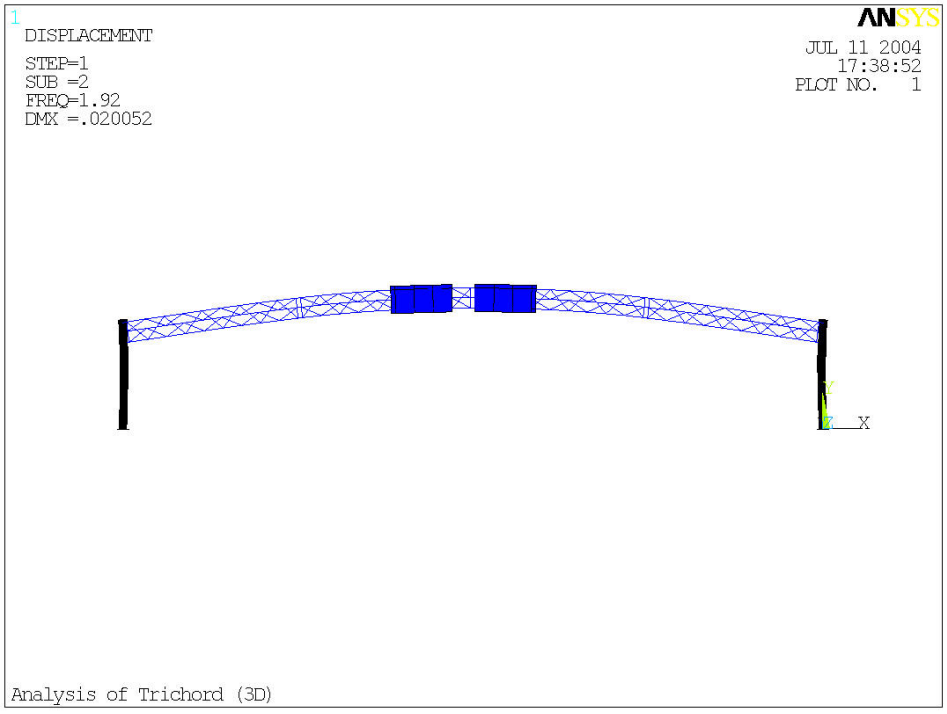

Fig. 3.66 Second mode for the tri-chord sign structure.

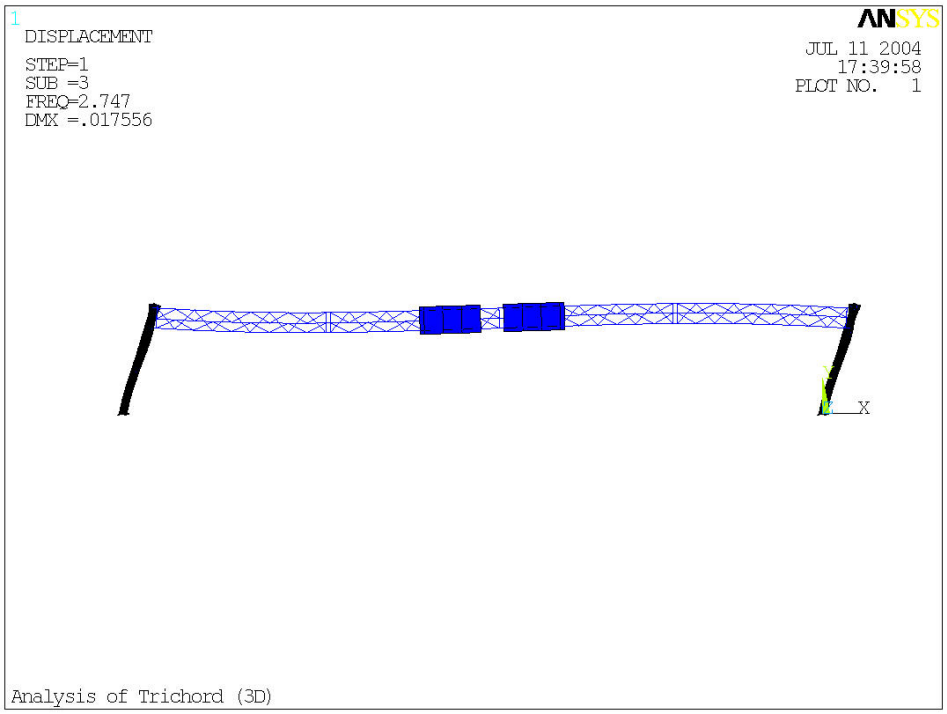

Fig. 3.67 Third mode for the tri-chord sign structure.

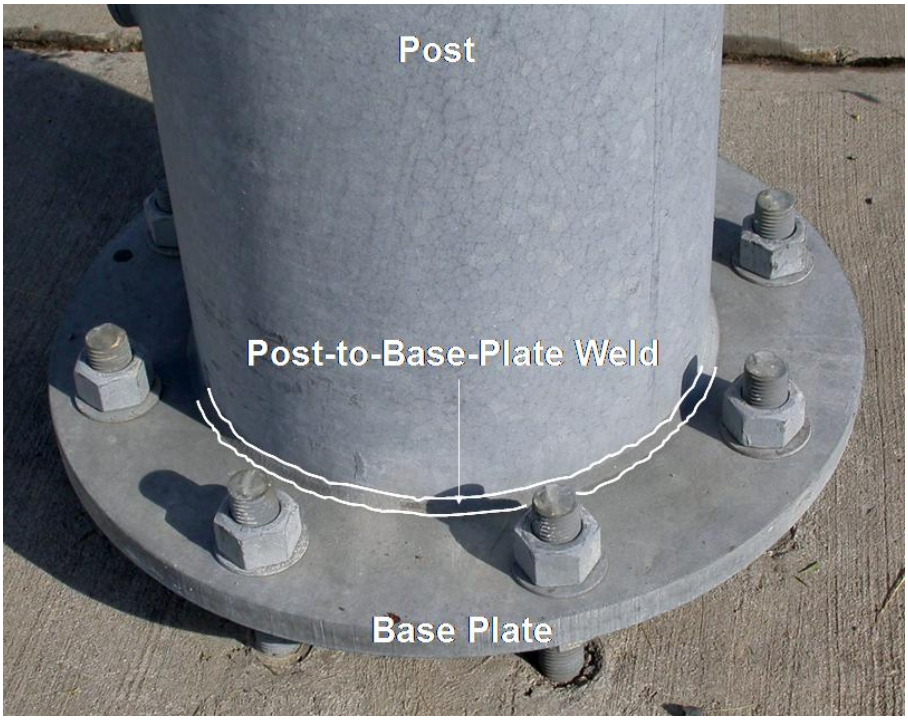

Fig. 3.68 Post-to-base-plate weld connection for a tri-chord sign structure.

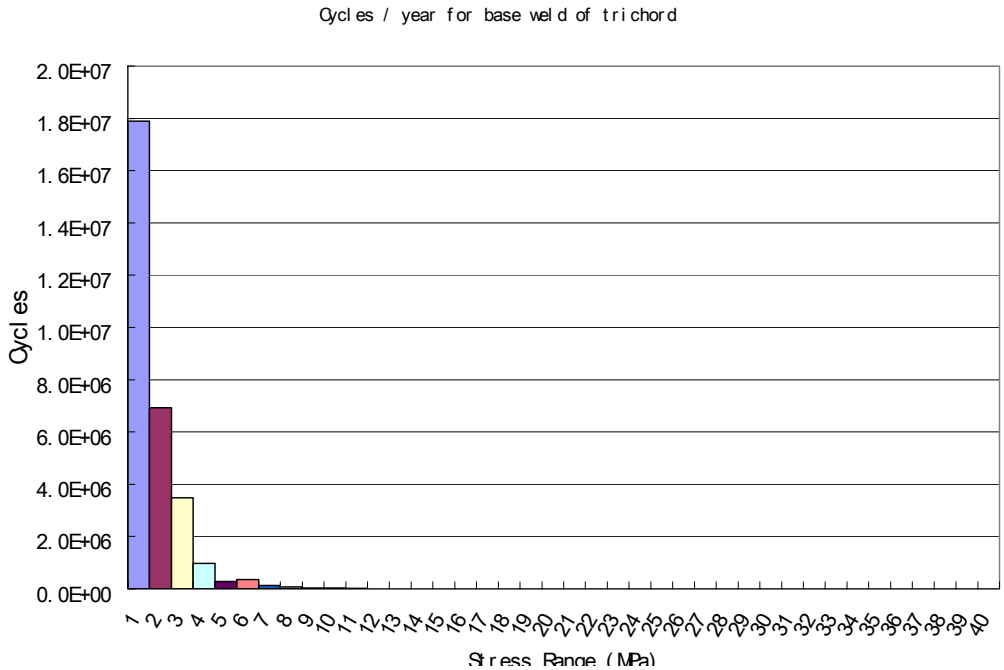

Fig. 3.69 Histogram for post-to-base-plate weld detail of tri-chord sign structure.

Fig. 3.70 Anchor rods detail of a tri-chord sign structure.

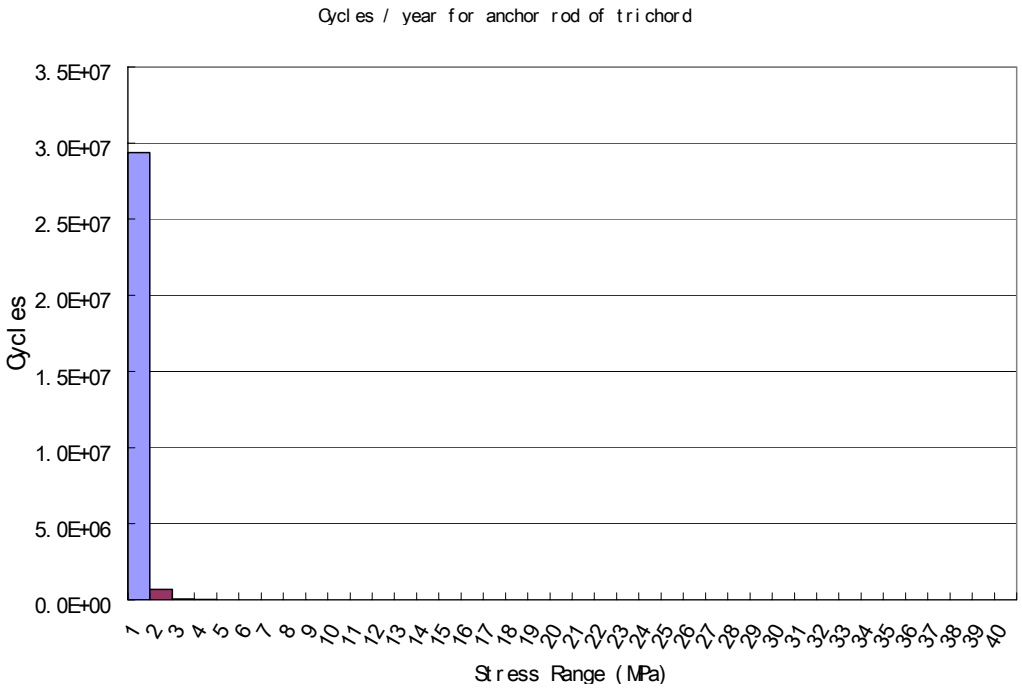

Fig. 3.71 Histogram for anchor rod.

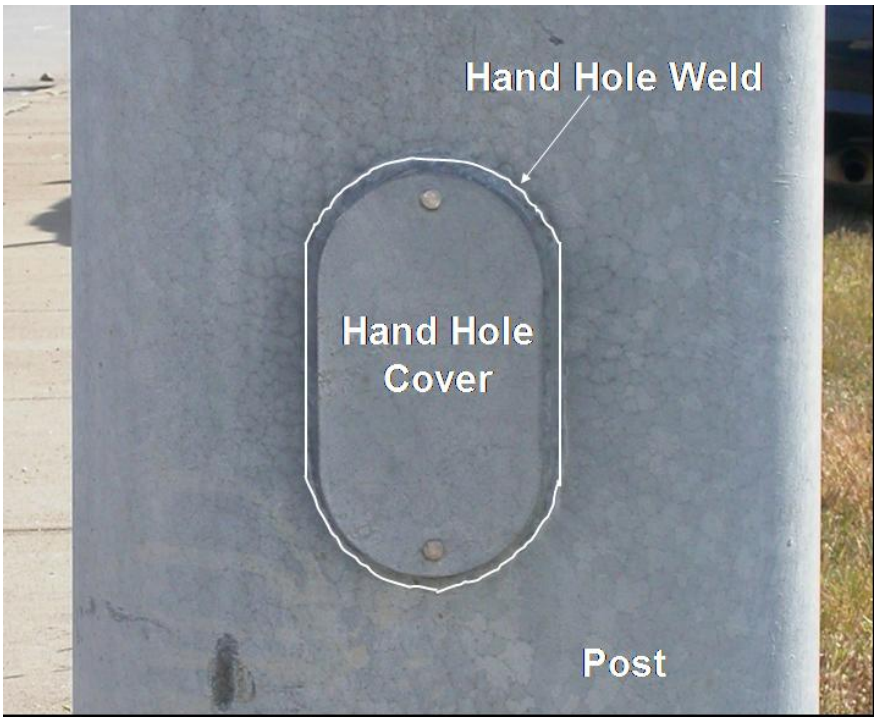

Fig. 3.72 Hand hole of a tri-chord sign structure.

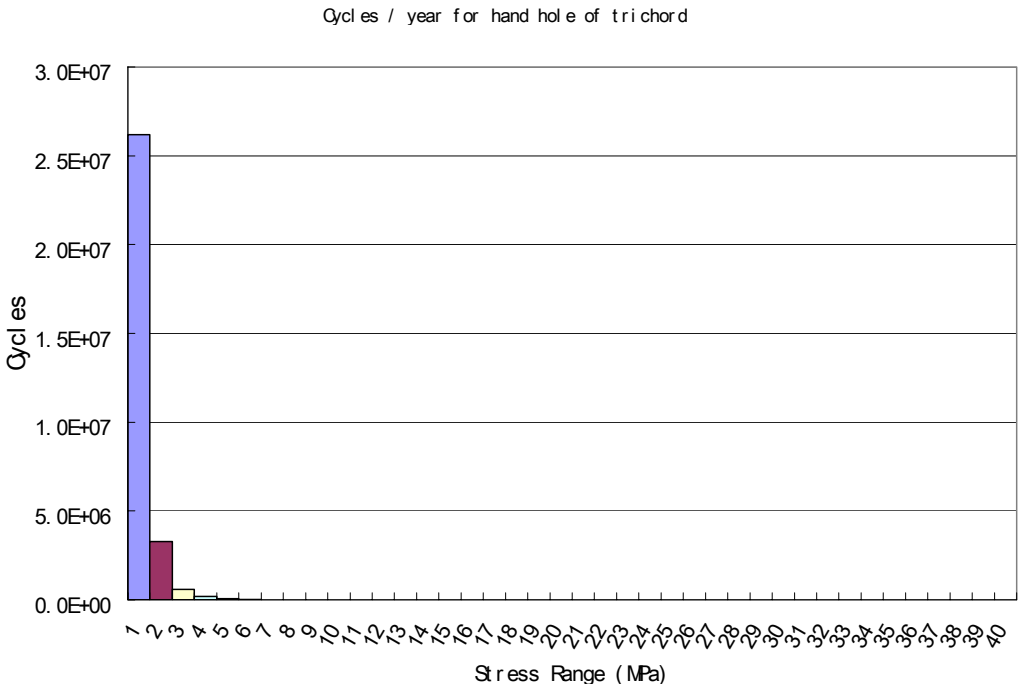

Fig. 3.73 Histogram for hand hole detail.

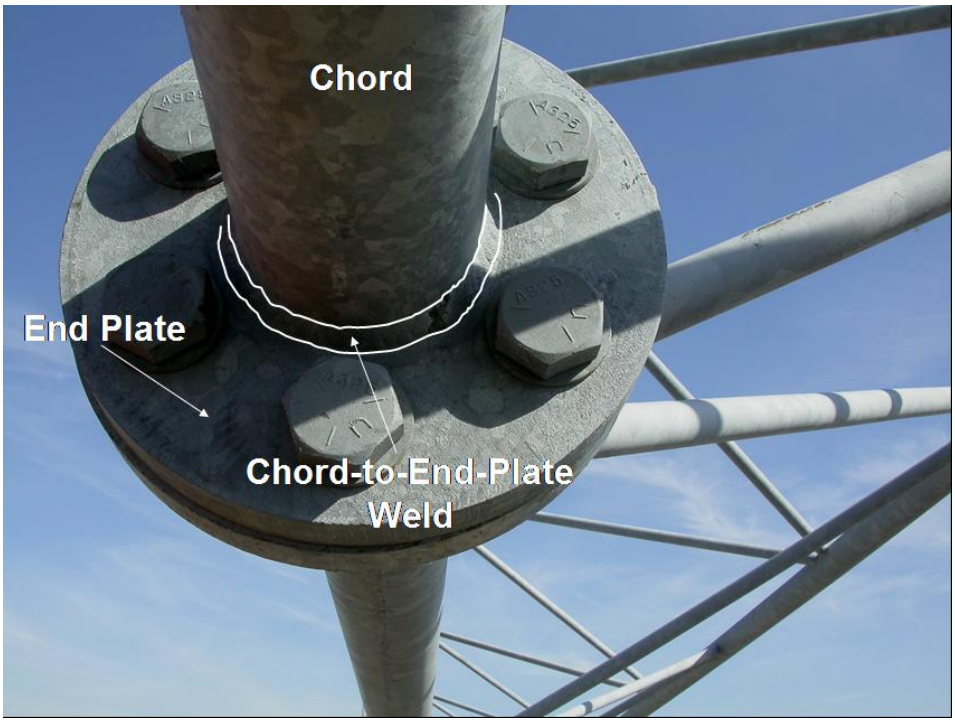

Fig. 3.74 Chord-to-end-plate weld connection for a tri-chord sign structure.

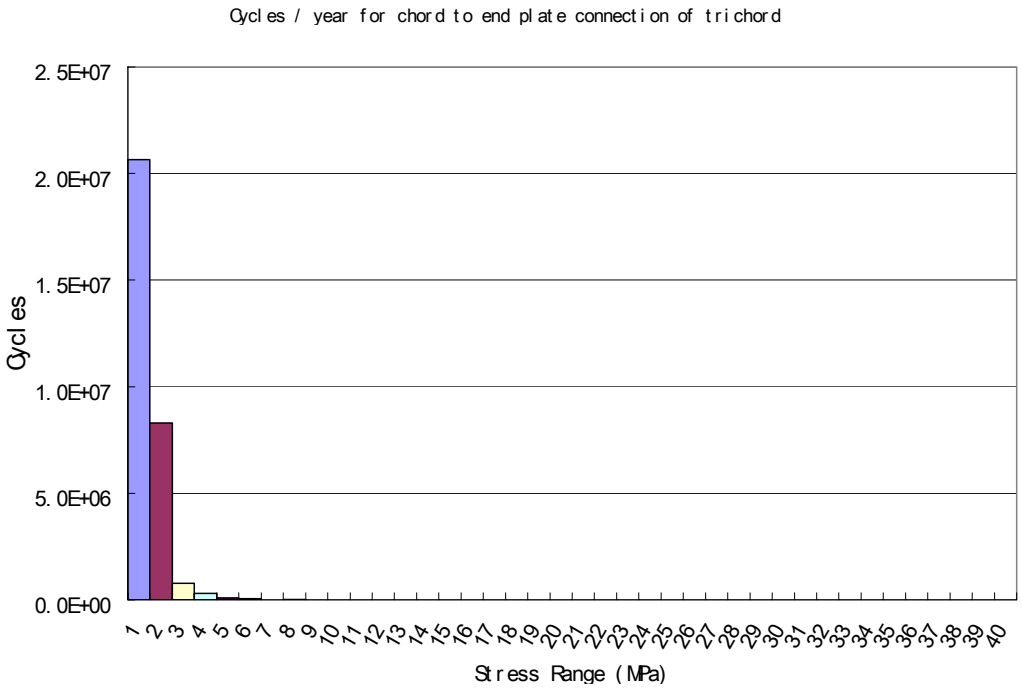

Fig. 3.75 Histogram for chord to transverse plate weld connection at middle span.

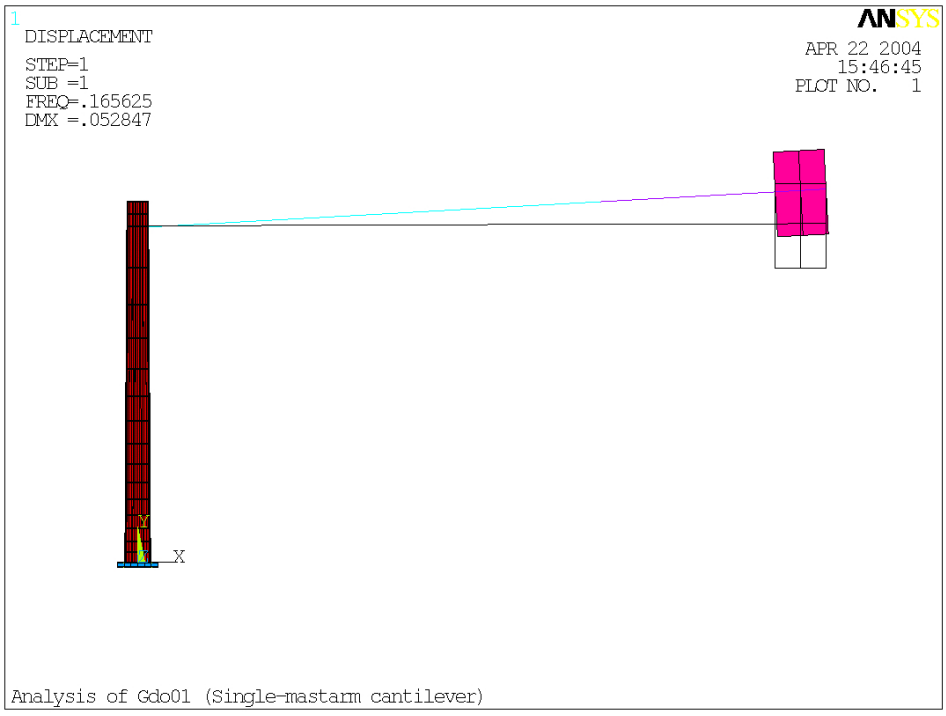

Fig. 3.76 First mode of the single-mastarm cantilever sign structure.

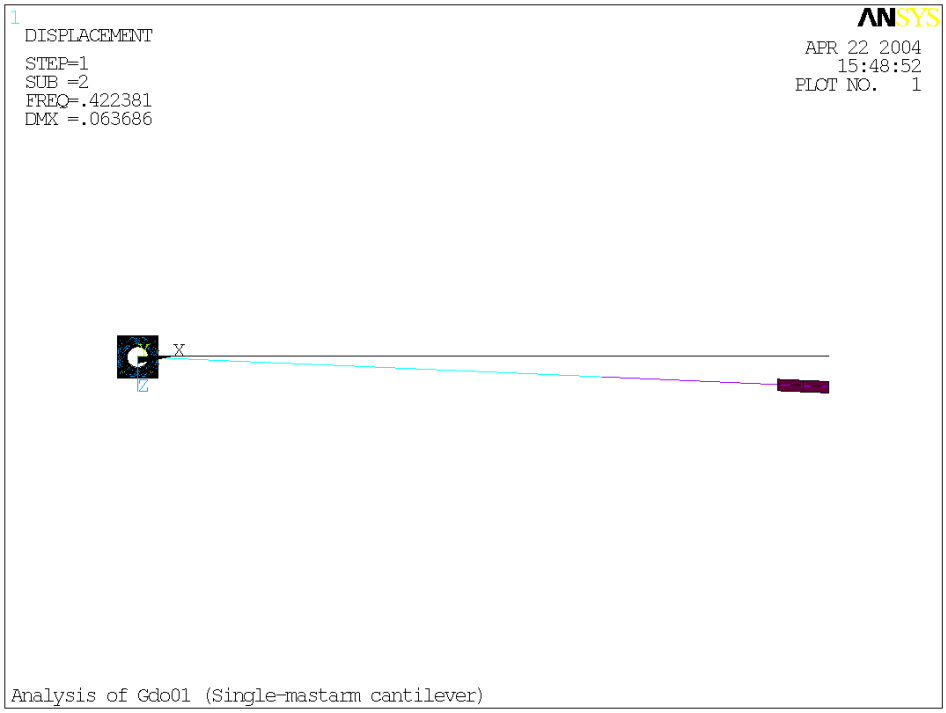

Fig. 3.77 Second mode of the single-mastarm cantilever sign structure.

CHAPTER 4

INSPECTION OF SIGN STRUCTURES

It is very important to detect fatigue damage in sign structures in the field and mitigate that damage to prevent the failures of sign structures. This process is critical to maintain safe operation of roads and highways. A regular inspection program for sign structures with nondestructive evaluation (NDE) methods is the best means to accomplish this task. NDE is briefly introduced in this chapter. Sign structure inspection intervals are suggested based on the results of a literature search, communication with inspection engineers, and analytical considerations. Requirements and the procedures for sign structure inspection and guidelines for component inspection of sign structures are discussed in detail in the second volume of this report titled, "Sign Structure Inspection Manual".

4.1 Introduction of NDE

NDE techniques can be used to detect defects in structural components without damaging the material. The NDE process is discussed by Grandt (2004) and can be summarized as the following: "At first, apply a stimulus, i.e. some form of electromagnetic or ultrasonic energy, to structural components. Sense and record the response in the structural components due to the stimulus. Try to find any indication from the received response and

interpret the meaning of the indication. The indication can be judged based on the interpretation to be a false indication, relevant indication or non-relevant indication. If the indication is a relevant indication, evaluate the indication and make a decision about the condition of the structural components."

The choice of an NDE inspection method can influence the results because every inspection method has inherent advantages and disadvantages. For different inspection situations, the most suitable method needs to be selected. The ideal inspection method should be economical, simple to apply, and reliable. For both bridge and sign structure applications, the inspection method must be convenient for field use by inspection personnel. So the selection of inspection methods should be based on these conditions. Also, the correct application of the technique is an important factor. The inspection personnel need to be well trained to operate any required equipment. Finally, human factors can play a significant role in the effectiveness of NDE methods. The mental attitude of the inspector, for example, can notably influence the outcome of the inspection (Grandt, 2004).

4.2 NDE Methods

This section summarizes the inspection techniques which are often used in sign structure inspection: visual inspection, dye-penetrant testing (PT), magnetic particle testing (MT), and ultrasonic testing (UT). In general, radiographic testing (RT) is not commonly used to inspect sign support structures (Dexter, 2002) and is not included in this section.

4.2.1 Visual Inspection

Visual inspection is the primary method of inspecting for cracks and other irregularities. It can be used independently or combined with other inspection techniques such as PT, MT, and UT. Visual inspection was clearly defined by Spencer (1996) as, "the process of examination and evaluation of systems and components by use of human sensory systems aided only by such mechanical enhancements to sensory input as magnifiers, dental picks, stethoscopes, and the like. The inspection process may be done using such behaviors as looking, listening, feeling, smelling, shaking, and twisting." Visual aids such as light sources or magnification devices may be used to aid in the visual inspection. For inspection of locations which are difficult to access, mirrors or borescopes can also be used.

The visual inspection technique has both advantages and disadvantages. The advantages are that it is a very simple yet very powerful method. However, the results of visual inspection are highly influenced by human factors, including the experience and the capabilities of the inspection personnel (Grandt, 2004). The size of the cracks that can be found is limited by the capability of human eyes. Visual inspection also requires close access - at most an arm's length away - to the inspection location. Additionally, only surface cracks can be found by visual inspection.

In order to minimize the disadvantages, several measures can be employed. A visual inspection should be performed by inspectors meeting the qualifications of the Bridge Inspector's Training Manual (Hartle et al., 1995) to reduce the influence of human factors. If higher sensitivity is needed, a problematic location of the sign structure that has already been

identified by visual inspection can be further inspected by other, more sensitive methods (PT, MT, or UT). For sign structures, a ladder, bucket truck, or reach-all truck can be used to gain close access to the mastarm or truss locations.

4.2.2 Dye-Penetrant (PT) Inspection

Initially, a visual inspection of the sign structure should be performed to assess the overall condition. If it is not clear whether a visual indication is a surface crack or just a false indication, further investigation can be performed using dye-penetrant (PT). When PT is used, the technique and procedure should be in conformance with ASTM E 165 (2002) “Standard Test Method for Liquid Penetrant Examination”.

Dye-Penetrant (PT) is one of the most common and least expensive inspection methods for locating surface defects. This technique is applicable to many types of materials, such as steel and aluminum. In this method, a low-viscosity fluid is applied to the surface of the test object and penetrates into surface cracks. After cleaning and drying of the surface, a developer is then applied to the surface to draw the penetrant fluid from the surface cracks by capillary attraction. The function of the developer is to provide both a contrasting background to view the penetrant indication and enlarge the indication. Through-thickness cracks can be detected if the developer is applied to the opposite surface.

There are two types of penetrants: fluorescent (type I) and non-fluorescent (type II). Fluorescent penetrants need to be viewed under ultraviolet light in a darkened room. Non-fluorescent penetrants can be viewed under visible light. The penetrant removal methods

can be classified as the following (Grandt, 2004): water-washable penetrant (method A), oil-based emulsifiers (method B), solvent-removable penetrant (method C), and water-based emulsifier (method D). The developers come in the following forms (ASTM, 2002): dry powder developers, aqueous developers, non-aqueous wet developers, and liquid film developers. By using different combinations of penetrant, penetrant removal method, and developer, the PT examination can be made suitable for any specific application.

For the field inspection of sign structure welds, two combinations are available: solvent-removable visible penetrant (type II and method C) and water-washable visible penetrant (type II and method A). The first combination is portable in the field and sensitive, but solvent penetrant removal can be labor-intensive. The second combination is the quickest and least expensive method, but it is the least sensitive method of all the penetrant inspection methods.

When used correctly, PT is a reliable method for detecting surface cracks on smooth surfaces. Additionally, it is inexpensive and requires less skill than MT and UT. However, inspection of sharp corners and complex shapes may be a challenge for PT. It is often difficult to distinguish between a crack and the plate/weld toe interface. Also, PT is somewhat labor-intensive should not be applied on too many locations of a sign structure.

4.2.3 Magnetic Particle (MT) Inspection

Before the use of magnetic particle (MT) in a sign structure, a visual inspection should be conducted to assess the overall condition. If a visual indication needs to be

identified as a crack or just a false indication, further investigation can be performed using MT. When MT is used, the technique and procedure should be in conformance with ASTM E 709 (2001) “Standard Guide for Magnetic Particle Examination”.

In a magnetic particle (MT) inspection, a ferromagnetic test piece (i.e. a steel plate) is magnetized by one of several methods (Grandt 2004) employing magnets or an applied electrical current, thus forming a magnetic field in that test piece. When the magnetic field in the test piece encounters a discontinuity, the magnetic field is distorted. Fine magnetic particles are sprayed or dusted on the test piece in order to detect the distortions. The particles should not be attracted to the test piece before it is magnetized and should be easily magnetized by the magnetic field in the test piece. There are two types of magnetic particles: dry particles and wet particles. Dry particles can work well on rough surfaces and for subsurface flaws. However, they are not sensitive to very small cracks. Wet particles are best used for detecting small surface cracks.

MT can be used to detect small surface or sub-surface defects if the depth of the defects is not too great. The necessary equipment is portable and easy to use in the field. Other advantages are that MT requires very little training to use and the inspection results can be easily interpreted. The major disadvantage of MT for weld inspection is that this method works most effectively on smooth surfaces. Hence, the accuracy of MT is reduced when used on irregular weld surfaces. But reasonable results can be obtained by an experienced inspector (Fisher, 1998).

4.2.4 Ultrasonic Inspection (UT)

Ultrasonic Inspection (UT) can also be used as a follow-up to visual inspections of the sign structure when an in-depth investigation is needed. UT is particularly useful for locating subsurface cracks and other discontinuities. When UT is used, the technique and procedure should be in conformance with ASTM E 164 (2003) "Standard Practice for Ultrasonic Contact Examination of Weldments".

UT uses sound waves at frequencies that range between 200 kHz and 25 MHz (Grandt, 2004) and are inaudible to the human ear. The sound waves are introduced into the test object at various surface locations by ultrasonic transducers. These waves travel through the test object and are received by other transducers. If a defect is in the propagation path of the sound waves, the received sound waves will be changed. Interpretation of the reflection and refraction of these sound waves at a particular surface can provide information about the size and location of defects in the test object.

Ultrasonic waves can travel in many materials, allowing UT to be widely used. Both surface and sub-surface cracks can be detected by UT. It is sensitive to even relatively small cracks. Only one side of the test object needs to be accessible for UT to be performed, although it is best if both sides are accessible. Additionally, portable equipment is available for field use. However, UT requires a high degree of skill and training to operate the equipment and understand the inspection results, which will substantially increase the cost of inspection. Rough surfaces may also reduce the accuracy of UT.

UT was used by the Michigan Department of Transportation to confirm the presence of cracks that were visually found at the end of the horizontal gusset plate connections (Cook et al., 2000). In conjunction with this effort, the "Procedure for Ultrasonic Testing of Gusset Plates on Cantilever Sign Supports" was developed for finding fatigue cracks and documenting the results.

4.3 In-Service Inspection of Sign Structures

Inspection of sign structures is essential to maintain their safety. It is required in the Standard Specifications for Structural Supports for Highway Signs, Luminaires and Traffic Signals (AASHTO 2001). Section 2.7 of that standard states that, "A regular maintenance program should be established that includes periodic inspection, maintenance, and repair of structural supports."

The effectiveness of sign structure inspection depends on good safety procedures, a well-developed inspection plan, and appropriate inspection methods. Sign structures should be inspected by trained inspectors who have an understanding of the load paths of the structure and the particular types of defects that could be expected in these structures. The inspection should be thorough to ensure that a complete examination of all critical components is achieved.

Inspection is a difficult and expensive process. It is not realistic or practical to inspect every portion of a sign structure for fatigue cracking with equal effort since the time and money that can be devoted for inspection is typically quite limited. Consequently, analytical

studies were conducted as part of this research to identify the details that are most susceptible to fatigue cracking. Accordingly, inspection of these areas should help to focus the inspection on the high-risk regions of sign structures, so as to facilitate the inspection and reduce the cost.

Requirements and the procedures of sign structure inspection, as well as guidelines for inspection of important sign structure details, are presented in detail in the "Sign Structure Inspection Manual" attached as a second volume of this report.

4.4 Inspection Frequency

The choice of interval for sign structure inspection is a very important issue that will have a significant impact on both the safety of sign structures and the cost of labor and equipment for inspection. An effort was made to study the inspection interval needed. The recommended inspection interval involves two aspects: a one-time initial inspection followed by a series of routine inspections. The initial inspection is concerned with detecting fabrication deficiencies, while the routine inspection assumes excellent fabrication and weld quality and is aimed at detecting routine fatigue damage. Both of these aspects of inspection are discussed below.

The one-time initial inspection is recommended to occur after the sign structure has been in service for at least two years. Not to be confused with an inspection that may occur in conjunction with the construction phase, the one-time initial inspection is an inspection that is conducted to detect the onset of any cracks or damage that may be the result of poor

fabrication quality or welding defects. The belief is that a serious flaw present during manufacturing the sign structure would result in a sizable crack that would manifest itself after a two-year period. The initial inspection is recommended for all sign structures, regardless of the type of sign.

After the one-time initial inspection, the sign structure would then be inspected on a regular interval. Based on an analytical evaluation of the fatigue life of different types of sign structures under natural wind loading, recommendations for maximum inspection intervals were developed. Sign structures were classified into two groups, Class A and Class B, according to the estimated severity of the fatigue damage caused by wind loads. Double-mastarm cantilever sign structures and single-mastarm cantilever sign structures belong to Class A. They are more susceptible to wind-induced fatigue damage than are other sign structures. Based on a review of many states' practice included in NCHRP report 469 (Dexter, 2002) and calculated fatigue lives in this research, it is recommended that Class A sign structures be inspected at least once each 4 years.

Overhead bridge structures (including tri-chord and box-truss sign structures) and monotube sign structures are classified as Class B. They are less susceptible to wind-induced fatigue damage. It is suggested that Class B sign structures be inspected at an interval of no more than 8 years according to NCHRP report 469 (Dexter, 2002).

4.4.1 Crack Propagation Calculation for Inspection Interval

Two analyses of fatigue crack propagation were conducted to evaluate the

recommended inspection intervals. For the first analysis, it is assumed that an initial elliptical 1.0 in. edge crack with a depth of 0.4 in. exists in the post-to-base-plate weld toe of a double-mastarm cantilever sign structure located at Fort Wayne, Indiana without being detected by visual inspection. The 1 in. length is a reasonably large crack size that could still possibly be missed in a visual inspection. The depth of 0.4 in. was selected because it is almost a through-post-wall crack and represents a very critical situation. In addition, the location of Fort Wayne was chosen since the wind environment there was found to be the most likely to produce short fatigue lives. At the first stage, the initial crack will propagate as an elliptical crack. After the depth of the crack reaches the thickness of the post wall, it will grow as a through-crack in the second stage to fracture.

Linear elastic fracture mechanics crack growth procedures were used to estimate the remaining life of the cracked member. An appropriate stress intensity factor K is defined as (Bannantine et al, 1990):

$$K = f(g)\sigma\sqrt{\pi a} \qquad (4.1)$$

where σis the applied remote stress in ksi, f(g) is a dimensionless geometric parameter, and a is the crack size in inches. For variable-amplitude loading, the applied stress range can be replaced by equivalent stress range $\Delta\sigma_e$ (Moses et al., 1987) and K can be replaced by stress intensity factor range ΔK.

In the first stage, when the crack is assumed to be an elliptical edge crack, the f(g) variable can be approximated as (Albrecht, et al. 1977; Delft, et al. 1986):

$$f(g) = F_E F_S F_W F_G \qquad (4.2)$$

where F_E is a correction for an elliptical crack front, F_S is the correction for free surface

(=1.12), F_W is the correction for finite width, and F_G is the correction for geometry (=1.0 according to Delft et al. (1986)). In the second stage, the crack is assumed to be centered on a finite-size center-cracked plate with a discontinuous geometry of fillet weld under tension. The factor f(g) can be represented as (James, 1976; Albrecht, 1977):

$$f(g) = F_G\left[1.77 + 0.277\left(\frac{2a}{W}\right) - 0.51\left(\frac{2a}{W}\right)^2 + 2.7\left(\frac{2a}{W}\right)^3\right] \qquad (4.3)$$

where W is the width of the plate (18 in. was used), and F_G is the geometry correction factor (2.1 was used for fillet weld toe (Delft, 1986)).

The growth rate behavior of a crack in structural steel can be idealized by three distinct phases: slow crack growth, stable crack growth, and rapid crack growth (Moses et al., 1987). These phases can be represented as straight lines in a log-log plot of da/dN versus ΔK (crack growth per cycle). A typical da/dN versus ΔK plot (Fuchs and Stephens (1980)) is shown in Fig. 4.1. The left boundary line is parallel to Y axis representing crack growth threshold ΔK_{th}. If ΔK is below this level, no crack growth occurs. ΔK_{th} is assumed to be 6.5 ksi$\sqrt{in}$ for structural steel (Moses et al., 1987). The right boundary line is also parallel to Y axis representing fracture toughness K_c. When the stress intensity factor reaches K_c, fracture occurs. For structural steels with yield strengths up to 50 ksi, K_c is roughly 50 ksi$\sqrt{in}$ (Moses et al. 1987). For the structural steels and weldments in these steels, the sloping central portion of the curve can be defined as (Barson and Rolfe, 1999):

$$\frac{da}{dN} = 3.6\times10^{-10}\,\Delta K^3 \qquad (4.4)$$

Based on Equation 4.1, 4.2, 4.3 and 4.4, the crack propagation can be calculated with a stress range histogram of the structural detail.

A natural wind load time history for a double-mastarm cantilever sign structure located in Fort Wayne, Indiana (as described in Chapter 3) was assumed to be the typical wind load time history for the crack propagation calculation. Then the stress range histogram presented in Chapter 3 was used in this calculation and was assumed to repeat for every year. The equivalent stress range for this stress time history was calculated to be 17.4 MPa (2.52 ksi) with a total cycle number of 985,663 for a year. The crack propagation calculation was conducted following the procedure proposed by Barson and Rolfe (1999). In the first stage, it took 3 years for the elliptical crack to reach the thickness of the post wall and the crack grew to 31.8 mm (1.25 in.). In the second stage, it was computed that the crack grew from 31.8 mm to 44.7 mm (1.25 in. to 1.76 in.) after 2.4 years and the crack reached the fracture point under the maximum stress range of 105 MPa (15.23 ksi).

A similar calculation was also performed for an initial crack with a different aspect ratio (size). In research conducted by Hassan and Bowman (1996), it was found that elliptical cracks typically had a length-to-depth ratio of 4 over 1 for cover plate details. So the initial crack was assumed to have a length of 1 in. and a depth of 0.25 in. It is obvious that this crack is not as critical as the previous crack due to smaller initial depth. Other assumptions are the same as the previous calculation. Following the same calculation procedure, it was found that this crack fractured during the first state, which was the elliptical crack stage. The final crack size was 50.7 mm (1.997 in.) in length and 12.7 mm (0.499 in.) in depth. It took 19 years for the final crack size to be reached under the typical wind load time history.

According to the first calculation, even for a cracked member with an initial crack size of 1 in. in length and 0.4 in. in depth under the most critical wind situation in Indiana, the

remaining life of the post-to-base plate weld connection would still allow at least one inspection to detect the crack. So the recommended inspection intervals are reasonable in this perspective.

The second calculation shows that if the initial crack size is not as severe as the size in the previous calculation, it is expected that 4 or 5 inspections will be conducted before rapid crack extension occurs, dramatically increasing the likelihood of finding the crack prior to failure. In addition, less critical sign structure types (the sign structures other than single and double-mastarm cantilever sign structure) and less critical locations (the locations other than Fort Wayne) will also help to significantly increase the number of times of inspection allowed and improve the chances of detecting cracks before failure.

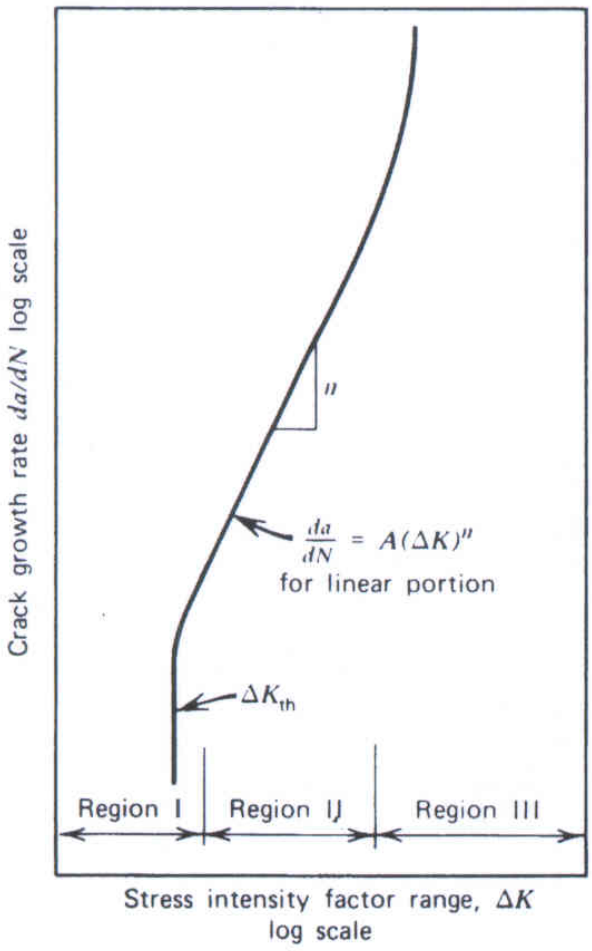

Fig. 4.1 Crack Growth versus Stress Intensity (Fuchs &Stephens 1980).

CHAPTER 5

CONCLUSIONS

5.1 Summary and Conclusions

Analytical research was performed on wind load simulation, dynamic stress analyses and fatigue analyses for five types of sign structures, including double-mastarm cantilever sign structures, box-truss sign structures, monotube sign structures, tri-chord sign structures, and single-mastarm cantilever sign structures. Important conclusions drawn from the analytical results are summarized as follows:

- The details of the double-mastarm cantilevered sign structure that produced the lowest fatigue lives, in ranked order from the shortest life to the greatest life, are: post-to-base plate socket welded connections, fillet welds in the built-up box connections, chord-to-end plate socket weld connections, and hand hole connections. The same order was obtained at all six geographic locations in Indiana considered in this research.
- The anchor rod, strut-to-gusset plate welded connection, and gusset plate-to-chord weld connection of the double-mastarm sign structure were all found to have essentially infinite lives. Finite fatigue lives can occur, however, if less than ideal fabrication and/or construction conditions occur.

- The computed fatigue life for given details in a sign structure varied considerably at different geographic sites. Variations in life were primarily due to significant differences in the wind environment at various sites, which reflected differences in the mean wind speed distribution at each site. Sign structures in Fort Wayne, Indianapolis and South Bend were generally found to have the shortest fatigue lives among the six locations in Indiana, while sign structures in Bloomington were found to have the longest fatigue lives. These results agree well with the predictions based on wind speed distribution curves from a Weibull distribution. It was observed that the main portion of the wind probability curves for Fort Wayne, South Bend, and Indianapolis were shifted right to relatively higher wind speeds as compared with the curves of Evansville and Bloomington. Consequently, it was found to be more likely for relatively higher wind loading to occur in Indianapolis, Fort Wayne and South Bend, which could lead to shorter fatigue lives.
- The life expectancy of the details in double-mastarm cantilever sign structures, when less than 50 years, was found to be greater by 13% to 37% when a VAFL approach per the AASHTO LRFD Bridge Specification was used in the damage prediction compared with the life predicted by an extension of the straight-line S-N curve. The variations in fatigue lives reflect the impact of fatigue damage caused by the stress cycles between the VAFL and the CAFL. The medium range stress cycles have a more significant impact on the fatigue life of the sign structure connection details for longer fatigue lives.
- Based on the results of the sensitivity investigation, it can be concluded that the variation in the cyclic fatigue lives with respect to different sets of simulated loads is reasonable

and at a comparable level with the results from a welded connection testing program.

- Galloping rather than natural wind may be the most critical loading to cause major fatigue damage to the single-mastarm cantilever sign structure.
- According to the dynamic analyses and fatigue analyses results of the sign structures, the major structural details in the box-truss sign structure, the monotube sign structure and the tri-chord sign structures sustain little wind-induced fatigue damage. It can be concluded these three types of sign structure are generally not as critical as the double-mastarm cantilever sign structure.
- In the box-truss sign structure, the chord-to-transverse-plate welded splice connection is more critical than the other major details. However, fatigue lives in excess of 50 years were obtained, which is a typical service life for such structures.
- In the tri-chord sign structure, the post-to-base-plate weld connection is more critical than the other details. However, fatigue lives were found to be longer than 50 years.
- Sign structures should undergo an initial inspection within two years after construction, followed by a regular periodic inspection. The initial inspection is intended to catch any weld connection detail problems that may become evident after the sign structure has been in service for a short period of time and has experienced a few significant loading events. The periodic inspection should then occur once every four years for the single-mastarm and double-mastarm cantilever sign structures, and once every eight years for the box-truss, monotube and tri-chord sign structures. Calculated fatigue lives based on a crack propagation analyses were found to be longer than the recommended sign structure inspection intervals.

5.2 Implementation of Study Results

The present study has examined the fatigue behavior of several different prototype Indiana sign structures subject to various wind loading environments. Based upon this examination the most critical detail locations with respect to fatigue and fracture in the sign structures included in this study were identified and an inspection guideline was prepared. Moreover, a plan for inspecting various types of sign structures was proposed based upon the crack propagation behavior of the prototype sign structures. The inspection plan and the inspection guide can be used as a starting point for formulating an inspection program and to help train inspectors who will be examining sign structures.

5.3 Suggested Future Work

Several aspects of this research merit future investigation. Based on the current study, the following future work is suggested:

- A new method to simulate the effect of galloping for single-mastarm cantilever sign structures is needed to accurately evaluate the fatigue performance. In the current research, the fatigue life of the single-mastarm cantilever sign structure was not calculated because natural wind gusts were assumed to be the most critical loading

causing fatigue damage, and this loading did not appear to control for these structures.

- An experimental program evaluating the fatigue performance of sign structures in the field is needed to verify the fatigue damage evaluation results from the analytical program. Currently, no experimental work or field observation data from Indiana sites are available to validate or calibrate the analytical prediction.
- A more comprehensive investigation on sign structures designed in ways other than the prototype sign structures is needed. This study is based on new prototype sign structure designs provided by the Indiana Department of Transportation. Older sign structures in Indiana may have different design details and dimensional variations that could produce different results.

LIST OF REFERENCES

American Association of State Highway and Transportation Officials (AASHTO) (2004). *AASHTO LRFD Bridge Design Specifications*, Washington, D. C.

American Association of State Highway and Transportation Officials (AASHTO) (2001). *Standard Specifications for Structural Supports for Highway Signs, Luminaires and Traffic Signals*, 4th Edition, Washington, D. C.

American Welding Society (2004). *Structural Welding Code-Steel D1.1*, Miami.

American Welding Society (2003). *Structural Welding Code-Aluminum D1.2*, Miami.

ANSYS, Version 7.0 Manual. (2002). ANSYS Inc., Southpointe, 275 Technology Drive, Canonsburg, PA 15317.

ASTM E165 (2002). *Standard Test Method for Liquid Penetrant Examination*, American Society for Testing Materials, West Conshohocken, PA.

ASTM E 709 (2001). *Standard Guide for Magnetic Particle Examination*, American Society for Testing Materials, West Conshohocken, PA.

ASTM E 164 (2003). *Standard Practice for Ultrasonic Contact Examination of Weldments*, American Society for Testing Materials, West Conshohocken, PA.

Albrecht, P., and Yamada, K. (1977). "Rapid Calculation of Stress Intensity Factors," *Journal of the Structural Division*, Vol. 103, No. ST2, pp. 377-389.

Bannantine, J. A., Comer, J. J., and Handrock, J. L. (1990). *Fundamentals of Metal Fatigue Analysis*, Prentice-Hall, Englewood Cliffs, New Jersey.

Bobillier, B., Chakrabarti, S., and Christiansen, P. (2001). "Physical Modeling of Wind Load on a Floating Offshore Structure," *Journal of Offshore Mechanics and Arctic Engineering*, Vol. 123, pp. 170-176.

Collins, T. J., and Garlich, M. J. (1997). "Sign structures under watch," *Road and Bridges*, July, pp. 38-44.

Cook, S. J., Till, R. D., and Pearson, L. (2000). "Fatigue Cracking of Horizontal Gusset Plates at Arm-to-Pole Connection of Cantilever Sign Structures," *Proceedings of the Structural Materials Technology IV: An NDT Conference*, Atlantic City, NJ, pp. 419-427.

Delft, D.R.V. van, Dijkstra, O. D., and Snijder, H. H. (1986). "The Calculation of Fatigue

Crack Growth in Welded Tubular Joints Using Fracture Mechanics," OTC 5352, Offshore Technology Conference, Houston, Texas, pp. 573-579.

Downing, S. D., and Socie, D. F. (1982). "Simple Rainflow Counting Algorithms," *International Journal of Fatigue*, Vol. 4, No. 1, pp. 31-40.

Dexter, R. J.,and Ricker, M. J. (2001). "Fatigue-Resistant Design of Cantilevered Signal, Sign and Light Supports," *National Cooperative Highway Research Program (NCHRP) Report 469*, Transportation Research Board, National Research Council, Washington, DC.

Edwards, J. A., and Bingham, W. L. (1984). "Deflection Criteria for Wind-Induced Vibrations in Cantilever Highway Sign Structures," *Report 110-79-2*, Center for Transportation Engineering Studies, North Carolina State University at Raleigh, Raleigh, NC.

Fisher, J. W., Frank, K. H., Hirt, M. A., and McNamee, B. M. (1970). "Effect of Weldments on the Fatigue Strength of Steel Beams," *National Cooperative Highway Research Program (NCHRP) Report 102*, Transportation Research Board, National Research Council, Washington, DC.

Fisher, J. W. (1984). *Fatigue and Fracture in Steel Bridge: Case Studies*, Wiley Interscience.

Fisher, J. W., et al. (1981). "Fatigue Behavior of Steel Light Poles," *Report No. FHWA/CA/SD-81/82*, California Department of Transportation, Sacramento, CA.

Fisher, J. W., Kaufmann, E. J., and Culp, J. D. (1991). "Fatigue Cracking in Highway Sign Anchor Rods," *Proceedings of the Ninth Structures Congress*, Indianapolis, IN, pp. 319-322.

Fisher, J. W., Kulak, G. L., Smith, I. F. C. (1998). *A Fatigue Primer for Structural Engineers*, National Steel Bridge Alliance (NSBA), May.

Foley, C. M., Fournelle, R. A., Ginal, S. J., and Peronto, J. L. (2004). "Structural Analysis of Sign Bridge Structures and Luminaire Supports," *Report No. 04-03*, Wisconsin Department of Transportation, Madison, WI.

Fuchs, H. O., and Stephens, R. I. (1980). *Metal Fatigue in Engineering*, John Wiley & Sons, New York.

Grandt Jr., A. F. (2004). *Fundamentals of Structural Integrity*, John Wiley & Sons Inc., Hoboken, NJ.

Gurney, T. R. (1979). *Fatigue of Welded Structures*, 2nd Edition, Cambridge University Press, Cambridge, UK.

Hartle, R. A., Amrhein, W. J., Wilson III, K. E., Baughman, D. R., Tkacs, J. J. (1995). *Bridge Inspector's Training Manual 90*, Report No. FHWA/PD-91/015, Federal Highway Administration.

Iowa Department of Transportation, and Collins Engineers Inc. (1999). *Manual for Inspection of Sign Structures, Bridge-Mounted Support Frames, Long Mast Arm Structures, and Highmast Lighting Towers.*

James, L. A. (1976). "Fatigue-Crack Propagation in Austenitic Stainless Steels," *Atomic Energy Review*, Vol. 14, No. 1, pp. 40-41.

Justus, C. G., Hargraves, W. R., and Yalcin, A. (1976). "Nationalwide Assessment of Potential Output from Wind Powered Generations," *Journal of Applied Meteorology*, Vol. 15, pp. 673-678.

Kaczinski, M. R., Dexter, R. J.,and Van Dien, J. P. (1998). "Fatigue-Resistant Design of Cantilevered Signal, Sign and Light Supports," *National Cooperative Highway Research Program (NCHRP) Report 412*, Transportation Research Board, National Research Council, Washington, DC.

Kaimal, J. C. (1968). "Spectral Characteristics of Surface-Layer Turbulence," *Journal of the Royal Meteorological Society*, Vol. 98, pp. 563-589.

Moses, F., Schilling C. G., and Raju, K. S. (1987). "Fatigue Evaluation Procedures for Steel Bridges," *National Cooperative Highway Research Program (NCHRP) Report 299*, Transportation Research Board, National Research Council, Washington, DC.

Repetto, M. P., and Solari, G. (2001). "Dynamic Alongwind Fatigue of Slender Vertical Structures," *Engineering Structures*, Vol. 23, pp. 1622-1633.

Seguro, J. V., and Lambert, T. W. (2000). "Modern Estimation of the Parameters of the Weibull Wind Speed Distribution for Wind Energy Analysis," *Journal of Wind Engineering And Industrial Aerodynamics*, Vol 85, pp. 75-84.

Simiu, E., and Scanlan R. H. (1986). *Wind Effects on Structures: An Introduction on Wind Engineering*, Second Edition, John Wiley & Sons, NY.

Spencer, F. W. (1996). *Visual Inspection Research Project Report on Benchmark Inspections*, Technical Report DOT/FAA/AR-96/65, U.S. Department of Transportation, Federal Aviation Administration, Washington , D.C., October.

Stevens, M. J., and Smulders, P. T. (1979). “The Estimation of the Parameters of the Weibull Wind Speed Distribution for Wind Energy Utilization Purposes,” *Wind Engineering*, 3 (2), pp. 132-145.